Shaking Table Test Allowing Interpretation of Damage to Structure in Terms of Energy Influx and Efflux through Soil-Structure Interface

REPORT OF RESEARCH PROJECT
1999 GRANT-IN-AID FOR SCIENTIFIC RESEARCH (B)
(No. 10450174)
The Ministry of Education, Science, Sports and Culture

March, 2000

Kazuo KONAGAI
Institute of Industrial Science
University of Tokyo

REPORT OF RESEARCH PROJECT
1999 GRANT-IN-AID FOR SCIENTIFIC RESEARCH (B)

Project No. **10450174**

Title of project:

SHAKING TABLE TESTS ALLOWING INTERPRETATION OF DAMAGE TO STRUCTURE IN TERMS OF THE ENERGY INFLUX AND EFFLUX THROUGH SOIL STRUCTURE INTERFACE

（地盤と構造物のエネルギー収支効果を反映した振動台模型実験による損傷累積過程の研究）

Head investigator: **Kazuo KONAGAI**

Investigator: **Yoshiaki NAKANO**

Grant-in-aid:	6,000,000 yen	1998
	4,600,000 yen	1999

Publication list (Peer reviewed):

1) Konagai, K., A. Mikami and T. Nogami: Simulation of Soil-Structure Interaction Effects in Shaking Table Tests, Geotechnical Earthquake Engineering and Soil Dynamics 1998, Seattle, *Geotechnical Special Technical Publication*, ASCE, **75(1)**, 482-493, 1998.
2) Konagai, K. and T. Nogami: Analog circuit to simulate dynamic soil-structure interaction in shake table test, *International Journal of Soil Dynamics and Earthquake Engineering*, **17(5)**, 279-287, 1998.
3) Konagai, K., T. Nogami, T., Katsukawa, T., Suzuki and A., Mikami: Real Time Control of Shaking Table for Soil-Structure Interaction Simulation, *Jour. of Structural Mechanics and Earthquake Engineering, JSCE*, **16(1)**, 91s-95s, 1999.
4) Konagai, K., O., Uemura, T., Katsukawa and T., Suzuki: Real Time Simulation of Soil-Structure Interaction Effects on Shaking Tables, *Proc., 10th Japan Earthquake Engineering Symposium*, **E1-13**, 1647-1652, 1998.
5) Konagai, K., A. Raquib and D., Maruyama: Simulation of Energy Influx and Efflux through Soil Structure Interface, *Proc., 12th World Conf., Earthquake Engineering* (CD Rom), No.1334, 2000.
6) Konagai, K., A. Raquib and D., Maruyama: Simple Expression of the Dynamic Stiffness of Grouped Piles in Sway Motion, *International Jour., Earthquake Engineering*, accepted for publication.
7) Nakano, Y., K., Kusu and Y., Hino: Tortional Response of RC Buildings Retrofitted with Steel Framed Braces, *Proc., 12th World Conf., Earthquake Engineering* (CD Rom), No.1129, 2000.

PREFACE

Nonlinear soil-structure interaction is a phenomenon associated with energy influx and efflux through a soil-structure interface. The energy accumulated in a structure is given as the difference between the energy influx and efflux, and is certainly responsible for compound fracture of the structure. Structures in active seismic zones may experience a number of earthquakes during their service lives. All events that a structure has experienced are responsible for continual accumulation of the damage, and thus, the cumulative energy is, if measured, an appropriate index for evaluating the remaining life of a structure. Needless to say in this discussion, both behaviors of a structure and its subsoil are to be treated with equal rigor in order for the energy flow to be rationally estimated.

Model experiments on a shaking table are quite useful for identification of important phenomena and verification of predictive theories regarding dynamic behavior of a prototype structure subjected to an earthquake, and sensors densely arranged on a structure model may allow us to discuss the compound fracturing of the structure model in terms of the energy that is accumulated in it. However, a shaking table is, in general, controlled so that it follows closely the input *free-field* motion, while in reality, a structure interacts with its foundation on or in the ground, and responds differently. This interaction thus causes the motion of the ground at the structure's base to deviate from the free-field motion. This effect may be partly incorporated by filling up a bin on the table with actual prototype soil and by putting a model on it. This method is particularly useful when non-linear features of the soil in the vicinity of a structure must be considered. But the process of preparing a soil model is rather difficult; and if prepared, it still cannot allow for the effect of wave-dissipation into an infinite soil medium existing in the field.

Shaking tables of many sizes have been used so far. Some are quite large, allowing models with dimensions of several meters to be shaken. However, they are not always large enough for all structural models of interest to be tested. Within the finite base size of a shaking table and within the limit of its dynamic loading capacity, not the whole structure but just one part of it, like some devices for vibration reduction, can be tested. In this case also, the input motion to the model's base must be affected by the presence of the model.

The purpose of this project was to develop a method for controlling a shaking table so that the soil-structure or base-structure interaction effect is incorporated. In order for the interaction effect to be reflected in a shaking table test, the signal equivalent to the

further displacement induced by the interaction is added in real-time to the input ground or base motion. This method, therefore, requires a device that can generate the signals corresponding to the base-structure interaction motions. To all intents and purposes, the expression of base stiffness must be simplified enough for the device to loose no time in responding to the input force, and producing the base-structure interaction motion.

As is the case of many reports, this report was an outgrowth of different peer-reviewed papers published in both domestic and international journals. Chapters in this report are, thus, based on these papers. However, they were so arranged that the outline of this study, and eventually, the remaining problems would be brought in full relief.

Acknowledgment here may be in order. I am indebted to the many people whose suggestions and criticisms have helped me with this project, especially, Dr. Toyoaki Nogami, Professor, Cincinnati University, Dr. Takeyasu Suzuki and Mr. Tota Katsukawa, Technical Research & Development Inst., Kumagai Gumi, Co., Ltd, Dr. Xiu Loo and Dr. Akihiko Nishimura, Railway Technical Research Institution. I should like to thank the students and staff members at Konagai Lab. and Nakano Lab., IIS, University of Tokyo, especially, Mr. Raquib Ahsan who have conducted difficult experiments and numerical simulations. Dr. Atsushi Mikami, former Research Associate, and Mr. Toshihiko Katagiri, technician at Konagai Lab., have devotedly tried out some new ideas. Regarding the results obtained through the experimental and numerical simulations, I had frequent opportunities to discuss with the members of the Committee for the Future Prospect of the Seismic Design of Bridges (Chairman: Prof. Yuzo Fujino, University of Tokyo), Japan Society of Steel Construction. The discussions were very constructive. Lastly, grateful acknowledgment is made to Ms. Yasuko Takahashi for her help in preparing figures and tables.

K. K.

Komaba, Tokyo
March, 2000

CONTENTS

INTRODUCTION

When a structure is subjected to a ground excitation, it interacts with its substructure i.e., foundation and soil. In other words, the motion of ground is also altered because of the vibration of the structure. Due to the semi-infinite extent of soil, this interaction provides a mechanism for energy dissipation, called radiation damping, through soil as outwardly propagating waves. For the shaking table tests conducted without taking the interaction into account, the input energy is totally consumed by the structure producing quite conservative results. On the other hand, tests conducted using physical ground model to incorporate associated non-linearity inherit two fold demerits. Firstly, the finite dimension of the ground model fails to provide radiation damping and thus yielding conservative results. Secondly the weight of the ground model causes an extra burden on the performance of the shaking table restricting superstructure models to a smaller size. Hence, when the observation of the behavior of a superstructure is the main concern, neither of the above methods seems to be satisfactory.

With a view to incorporate the interaction between soil and structure without using any physical ground model, Konagai et al. (1997~1998) introduced a new method for shaking table tests. In their method, appropriate soil-structure interaction motions are added to free-field ground motions to simulate soil-structure interaction effects. The method considers radiation damping which, in general, causes the total damping of a soil-structure system to be greater than that of the structure itself. Thus the incorporation of soil-structure interaction effects in a shaking table test leads to reducing the demands on the capacity of shaking tables. This dynamic interaction is a phenomenon associated with the influx and efflux of energy which is generated by the

earthquake excitation and transmitted through the soil-structure interface. It is noted that the difference between the influx and efflux is exactly the energy stored up within a structure, and thus, is closely related to the extent of damage to the structure. If these interaction effects are rationally simulated in shaking table tests, one will obtain the necessary pieces of information for interpreting the failure processes of prototype structures in terms of energy.

The method was initially developed with the assumption that soil behaves linearly. In the present report, the method is extended to take the 'far field' soil non-linearity into account through an equivalent linear approach. The non-linearity produced in the vicinity of foundations, which is usually associated with large strain and separation between soil and foundation, has not been considered in this study. In this method the dynamic soil parameters are varied in real time by means of a digital signal processor. The method, on one hand, captures the non-linear soil behavior of softening and re-hardening during the course of an earthquake, and on the other hand, allows testing of a bigger superstructure model by obviating the need of a heavy physical ground model.

This report introduces in its first half (***Chapters* 1~3**) simple descriptions of foundation stiffness parameters in terms of a limited number of frequency-independent parameters: the descriptions allowing soil-structure interaction motions to be simulated on a shaking table. The latter half (***Chapter* 4**) then presents a method for simulating soil-structure interaction effects in shaking table tests, in addition to some pieces of equipment contrived for better control of shaking tables. Simple examples of soil-structure interaction simulations using the present method are also given in this chapter.

In the course of this study, the idea of treating a pile group beneath a super-structure as a single upright beam has yielded **BASPIA** (**B**eam **A**nalogy for **S**oil-**P**ile group **I**nteraction **A**nalysis), a program allowing soil-pile group interaction analysis to be made with less time and effort. **BASPIA** includes ***TLEM*** (**T**hin-**L**ayered **E**lement **M**ethod) as a solver that describes a soil stratum as an infinite stratified medium with the inclusion of a cylindrical hollow, in which a foundation is fitted. **BASPIA** with the restricted version of ***TLEM*** for WINDOWS is a freeware that can be downloaded from the following URL:

http://norway.iis.u-tokyo.ac.jp/BASPIA.htm

The manuals of **BASPIA** and ***TLEM*** (Ver. 1.2) are provided in **APPENDIX 3**.

REFERENCES

Konagai, K., Mikami, A. and Nogami, T. [1998] "Simulation of Soil-Structure Interaction Effects in Shaking Table Tests," Geotechnical Earthquake Engineering and Soil Dynamics 1998, Seattle, *Geotechnical Special Technical Publication*, ASCE, **75(1)**, 482-493.

Konagai, K. and Nogami, T. [1998] "Analog circuit to simulate dynamic soil-structure interaction in shake table test," *International Journal of Soil Dynamics and Earthquake Engineering*, **17(5)**, 279-287.

Konagai, K., Nogami, T., Katsukawa, T., Suzuki, T. and Mikami, A. [1998] "Real Time Control of Shaking Table for Soil-Structure Interaction Simulation," *Jour. of Structural Mechanics and Earthquake Engineering, JSCE,* **16(1)**, 91s-95s.

Konagai, K., Uemura, O., Katsukawa, T. and Suzuki, T. [1998] "Real Time Simulation of Soil-Structure Interaction Effects on Shaking Tables," *Proc., 10th Japan Earthquake Engineering Symposium*, **E1-13**, 1647-1652.

Chapter 1

SIMULATION OF SOIL -STRUCTURE INTERACTION EFFECT ON SHAKING TABLES

1.1. TWO PRIMARY CAUSES OF SOIL-STRUCTURE INTERACTION

In this study, a soil-structure system is divided into two substructures, the superstructure and the unbounded soil extending to infinity; the latter includes an embedded foundation as illustrated in **Figure 1.1**, because a shaking table represents exactly the latter substructure of soil. The multi-step method is used to describe two primary causes of soil-structure interaction - the inability of the foundation to match the free-field deformation, and the effect of the dynamic response of the superstructure on the movement of its supporting soil-foundation system. In the lower substructure of soil,

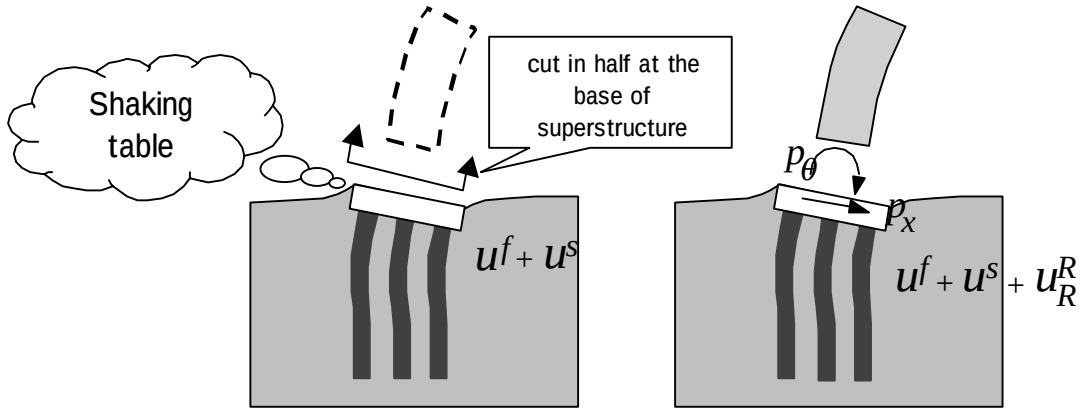

Figure 1.1 Two primary causes of soil-structure interaction

an earthquake will cause soil displacements, $\{\mathbf{u}^f\}$. The foundation embedded in this soil deposit, however, will not follow the free-field deformation pattern. This deviation of the displacements from the free-field soil displacements, $\{\mathbf{u}^f\}$, is denoted by $\{\mathbf{u}^s\}$. The mass of the super-structure then causes it to respond dynamically, and the forces, $\{\mathbf{p}\}$, transmitted to the lower substructure of soil and foundation will produce further deformation of soil, $\{\mathbf{u}^R\}$ (***inertia interaction***), that would not occur in a fixed base structure. Thus, the displacements of soil, $\{\mathbf{u}\}$, are eventually expressed by the following equation as:

$$\{\mathbf{u}\} = \{\mathbf{u}^f\} + \{\mathbf{u}^s\} + \{\mathbf{u}^R\} \tag{1.1}$$

Consider the case that a foundation has two degrees of freedom in sway and rocking (x, θ) at the base of its super-structure as illustrated in **Figure 1.1**. The interaction forces, $\{\mathbf{p}\}$ ($=\{p_x \quad p_\theta\}^T$), from the super-structure cause the inertia interaction motions, $\{\mathbf{u}^R\}$, in the frequency domain to be:

$$\begin{Bmatrix} u_x^R \\ u_\theta^R \end{Bmatrix} = \begin{bmatrix} H_{xx}(s) & H_{x\theta}(s) \\ H_{\theta x}(s) & H_{\theta\theta}(s) \end{bmatrix} \begin{Bmatrix} p_x \\ p_\theta \end{Bmatrix} \tag{1.2}$$

where,

$$\begin{bmatrix} H_{xx}(s) & H_{x\theta}(s) \\ H_{\theta x}(s) & H_{\theta\theta}(s) \end{bmatrix} = [\mathbf{H}] \tag{1.3a}$$

is the flexibility (compliance) at the top of the foundation, and

$$s = i \cdot \omega \tag{1.3b},$$

in which $i = \sqrt{-1}$ and ω is the excitement circular frequency. In the present method, a shaking table's motion is controlled directly following the above-mentioned process of soil-structure interaction.

In the present method, the motion of a shaking table is controlled directly following the actual process of soil-structure interaction. **Figure 1.2** shows a schematic view of the set-up of a shaking table test, in which a superstructure model is placed directly on the table without a physical ground model. Soil-structure interaction effects are simulated by adding appropriate soil-structure interaction motions to free-field ground motions at the shaking table. In the simulation, first, the transducers at the base of the foundation pick up the signals of the base forces, p_x and p_θ in sway and rocking motions, respectively. These two amplified signals are then applied to the circuits H_{xx}, $H_{\theta x}$, $H_{x\theta}$ and $H_{\theta\theta}$ to produce the outputs corresponding to the soil-structure interaction motions, u_x^R and u_θ^R. The output signals are then added to the signals of the base input motions, $u_x^f + u_x^s$ and $u_\theta^f + u_\theta^s$, to produce the signals of foundation motions, $u_x^f + u_x^s + u_x^R$ and $u_\theta^f + u_\theta^s + u_\theta^R$. The method is, thus, based on the premise

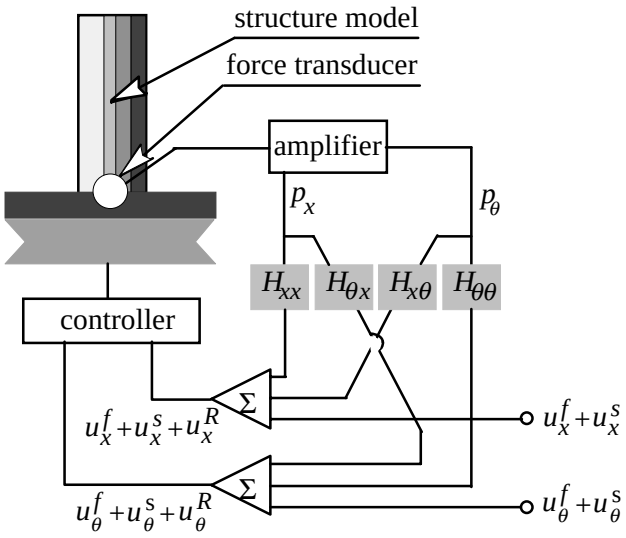

Figure. 1.2 Present setup in a shaking table test for soil-structure interaction simulation

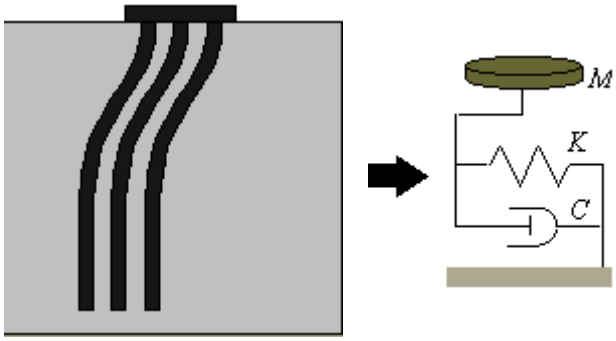

Figure 1.3. Modeling of a pile-group as a simple-damped oscillator

that $u_x^f + u_x^s$ and $u_\theta^f + u_\theta^s$ are known beforehand as the base input motions. The signals of the foundation motions are finally translated into the shaking table motions by the shaking table controller.

This method, therefore, requires a device that can generate signals identical to the transient motion of its base on a soil medium of infinite extent. To all intents and purposes, the expression of soil stiffness, $[\mathbf{k}]$ $(=[\mathbf{H}]^{-1})$, must be simplified enough for the device to loose no time in responding to the input force $\{\mathbf{p}\}$, and producing the soil-structure interaction motion, $\{\mathbf{u}^R\}$. As will be shown later, the stiffness function for a sway motion of a pile-cap, for example, can be closely approximated by a simple-damped oscillator with spring, dashpot and mass parameters, K, C and M (**Figure 1.2**). The parameters K, C and M are varied with time to reflect the

non-linear behavior of soil. In order to obtain the appropriate variation of these parameters with time a non-linear analysis of ground response is necessary. From the non-linear ground response analysis, it is possible to obtain the non-linear stress-strain histories at different points of the ground profile for a particular base excitation. The non-linear stress-strain histories are then idealized to obtain histories of equivalent linear soil parameters like secant shear modulus and damping ratio. Using the equivalent linear soil parameters of a particular time, a linear foundation-soil interaction analysis is performed to obtain the appropriate values of the parameters of the stiffness function at that time. Thus by performing similar analyses repeatedly to cover the total duration of the excitation, variations of these parameters with time can be obtained. During shaking table tests the parameters of the stiffness function are changed in real time according to the derived variations by means of a digital signal processor. The steps of the present method are discussed in detail in ***Chapter* 4** (**4.4.3,** p.61~).

1.2 PHYSICAL INTERPRETATION OF DYNAMIC SOIL STIFFNESS

As has been suggested above, a flexibility or stiffness function for the motion of a foundation embedded in or resting on the lower substructure of soil can often approximated by a simple oscillator with an inclusion of a viscous damper. A simple analysis will be sufficient to illustrate a physical interpretation of this viscous damper.

Observation of wave fronts radiating from a foundation offers important insights into soil-structure interaction. This is also a very useful way to examine simple expressions of soil-structure interaction. Konagai et al. (1987) used a special experiment method to directly observe the wave front radiating from a foundation subjected to an impulse (**Figure 1.4**). In their method, a model foundation is put on, or embedded in a soft and transparent soil model which is made of urethane gel with a thin gelatin plate sandwiched upright in its middle. The elastic constants of the gelatin plate are almost identical to those of the surrounding urethane gel. Since the gelatin has an extremely high photo-elastic sensitivity compared with the urethane gel, the gelatin plate allows the visual observation of the radial propagation of shear waves in the vicinity of the foundation. A vertical impulse was applied to a model of a rigid surface disk. **Figure 1.5** shows a snap shot of the wave front radiating outwardly into the homogeneous ground model. The hemispherical shape of the wave front suggests that the wave decays as it travels away in the radial direction, r. This wave with the velocity c, thus, will presumably be approximated by:

$$u^R = q(r) \cdot f(r - ct) \tag{1.4}$$

where, $q(r)$ describes how the wave attenuates as it travels away. On the soil-disk interface ($r = r_0$) having the contact area, A, shear force, p, is roughly described as:

$$\begin{aligned} p \cong \tau A = -\left\{ A\mu \frac{\partial u^R}{\partial r} \right\}_{r=r_0} &= -A\mu \left\{ \frac{dq}{dr} f + q \frac{\partial f}{\partial r} \right\} \\ &= -A\mu \left\{ \frac{dq}{dr} f - \frac{q}{c} \frac{\partial f}{\partial t} \right\}_{r=r_0} \\ &= -A\mu \left\{ \frac{q'}{q} u^R - \frac{1}{c} \dot{u}^R \right\} \end{aligned} \tag{1.5}$$

in which μ is the elastic modulus of soil.

The force p thus turns out to comprise two components proportional to the displacement, u^R, and the velocity, $\dot{u}^R$, of the disk, respectively. Equation (1.5) is thus

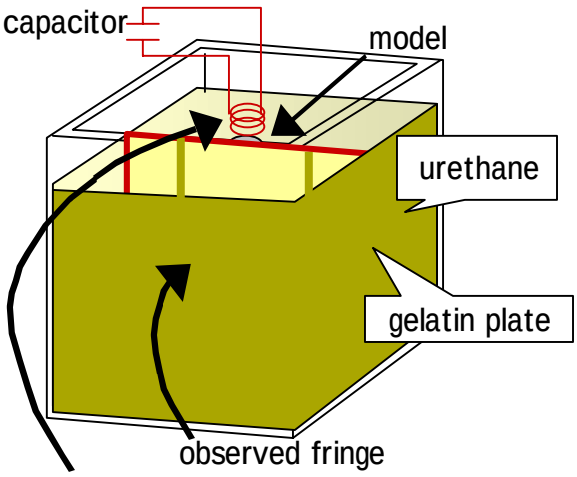

A suuden discharge of a capacitor through a solenoid coil serves as an inpulsive energy source

Figure. 1.4. Visualization of wave fronts [Konagai et al., 1987]

A jelly-like soft soil model of urethane with an upright and flexible gelatin plate sandwiched in its interior was prepared in an acrylic box. An impulse was then applied to a foundation resting on or embedded in the soil model. Since photo-elastic sensitivity of gelatin, when compared with that of urethane, is extremely high, cross sections of sharp wave fronts induced by the impulse and transmitted through the 3D soil model are clearly visualized on the inner plane of gelatin through a polariscope arrangement.

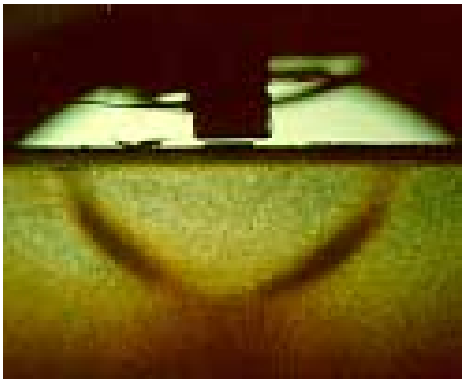

Figure 1.5. Hemispherical wave front from a rigid disk [Konagai et al., 1987, 1998]

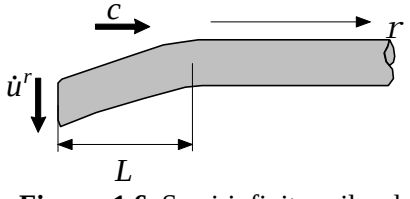

Figure. 1.6. Semi-infinite soil rod

rewritten as:

$$p = K \cdot u^R + C \cdot \dot{u}^R \tag{1.6}$$

where,

$$K = \left\{ - A\mu q'(r) / q(r) \right\}_{r=r_0} \tag{1.7a}$$

$$C = \left\{ A\mu q(r) / c \right\}_{r=r_0} \tag{1.7b}$$

Since $q(r)$ decreases as r increases, $-q'(r)$ in Equation (1.7a) is noted to be a positive value, and consequently, both parameters, K and C are positive. Equation (1.6), thus, implies that the stiffness of the soil-disk system is mechanically identical to an assembly of the spring K and the damper C arranged in parallel.

A simple semi-infinite soil rod with a constant cross-section ($q(r) = q(r_0) = 1$, **Figure 1.6**), offers further clearer physical insight into the reaction from the soil. Only shear deformation is allowed to take place in this rod. The soil stiffness at the end of the rod is simply given by:

$$k = \frac{\mu A}{L} \tag{1.8}$$

with L as the deformed length of the rod. For a static load applied to the end of the rod, the entire length of the rod is deformed ($L = \infty$), and eventually:

$$k = K = \frac{\mu A}{L} = 0 \tag{1.9a}$$

Equation (1.9a) is consistent with Equation (1.7a) because $-q'(r)$ is noticed to be 0 for this rod of constant cross-section. When a dynamic load p causes the rod's end to be driven with the velocity $\dot{u}^R$, the entire length of the rod does not move all at once within a finite time t. At this particular time t, displacement u^R and the deformed rod length L are $\dot{u}^R t$ and ct, respectively. The reaction force p is thus given as:

$$p = k \cdot u^R = \frac{\mu A}{ct} \dot{u}^R t = \frac{\mu A}{c} \dot{u}^R = C\dot{u}^R \tag{1.9b}$$

It is obvious that Equation (1.9b) is consistent with Equation (1.7b) because the specific energy does not decrease as the wave travels through the rod of constant cross-section calling for $q(r) = q(r_0) = 1$.

An added mass parameter, M, if necessary, can be attached to the simplified model for better approximation of the soil stiffness, leading to a slight modification of Equation (1.6) as:

$$p = M \cdot \ddot{u}^R + K \cdot u^R + C \cdot \dot{u}^R \tag{1.10}$$

The soil stiffness is thus written in the frequency domain as:

$$k = \left(K - \omega^2 M \right) + i\omega C \tag{1.11}$$

implying that the stiffness is eventually a complex function of circular frequency ω. Its

real part is a downward open parabola to the right, whereas its imaginary part increases linearly with increasing frequency.

1.3 SUMMARY

The above expression for the soil stiffness may be based on oversimplified conditions, but gives us an idea that the stiffness for any of lateral, vertical or rotational response mode will be approximately described by a limited number of simple frequency-independent parameters. It is, however, certainly necessary to have a rational numerical tool allowing rigorous stiffness parameters to be examined, and to be compared with the simplified expressions. Especially, thorough discussions on piles grouped beneath super structures are essential in the course of this study; the discussion follows in ***Chapters* 2** and **3**.

REFERENCES

Konagai, K., Koizumi, Y. and Ogawa, S. [1987] "Experiments on Soil-Pile Interaction using Electromagnetic-Induction-Type Impulse Generator," *Dynamic Response of Pile Foundations -- Experiments, Analysis and Observation, Geotechnocal Special Technical Publication, ASCE,* **11**, 99-109.

Konagai, K. and Nogami, T. [1998] "Analog circuit to simulate dynamic soil-structure interaction in shake table test," *International Journal of Soil Dynamics and Earthquake Engineering*, **17(5)**, 279-287.

Chapter 2

SIMPLE EXPRESSION OF THE DYNAMIC STIFFNESS OF GROUPED PILES

2.1 INTRODUCTION

Piles, grouped beneath a superstructure, interact with the surrounding soil during an earthquake, and the dynamic pile-soil-pile interaction often affects the motion of the superstructure to a considerable extent. Straightforward evaluation of the pile-soil-pile interaction, however, is cumbersome especially in dealing with tens or hundreds of piles grouped together. Hence a simplified approach for the evaluation of such dynamic pile-soil-pile interaction is highly desirable for the purpose of treating the dynamic behavior of an entire soil-foundation-structure system. Some research has been carried out with the objective of developing such a simplified approach. Attempts include the Ring-Pile method [Takemiya, 1986] and Closely-Spaced-Plates model [Ohira and Tazo, 1985]. In these methods, respectively, piles with the soil caught among them are re-grouped into several concentric cylinders (piles arranged in concentric circles) and into soil-pile-striped upright plates, allowing close evaluation of interaction effects to be made with less time and trouble. This chapter presents a further simplified approach in which a group of piles is viewed as a single equivalent upright beam.

Careful examination of the deflections of grouped piles reveals that most piles are indeed flexible in practice in the sense that they do not deform over their entire lengths. Instead, pile deflections become negligible below their active lengths. With the active lengths provided for different soil-pile systems, it is shown in the latter half of this chapter that pile-cap (grouped-piles-head) stiffness can be approximated in terms of the

mass, damping and stiffness parameters; the parameters are invariant of frequency and are dependent only on the mechanical properties of soil and pile. The method presented in this report requires real-time manipulation of soil-structure interaction parameters in accordance with the development of non-linear features of soils and piles. The present simple expression of pile-cap stiffness, thus proves to be useful despite the availability of efficient numerical programs for analyzing pile-soil-pile interaction.

2.2 EQUIVALENT SINGLE UPRIGHT BEAM

In discussing the equivalent upright beam, straightforward evaluation of pile-soil-pile interaction is first necessary to provide rigorous solutions. Based on the numerical scheme presented by Tajimi and Shimomura [Thin-Layered Method, 1976] that allows soil-embedded foundation interaction effects to be rigorously evaluated, a numerical program "***TLEM***"(Ver. 1.1) has been developed for soil-pile group interaction analyses [Konagai, 1998d]. The Thin-Layered Element Method is a method for describing soil strata rather than for foundations. In this method, a soil deposit is treated as an infinite stratified medium with the inclusion of a cylindrical hollow in which the foundation is fitted. The piles are assumed to be upright Timoshenko or Beronoulli-Euler beams. The evaluation of pile-soil-pile interaction effects in this program is based on the superposition method that was originally proposed by Poulos [1968, 1971]. In this approximation, only two piles are considered in the formulation of a global flexibility matrix, and other piles' effects on these two piles are totally ignored (**Figure 2.1**). Kanya and Kausel [1982] have shown that the superposition scheme gives reasonable results not only for static loads but for dynamic loads as well.

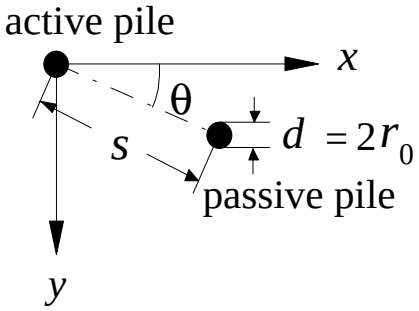

Figure 2.1 Active and passive piles

In contrast to the above approach, the present single upright beam is a composite of n_p piles and the soil caught among them embedded in a horizontally stratified infinite soil deposit with material damping of the frequency-independent hysteretic type (**Figure 2.2**). Following the *TLEM* assumption, the soil deposit overlying its rigid bedrock should include a cylindrical hollow of radius R_0. The cross-section, πR_0^2, of this hollow is assumed to be identical to the beam's cross-section A_G enclosed with the broken line circumscribing the outermost piles in the group (**Figure 2.2a**). The motion of the hollow is assumed to be compatible with that of the beam. The soil-pile composite together with its exterior soil is divided into n_L horizontal slices as shown in **Figure 2.2**. The following assumptions are adopted to derive the stiffness matrix of the equivalent single beam:

(1) Pile elements within a horizontal soil slice are all deformed at once keeping their intervals constant, and the soil caught among the piles moves in a body with the piles.
(2) Frictional effects due to bending of piles (external moments on each individual pile from soil) are ignored.
(3) The top ends of piles are fixed to a rigid cap.
(4) All upper or lower ends of the sliced pile elements arranged on the cut-end of a soil slice remain on one plane (Note this assumption does not necessarily mean that each pile's cross-section remains in parallel with this plane. See **Figure 2.2b**).

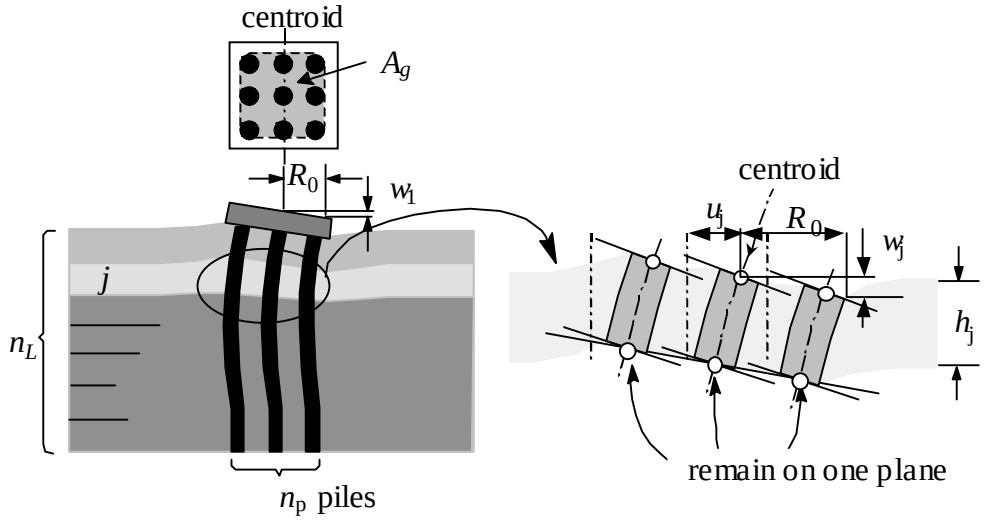

(a) soil-grouped piles system **(b)** sliced elements

Figure 2.2 Assumptions for evaluation of equivalent single beam

With assumptions (1) and (4), there are only two degrees of freedom for each cut-end of all slices of the soil-pile composite, namely, sway and rocking motions respectively designated as $\{\mathbf{u}\}(=\{u_1 \quad u_2 \quad \cdots \quad u_{N_L}\}^T)$ and $\{\mathbf{w}\}(=\{w_1 \quad w_2 \quad \cdots \quad w_{N_L}\}^T)$ (**Figure 2.2b**). The rocking motions are expressed in terms of the anti-symmetric vertical motion $\{\mathbf{w}\}$ at the outermost edge ($r = R_0$) of the equivalent beam with respect to the beam's centroid. In sway motions, all n_p piles are equally displaced (assumption (1)), causing the bending stiffness, EI, of the equivalent beam to be simply n_p times as large as the bending stiffness of an individual pile. Assumptions (3) and (4) imply that axial motions of the piles control the overall anti-symmetric rocking motion of the equivalent beam just as reinforcements in a concrete beam do. Therefore, another bending stiffness parameter, EI^G, is introduced to describe the rocking motion of the beam. This stiffness parameter EI^G is evaluated following the same procedure as that used for the evaluation of bending stiffness of a reinforced concrete beam (See **APPENDIX I**). Lateral external forces $\{\mathbf{p}_x\}$ and moments $\{\mathbf{M}\}$ are finally described in matrix notation in terms of $\{\mathbf{u}\}$ and $\{\mathbf{w}\}$ as specified in Equation (A12) in **APPENDIX I**:

$$\begin{Bmatrix} \mathbf{p}_x \\ \cdots \\ \dfrac{\mathbf{M}}{R_0} \end{Bmatrix} = \begin{bmatrix} [\mathbf{L}][\mathbf{D}]^{-1}[\mathbf{L}] & \vdots & \text{1st column of } [\mathbf{L}][\mathbf{D}]^{-1}/R_0 \text{ and zeros for other columns} \\ \cdots\cdots\cdots & & \cdots\cdots\cdots \\ \text{1st row of } [\mathbf{D}]^{-1}[\mathbf{L}]/R_0 \text{ and zeros for other rows} & \vdots & [\mathbf{Q}] \text{ with } D_{1,1}^{-1} \text{ added to the upper - left corner} \end{bmatrix} \begin{Bmatrix} \mathbf{u} \\ \cdots \\ \mathbf{w} \end{Bmatrix} \quad (2.1)$$

where, $[\mathbf{L}]$, $[\mathbf{D}]$ and $[\mathbf{Q}]$ are assembled global matrices corresponding to the individual layer parameters of $1/h_j$ (h_j = thickness of the j-th layer), h_j / EI and $EI^G / R_0^{\,2} h_j$, respectively, (See Equations (A2), (A4) and (A10) in **APPENDIX I** defining $[\mathbf{L}]$, $[\mathbf{D}]$ and $[\mathbf{Q}]$, respectively).

"***TLEM***" has been upgraded for evaluation of the behaviors of an equivalent single beam (Ver. 1.2). **Figure 2.3** shows pile cap stiffnesses k_{xx} for sway motions of 2×2 and 3×3 steel pile groups (**Table 2.1**) plotted as functions of frequency. The results for the equivalent beams are shown as open circles. Each pile group is embedded in the same homogeneous soil deposit (**Table 2.2**) equally divided into 20 slices. Downward dips in these plots of k_{xx} occur at essentially the resonance frequencies of the soil stratum for vertical shear wave propagation. As a whole, however, every real part of the pile cap stiffnesses decreases slowly as the frequency increases, whereas its imaginary part representing the damping of a soil-pile group system shows a general upward trend to the right. The curves for the equivalent single beams agree well with rigorous solutions from "***TLEM***" (Ver. 1.1).

Table 2.1 Parameters for steel piles

E_p (tf/m^2)	ρ (t/m^3)	r_0 (m)	Thickness (m)	Length (m)
2.1×10^7	7	0.3	0.0089	20

Table 2.2 Parameters for soil

ρ (t/m^3)	v_T (m/s)	ν
1.5	80	0.49

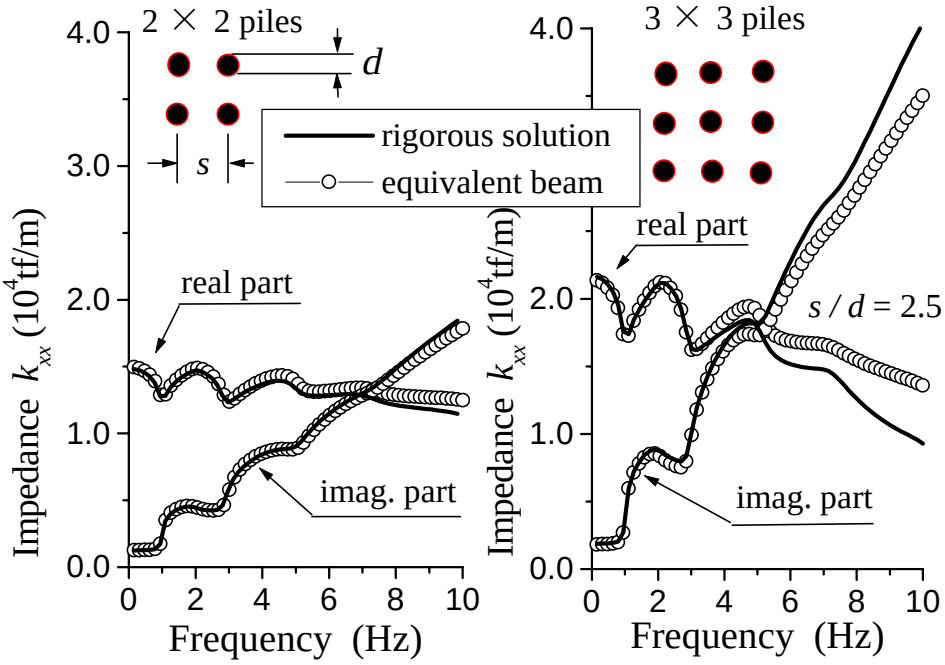

Figure 2.3 Variations of stiffness parameters for sway motions of pile groups

Assumption (1) taken in this chapter to derive the stiffness matrix of the equivalent-upright beam (Equation (2.1)) implies that the spacing between piles, *s*, should be within a certain limit. To investigate this constraint on the spacing between piles, the results of the program "*TLEM*" (Ver. 1.2) were compared with the rigorous results obtained from "*TLEM*" (Ver. 1.1). Here, hollow cylindrical steel piles (**Table 2.1**) embedded in a homogeneous soil with the density ρ and the shear wave velocity v_T (**Table 2.2**) were considered. The variations of the ratios between approximate and rigorous solutions with respect to normalized frequency $\omega s / v_T$ are shown in **Figure 2.4** for three different values of spacing ($s/d = 2.5$, $s/d = 3.33$ and $s/d = 5.0$). For a wide range of cases examined, "*TLEM*" (Ver. 1.2) is found to produce insignificant error below a certain limit of spacing, $s/d < 3$. Below this limit, however, it is noted

that the error can yet become significant as the non-dimensional frequency increases beyond a certain limit (See thick lines in **Figure 2.4** for large number of piles).

An earthquake causes the free-field ground motion $\{\mathbf{u}^f \ \vdots \ \mathbf{w}^f\}^T$ in which vertical displacement vector $\{\mathbf{w}^f\}$ can be ignored in many of the practical cases encountered. The piles in this soil deposit, however, will not follow the free-field deformation pattern. This deviation of the displacements from the free-field soil displacements is denoted by $\{\mathbf{u}^s \ \vdots \ \mathbf{w}^s\}^T$. Equation (2.1) is also used to evaluate effective foundation input motion $\{\mathbf{u}^f + \mathbf{u}^s \ \vdots \ \mathbf{w}^f + \mathbf{w}^s\}^T$. The effects of soil-embedded-foundation kinematic interaction are portrayed in the form of two kinematic displacement factors in sway and rocking motions

$$T_{e,sway} = \frac{u_1{}^f + u_1{}^s}{u_1{}^f}, \quad T_{e,rocking} = \frac{w_1{}^f + w_1{}^s}{u_1{}^f} \cong \frac{w_1{}^s}{u_1{}^f} \qquad \text{(2.2a), (2.2b)}$$

plotted as functions of frequency. In Equation (2.2b), the vertical component of free-field ground motion $w_1{}^f$ is ignored.

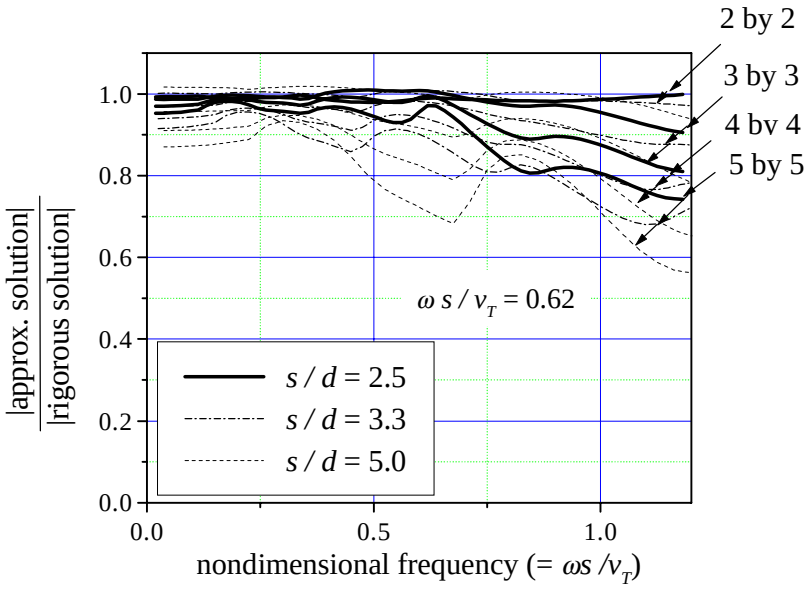

Figure 2.4 Variation of ratios between approximate and rigorous solutions with respect to normalized frequency $\omega s / v_T$

Figure 2.5 shows the kinematic displacement factors of a 2×2 PC pile group plotted as functions of non-dimensional frequency $\omega s / v_T$ ($s / d = 2$, See **Tables 2.3** and 2.**4**), and they are in good agreement with rigorous solutions by Fan et al. (1982).

It is again to be remembered that the piles behaving in accordance with assumption (1) are completely equal with each other not only in their deformations but also in lengthwise distributions of internal force and moment. The dynamic pile-soil-pile interaction effects are thus excluded. Even for a static loading, any discussion based on the assumption does not reflect the fact that outermost piles sustain heavier loads than those on inner piles (static pile-soil-pile interaction). Yet, the present single upright beam, as has been shown above, satisfactorily approximates the motions of a pile group with a reduced number of parameters. These parameters allow the stiffness parameters of a pile cap to be described in a further simplified manner; a discussion of lateral translation follows in **Section 2.3**.

Table 2.3 Parameters for piles

$E_p I_p$ (tf m^2)	ρ (t/m^3)	r_0 (m)	length (m)
2.4×10^5	2.0	0.5	15

Table 2.4 Parameters for surface soil deposit

ρ (t/m^3)	v_T (m/s)	ν	Thickness (m)
1.75	100	0.40	20

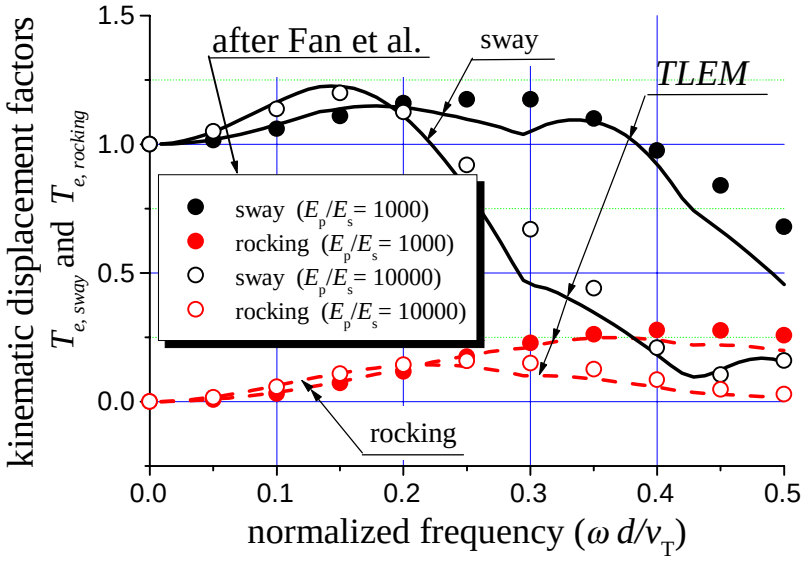

Figure 2.5 Kinematic displacement factors of pile groups

2.3. ACTIVE PILE LENGTH AND PILE CAP STIFFNESS

2.3.1 *Active pile length*

In practice, most laterally loaded piles are 'flexible' in the sense that they do not deform over their entire length *L*. Instead, pile deflections become negligible below an active length L_a (**Figure 2.6**). This length depends on how stiff the pile is in comparison with the surrounding soil. In engineering practice, Chang's formula is widely used; in this a pile is supported by discrete soil springs $K_h d$, and the characteristic parameter is introduced as $\beta = \sqrt[4]{K_h d / 4EI}$ with K_h designating the coefficient of subgrade reaction and *d* the pile diameter. The length given by $1/\beta$ is thus directly relevant to the active pile length L_a. When a soil is treated as an elastic continuum, however, it is to be recognized that K_h is not an inherent constant in the soil, but rather dependent on d. In addition, the active pile length is more rationally evaluated by replacing $K_h d$ with the shear modulus of soil μ. Some formulas for rather extreme soil profiles have been presented by Randolf(1981), Velez (1983) and Gazetas (1983), and in general, L_a is closely related to the following parameter L_0:

$$L_0 = \sqrt[4]{\frac{EI}{\mu}} \tag{2.3}$$

where, EI = bending stiffness of the pile, and μ = shear modulus of soil (representative value). The active length L_a is thus given as:

$$L_a = \alpha_0 L_0 \tag{2.4}$$

with the parameter α_0 reflecting different soil profiles. For an n_p pile group, EI in Equation (2.3) will presumably be replaced with EI ($= n_p E_p I_p$) specified by Equation (A5) in **APPENDIX I**.

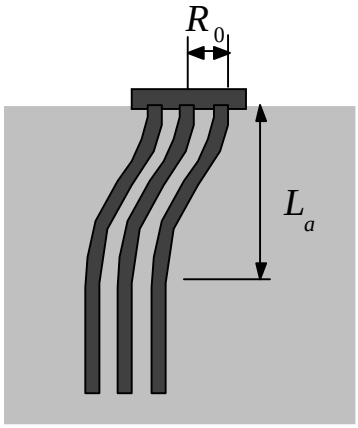

Figure 2.6 Active length of pile

2.3.2 *Pile cap stiffness*

It is assumed that only the soil above the active pile length, L_a, is deformed as shown in **Figure 2.7a**. The upper soil is then divided into vertical soil columns. Given the prescribed vibration mode $\psi(z/L_a)$ that satisfies $\psi(0)=1$ and $\psi(1)=0$, these columns can be replaced with simple-damped oscillators. Reducing the cross-section of each soil column, the soil deposit above L_a is modeled by an infinite plane supported by Winkler-type springs (**Figure 2.7b**). Lame's constants λ_p, μ_p (μ_p = shear modulus) and mass density ρ_p of the soil plane and Winkler-type spring constant k_p for the model are expressed in terms of ψ as:

$$\lambda_p = \int_0^{L_a} \lambda(z)\left(\psi(z/L_a)\right)^2 dz\,,\quad \mu_p = \int_0^{L_a} \mu(z)\left(\psi(z/L_a)\right)^2 dz\,,\quad \rho_p = \int_0^{L_a} \rho(z)\left(\psi(z/L_a)\right)^2 dz$$

and $$k_p = \int_0^{L_a} \mu(z)\left(\frac{d\psi(z/L_a)}{dz}\right)^2 dz \qquad \text{(2.5a)-(2.5d)}$$

A frequency parameter, ω_0, is introduced herein as:

$$\omega_0 = \sqrt{\frac{k_p}{\rho_p}} \qquad (2.6)$$

For a homogeneous soil, parameters λ_p, μ_p and ρ_p in Equations (2.5a)-(2.5c) are rewritten as

$$\lambda_p = \lambda\alpha_1 L_a\,,\qquad \mu_p = \mu\alpha_1 L_a \qquad \text{and} \qquad \rho_p = \rho\alpha_1 L_a \qquad \text{(2.7a)-(2.7c)}$$

with $$\alpha_1 = \int_0^1 \left(\psi_1(\zeta)\right)^2 d\zeta\,.$$

Even for inhomogeneous soils too, similar expressions may be derived with λ, μ, and ρ interpreted as representative values of $\lambda(z)$, $\mu(z)$ and $\rho(z)$, and the parameter α_1 portraying different soil profiles.

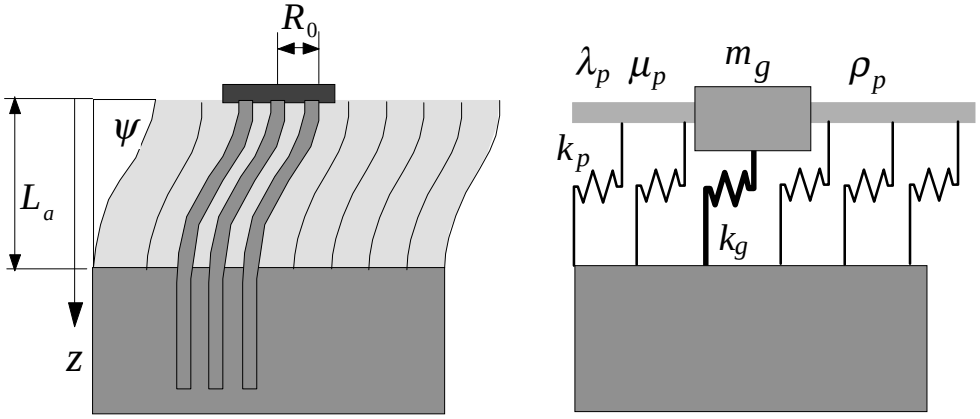

(a) Vertically sliced soil above L_a **(b)** Equivalent model

Figure 2.7 Soil deformation

The expression of soil stiffness, k_s, for the lateral motion of a massless body embedded in the soil plane in **Figure 2.7b** is completely identical to that given in Novak et al. [1978] regardless of the presence of Winkler-type springs k_p, i.e.:

$$k_s = \pi\mu_p a_0^{\,2} \frac{4K_1(b_0)K_1(a_0) + a_0K_1(b_0)K_0(a_0) + b_0K_0(b_0)K_1(a_0)}{b_0K_0(b_0)K_1(a_0) + a_0K_1(b_0)K_0(a_0) + b_0a_0K_0(b_0)K_0(a_0)} \tag{2.8}$$

where K_0 and K_1 are modified Bessel functions of the first and second order, respectively. Both a_0 and b_0 are normalized circular frequencies. As shown in **APPENDIX II**, the only difference from Novak's solution, owing to the presence of Winkler-type springs k_p appears as an inclusion of the frequency parameter ω_0 in a_0 and b_0 as:

$$a_0 = \frac{\omega_0 R_0}{v_T}\eta, \quad b_0 = \frac{\omega_0 R_0}{v_L}\eta \quad \text{with} \quad \eta = \sqrt{1 - \left(\frac{\omega}{\omega_0}\right)^2} \tag{2.9a)-(2.9c)}$$

in which ω is the circular frequency, and

$$v_{T_p} = \sqrt{\mu_p / \rho_p} \quad (= \text{transverse wave velocity in the plane}) \tag{2.9d}$$

$$v_{L_p} = \sqrt{(\lambda_p + 2\mu_p)/\rho_p} \quad (= \text{longitudinal wave velocity in the plane}) \tag{2.9e).}$$

Since a_0 and b_0 are respectively functions of v_{T_p} and v_{L_p}, Equation (2.8) is in turn a function of the Poisson's ratio ν. The expression of Equation (2.8) for a Poisson's ratio equal to 0.5 is obtained by taking a limit as $\nu \to 0.5$ in Equation (2.8), i.e.:

$$k_s = 2S^* + m_s\omega^2 \tag{2.10}$$

where $m_s\,(=\rho_p \pi R_0^{\,2})$ is the soil mass of the same volume as the cylindrical hollow in the soil plane, and

$$S^* = 2\pi\mu \frac{a_0K_1(a_0)}{K_0(a_0)} \tag{2.11}$$

Table 2.5 Values of ξ_k and ξ_m

Poisson's ratio, ν	ξ_k	ξ_m
0.50	2.000	1.0000
0.47	1.831	0.5336
0.45	1.741	0.3740
0.43	1.667	0.2628
0.40	1.580	0.1428
0.35	1.476	0.0352
0.25	1.351	0
0.20	1.311	0
0.10	1.252	0
0.00	1.213	0

It is found that the stiffness k_s for any Poisson's ratio other than 0.5 can be approximately expressed in the same form as Equation (2.10) but with a small modification [Nogami and Konagai, 1986], i.e.:

$$k_s = \xi_k(\nu) \cdot S^* + \xi_m(\nu) \cdot m_s \omega^2 \tag{12}$$

where, $\xi_k(\nu)$ and $\xi_m(\nu)$ are functions dependent only on Poisson's ratio ν. The values $\xi_k(\nu)$ and $\xi_m(\nu)$ are given in **Table 2.5.**

Konagai et al. [1992, 1998b] have shown that assuming plane stress condition over the entire extent of the soil plane allows k_s to approximate closely the rigorous solution of the soil stiffness, and thus, Poisson's ratio ν in Equation (2.12) must be replaced with ν^* for a plane-stress medium, which is expressed as:

$$\nu^* = \frac{\lambda_p{}^*}{2(\lambda_p{}^* + \mu_p)} \tag{2.13}$$

where, $\lambda_p{}^* = \dfrac{2\lambda_p \mu_p}{\lambda_p + \mu_p}$ (2.14)

It is noted that ν^* ranges from 0 to 1/3, and thus, $\xi_m(\nu^*)$ in Equation (2.12) is completely equal to zero. Equation (2.12) is then rewritten as;

$$k_s = \xi_k(\nu^*) \cdot S^* \tag{2.15}$$

The function $K_1(a_0)/K_0(a_0)$ is approximated by $1 + 0.4/a_0$, when the absolute value of a_0 is larger than 0.01 [Konagai and Nogami, 1998a]. This simplification leads to:

$$k_s = 2\pi\mu_p \xi_k(\nu^*) \frac{a_0 K_1(a_0)}{K_0(a_0)} \cong 2\pi\mu_p \xi_k(\nu^*) \cdot a_0(1 + 0.4/a_0) \tag{2.16}$$

Two limiting cases of $\omega \to 0$ and $\omega \to \infty$ are addressed herein. For the static case ($\omega \cong 0$), η of Equation (2.9c) approaches 1. Replacing ω_0 and v_{T_p} in Equation (2.9a) with those specified in Equations (2.6) and (2.9d), respectively, non-dimensional frequency a_0 in the static case is expressed as:

$$a_0 = \sqrt{\frac{k_p}{\mu_p}} R_0 \tag{2.17}$$

Substituting into Equation (2.17) Equations (2.5d) and (2.5b) which specify k_p and μ_p, respectively, Equation (2.17) is rewritten as:

$$a_0 = \frac{\alpha_2}{\alpha_1} \frac{R_0}{L_a} \tag{2.18}$$

where, $\alpha_2 = \int_0^1 \left(\dfrac{d\psi(\zeta)}{d\zeta} \right)^2 d\zeta$ with $\zeta = z/L_a$

Equation (2.16) is thus simply written as:

$$k_s \cong 2\pi\xi_k\alpha_1\mu L_a\left(\frac{\alpha_2}{\alpha_1}\frac{R_0}{L_a}+0.4\right)=\mu L_a\left(2\pi\xi_k\alpha_2\frac{R_0}{L_a}+0.8\pi\xi_k\alpha_1\right) \tag{2.19}$$

For the dynamic case ($\omega\to\infty$), non-dimensional frequency a_0 converges on:

$$a_0 = i\frac{\omega R_0}{v_{T_p}} = ia \tag{2.20}$$

Equation (2.16) is thus approximated by:

$$k_s \cong \mu L_a\left(i\cdot 2\pi\xi_k\alpha_1\cdot a+0.8\pi\xi_k\alpha_1\right) \tag{2.21}$$

From Equations (2.19) and (2.21), soil stiffness will presumably be approximated as:

$$k_s \cong \mu L_a\left\{\left(2\pi\xi_k\alpha_2\frac{R_0}{L_a}+0.8\pi\xi_k\alpha_1\right)+i\cdot 2\pi\xi_k\alpha_1\cdot a\right\} \tag{2.22}$$

Even without the soil above the active pile length, the pile group exhibits its own stiffness, k_g (**Figure 2.7b**), which is described as:

$$k_g \cong \alpha_3\frac{EI_p}{{L_a}^3}=\alpha_3\frac{\mu {L_0}^4}{{L_a}^3}=\frac{\alpha_3}{{\alpha_0}^3}\mu L_0 \tag{2.23}$$

where, $\alpha_3=\int_0^1\left(\frac{d^2\psi(\zeta)}{d\zeta^2}\right)^2 d\zeta$

Both k_s and k_g sustain the mass m_g of the embedded pile group with soil caught among the piles. This mass m_g is approximated by:

$$m_g \cong \int_0^{L_a}\rho_s\pi{R_0}^2\psi(z)^2\,dz=\rho_s\pi{R_0}^2L_a\alpha_1 \tag{2.24}$$

Therefore the overall stiffness k_{xx} of the pile cap for sway motion is given as:

$$k_{xx}=k_s+k_g-m_g\omega^2 \tag{2.25}$$

From Equations (2.22), (2.23) and (2.24), Equation (2.25) is rewritten as:

$$k_{xx}\cong\mu L_a\left[\left\{2\pi\xi_k\alpha_2\frac{R_0}{L_a}+\left(0.8\pi\xi_k\alpha_1+\frac{\alpha_3}{{\alpha_0}^3}\right)\right\}+i\cdot 2\pi\xi_k\alpha_1\cdot a-\pi\alpha_1\cdot a^2\right] \tag{2.26}$$

Substituting Equation (2.3) into Equation (2.26), one obtains:

$$k_{xx}\cong\mu L_0\left[\left\{2\pi\xi_k\alpha_2\frac{R_0}{L_0}+\left(0.8\pi\xi_k\alpha_0\alpha_1+\frac{\alpha_3}{{\alpha_0}^2}\right)\right\}+i\cdot 2\pi\xi_k\alpha_0\alpha_1\cdot a-\pi\alpha_0\alpha_1\cdot a^2\right] \tag{2.27}$$

It is now obvious that k_{xx} in Equation (2.27) has the following simple form with frequency-independent stiffness k_0, and damping and mass parameters c_0 and m_0 respectively:

$$k_{xx}\cong k_0+i\cdot c_0\cdot a-m_0\cdot a^2 \tag{2.28}$$

where,

$$\frac{k_0}{\mu L_0} = c_1 \frac{R_0}{L_0} + c_2, \quad \frac{c_0}{\mu L_0} = c_3 \text{ and } \frac{m_0}{\mu L_0} = c_4 \qquad \text{(2.29a)-(2.29c)}$$

with $c_1 = 2\pi\xi_k\alpha_2$, $c_2 = 0.8\pi\xi_k\alpha_0\alpha_1 + \frac{\alpha_3}{\alpha_0^{\,2}}$, $c_3 = 2\pi\xi_k\alpha_0\alpha_1$ and $c_4 = \pi\alpha_0\alpha_1$. (2.30a)-(2.30d)

The above equations show some important features of the pile cap stiffness. Among the parameters specified in the above equations, c_1, c_2, c_3 and c_4 are dependent on the shape function $\psi(\zeta)$, which may not differ drastically in different soil-pile systems as long as piles exhibit a flexible nature, and $k_0 / \mu L_0$ alone includes a term proportional to R_0 / L_0. Equation (2.28) was derived with the intention of showing what could be the most important key parameters that determine k_{xx}. The assumption taken to derive the equation is good enough for this purpose, but certainly is an oversimplification of reality. Since soils below active pile lengths are not allowed to deform at all, the assumption is liable to lead to overestimation of the stiffness parameter k_0 and underestimation of the damping parameter c_0. Therefore, parameters c_1, c_2, c_3 and c_4 were obtained not directly from Equations (2.30a)-(2.30d), but in such a way that the overall error would be minimized for the variety of soils and pile parameters examined. The parameters that have been considered are: 1) pile parameters such as group-pile stiffness, EI ($= n_p E_p I_p$), and active pile length ratio, L_0 / L; and 2) soil parameters including shear modulus μ and material damping D. In this discussion, only a homogeneous soil profile with a square arrangement of piles is considered. The best fit of the values from Equation (2.28) to rigorous solutions of k_{xx} was obtained by setting c_1, c_2, c_3 and c_4 at 2π, $\pi/2$, 2π and $\pi/4$, respectively. Some representative cases are shown in **Figures 2.8a-2.8f**.

The present simple expression of k_{xx} (Equation (2.28)) allows the effects of overall site non-linearity to be reflected by simply replacing the shear modulus of the intact soil, μ, with the complex modulus, $\mu'(1+iD)$; this describes equivalent-linear features of the soil experiencing dynamic loading, and is obtained from shear-modulus-reduction and damping ratio curves of the soil. This manipulation, however, causes the stiffness and damping parameters k_0 and c_0 in Equations (2.29a) and (2.29b) to be slightly dependent on frequency as:

$$\frac{k_0}{\mu' L_0} = \left(2\pi \frac{R_0}{L_0} + \frac{\pi}{2}\right) - 2\pi D \cdot a \qquad \text{(2.31a)}$$

$$\frac{c_0}{\mu' L_0} = 2\pi + \left(2\pi \frac{R_0}{L_0} + \frac{\pi}{2} - \frac{\pi}{4}a^2\right) D \qquad \text{(2.31b)}$$

When the effect of D cannot be ignored in Equations (2.31a) and (2.31b), appropriate

values of k_0 and c_0 must be determined taking into account the most probable predominant frequency a in the soil-structure interaction reality. **Figures 2.8a-2.8b** show that introducing the complex shear modulus of soil, the effect of material damping has properly been taken into account.

The downward dips in these non-dimensional plots of rigorous variations of k_{xx} vs. frequency occur at essentially the resonance frequencies of the soil stratum for vertical shear wave propagation. Thus the results from '*TLEM*' analyses with a perfectly rigid base laid under the soil stratum correspond to cases where this effect is most pronounced. It is therefore more likely that the solutions adhere along the ridges of these plots as the bases become more flexible. As can be seen from **Figure 2.8c**, Equation (2.28) underestimates slightly the real part of stiffness, and overestimates its imaginary part for lower values of shear modulus of soil.

From the study of a wide range of pile parameters (viz. number of piles, diameter of individual piles and length of piles), it was found that Equation (2.28) is valid irrespective of pile and soil parameters as long as the active-pile-length ratio, L_0 / L, is within a certain limit. Beyond this limit, the behavior of piles deviates from the 'flexible' nature. **Figures 2.8d-2.8f** show this trend of the deviation of Equation (2.28) from the results of "*TLEM*" (Ver. 1.2) as the ratio L_0 / L increases. In these figures, L_0 / L are changed by arbitrarily changing the number of piles and/or diameter of individual piles. These figures show that the allowable limit of L_0 / L is 0.3 or less.

A similar expression must also be derived for the dynamic stiffness of grouped piles in rocking motion and for the coupled stiffness between lateral sway and rocking motions. In this extension also, active pile length, if rationally estimated, would allow the pile-cap stiffness to be approximately described in a similar manner. Further detailed study on this point will be addressed in a later publication.

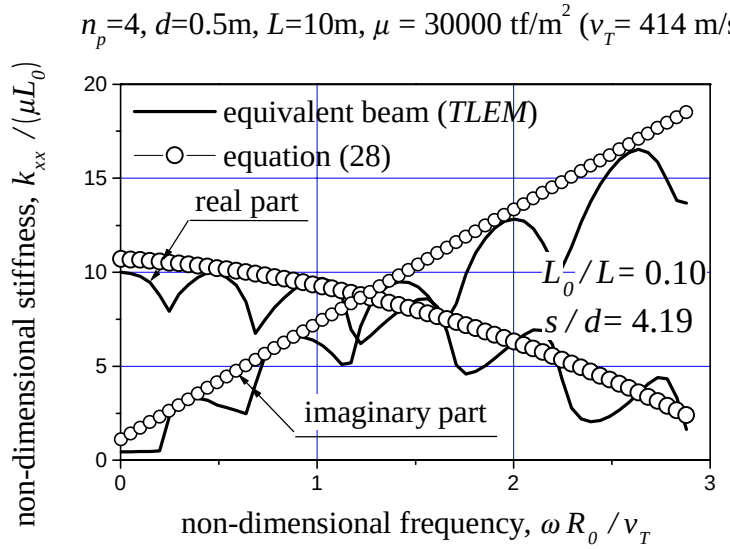

Figure 2.8a Variation of stifness for sway motion of pile cap (D = 0.05)

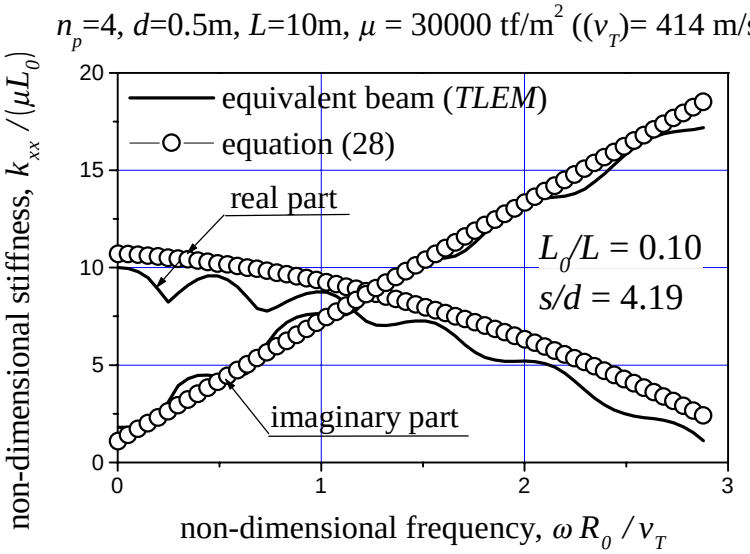

Figure 2.8b Variation of stiffness for sway motion of pile cap (D = 0.20)

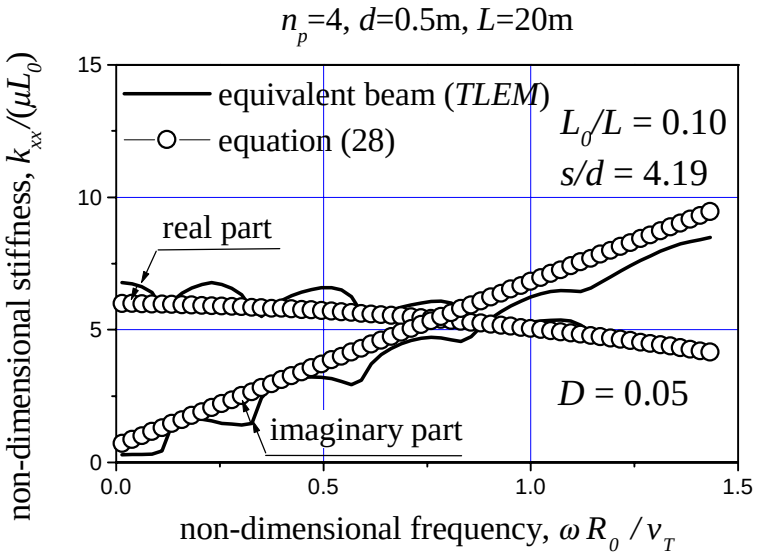

Figure 2.8c Variation of stiffness for sway motion of pile cap (μ = 1875 tf/m^2 , v_T = 103.5 m/s)

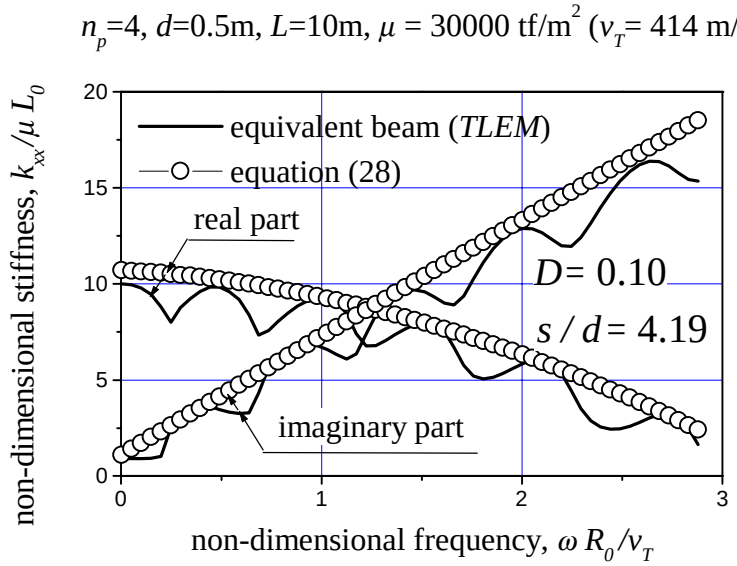

Figure 2.8d Variation of stiffness for sway motion of pile cap (L_0/L = 0.10)

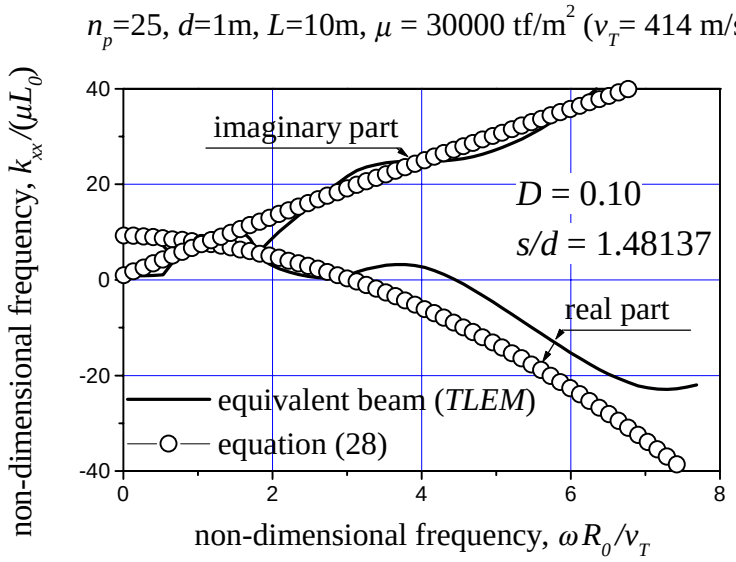

Figure 2.8e Variation of stiffness for sway motion of pile cap (L_0/L = 0.31)

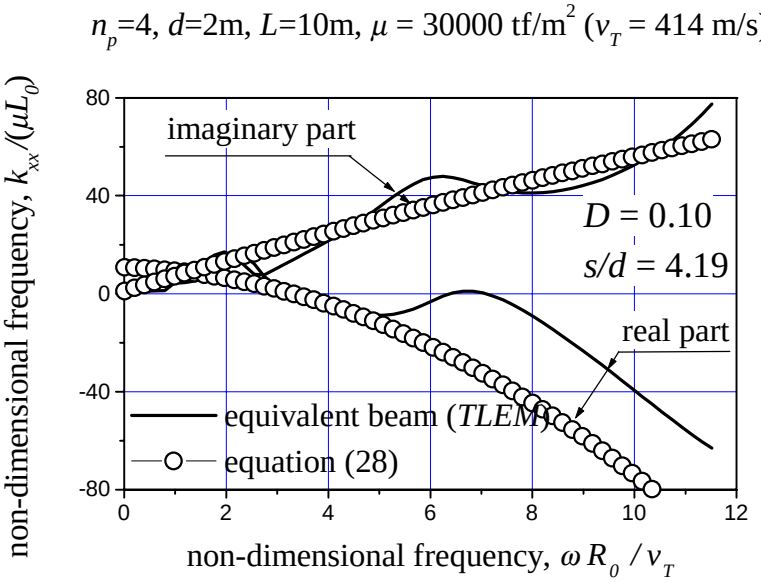

Figure 2.8f Variation of stiffness for sway motion of pile cap (L_0/L = 0.40)

2.4. SUMMARY

Piles grouped beneath a superstructure can be viewed as a single equivalent upright beam when the piles are closely spaced. The stiffness matrix presented herein (Equation (2.1)) yields close approximations of both dynamic pile-cap stiffness and kinematic displacement factors. This idealization of grouped piles as a single equivalent upright beam and the concept of the active pile length have facilitated the derivation of a simple expression of pile-cap stiffness in terms of frequency-independent mass, damping and stiffness parameters (Equations (2.29a)-(2.29c)). This expression is valid irrespective of pile and soil parameters as long as the pile group exhibits a "flexible" nature with its active-pile-length ratio, L_0 / L, kept less than 0.3. The present simple expression of pile-cap stiffness also allows the effects of overall site non-linearity to be reflected by simply replacing the shear modulus of the intact soil, μ, with the complex modulus, $\mu'(1+iD)$, which describes equivalent-linear features of the soil experiencing the seismic motion.

A similar expression must also be derived for the dynamic stiffness of grouped piles in rocking motion and for the coupled stiffness between lateral sway and rocking motions. Moreover, there is further scope to extend this study for inhomogeneous soil-profile and the local non-linearity of soil that develops in the vicinity of piles. In these extensions also, active pile length, if rationally estimated, would allow pile-cap stiffness to be approximately described in a similar manner. This will be discussed in future publications.

REFERENCES

Fan, K., Gazetas, G., Kanya, A., Kausel, E. and Ahmad, S. [1991] "Kinematic Seismic Response of Single Piles and Pile Groups," *Jour., Geotechnical Engineering*, ASCE, **117(12)**, 1860-1879.

Gazetas, G. and Dobry, R. [1984] "Horizontal Response of Piles in Layered Soils," *Journal of Geotechnical Engineering*, ASCE, **110(1)**, 20-40.

Kanya, A. and E. Kausel [1982] "Dynamic Stiffness and Seismic Response of Pile Groups," NSF report, **NSF/CEE-82023**.

Konagai, K. and Maehara, M. [1992] "Study on Hypotheses for Simple Numerical Evaluation of Soil-Embedded Structure Interaction," *Bull., Earthquake Resistant Structure Research Center*, **25**, 39-60.

Konagai, K. and T. Nogami [1998a] "Analog circuit to simulate dynamic soil-structure interaction in shake table test," *International Journal of Soil Dynamics and Earthquake Engineering*, **17(5)**, 279-287.

Konagai, K., A. Mikami and T. Nogami [1998b] "Simulation of Soil-Structure Interaction Effects in Shaking Table Tests," Geotechnical Earthquake Engineering and Soil Dynamics

1998, Seattle, *Geotechnical Special Technical Publication*, ASCE, **75(1)**, 482-493.

Konagai, K., Nogami, T., Katsukawa, T., Suzuki, T. and Mikami, A. [1998c] "Real Time Control of Shaking Table for Soil-Structure Interaction Simulation," *Jour. of Structural Mechanics and Earthquake Engineering*, JSCE, **598/I-44**, 203-210.

Konagai, K. [1998d] "Guide to *TLEM*," program manual **No. 5**, Konagai Lab., IIS, Univ. of Tokyo.

Nogami, T. and Konagai, K. [1988] "Time Domain Flexual Response of Dynamically Loaded Single Piles," *Journal of Engineering Mechanics*, ASCE, **114(9)**, 1512-1525.

Novak, M., Nogami, T. and Aboul-Ella, F. [1978] "Dynamic Soil Reactions for Plane Strain Case," *Proc., ASCE,* 104(EM4), 953-959.

Ohira, A., Tazo, T, Nakahi, S. and Shimizu, K. [1985] "Study of Dynamic Behavior of Piles in Soft Soils," *Journal of Structural Engineering / Earthquake Engineering*, 362/I-4, 417-426.

Randolph, M. F. [1981] "Response of Flexible Piles to Lateral Loading," *Geotecnique*, **31(2)**, 247-259.

Tajimi, H. and Y. Shimomura [1976] "Dynamic Analysis of Soil-Structure Interaction by the Thin Layered Element Method," *Transactions of the Architechtual Institute of Japan*, **243**, 41-51.

Takemiya, H. [1986] "Ring-Pile Analysis for a Grouped Pile Foundation Subjected to Base Motion," Structural Engineering/Earthquake Engineering, **3(1)**, 195s-202s.

Velez, A., Gazetas, G., and Krishnan, R. [1983] "Lateral Dynamic Response of Constrained Head Piles," *Journal of Geotechnical Engineering*, ASCE, **109(8)**.

Poulos, H. G. [1968] "Analysis of the Settlement of Pile Groups," *Geotechnique*, **18**, 449-471

Poulos, H. G. [1971] "Behavior of Laterally Loaded Piles," *Jour., Soil Mechanics and Foundation Division*, ASCE, **97(SM5)**, 733-751.

Chapter 3

SIMPLE EXPRESSION OF THE DYNAMIC FLEXIBILITY OF RIGID EMBEDDEDFOUNDATIONS

3.1 INTRODUCTION

Flexible piles have been the focus of the previous discussion in ***Chapter* 2**. The idealization of grouped piles as a single equivalent upright beam and the concept of the active pile length have facilitated the derivation of a simple expression of the pile-cap stiffness in terms of frequency-independent mass, damping and stiffness parameters. This simple approximation, however, is not appropriate for a rigid embedded body subjected to dynamic loading. Moreover, the rigidity of the foundation prevents it from following closely horizontal component of the free-field deformation pattern $\{\mathbf{u}^f\}$.

It is shown in this chapter that salient features of soil - stiff embedded foundation interaction are often insensitive to the detailed variations of soil profiles, and this fact enables us to apply the present method for soil-structure interaction simulation to real complex conditions. Nonlinear effects of soil will presumably be taken into account by changing the frequency-independent mass, spring and damping parameters with change in the soil shear modulus. Therefore, it is worthwhile to examine if rather secondary factors can be eliminated so that the simulations have a good balance between mathematical rigor and uncertainty in the complex environment.

3.2 KINEMATIC INTERACTION

A foundation of radius R_0 is assumed to be embedded in a soil deposit underlain by a semi-infinite bed-rock as shown in **Figure 3.1**. The inability of the rigid embedded foundation to conform to the deformation of soil thus causes the motion of the soil-structure interface to deviate by $\{\mathbf{u}^s\}$ from the free-field motion $\{\mathbf{u}^f\}$ (kinematic interaction). The foundation input motion must thus be modified to incorporate the effect of the kinematic interaction. The foundation-input motion $\{\mathbf{u}^f\}+\{\mathbf{u}^s\}$ for the system illustrated in **Figure 3.1** is estimated rigorously by using the thin layered element method (Tajimi and Shimomura, 1976). **Figure 3.2** shows the variation of $\left(u^f{}_x + u^s{}_x\right)/u^f{}_x$, i.e., the foundation-input motion at the ground surface, which is normalized by the free-field motion $u^f{}_x$. The ratio is nearly a real function of frequency, and decreases gradually as the frequency increases beyond the first fundamental natural circular frequency ω_0 of the soil deposit. This implies that the contribution of the fundamental vibration mode ψ_1 of the soil deposit to the foundation-input motion is predominant, because the rigidity of the embedded foundation keeps it from following the motion of higher modes. Therefore, it might be acceptable to approximate the foundation input motion excluding the higher modes of vibration. To examine this point, the free-field motion is calculated by taking into account only the first mode of vibration ψ_1, and compared with the rigorous solution. **Figure 3.3** shows the variation of the approximate solution of $\left(u^f{}_{x,1st\ mode}\right)/u^f{}_x$. The similarity is immediately apparent when **Figure 3.3** is compared with **Figure 3.2**, and thus, provides a firm basis for this approximation.

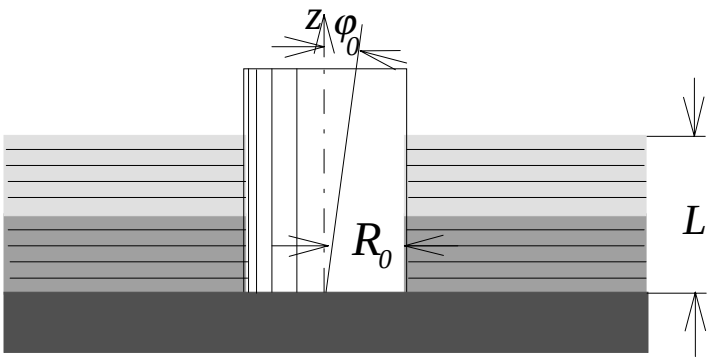

Figure . 3.1 Foundation embedded in thin-layered soil deposit

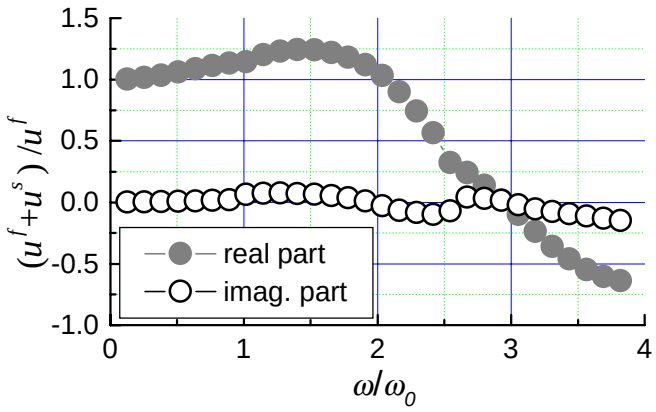

Figure 4.2 Foundation input motion

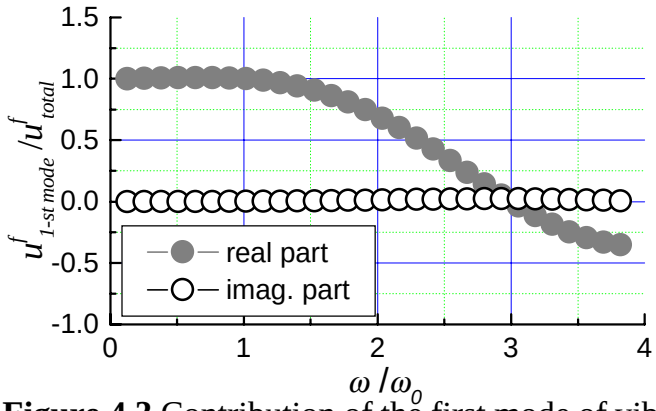

Figure 4.3 Contribution of the first mode of vibration to free-field motion

3.3 SIDE SOIL STIFFNESS FOR ROCKING MOTION

When the embedded foundation experiences an intense earthquake motion, the surface soil deposit exhibits more pronounced nonlinear features than the bed-rock. As a result, soil shear moduli at different depths in the surface layer vary with time. On the contrary, densities and Poisson's ratios of soils are very little or negligibly influenced by the soil nonlinearity. Thus the rocking stiffness of an embedded foundation reflects the overall change in soil shear moduli throughout the depth.

The following linear variation of shear wave velocity with respect to the depth z is assumed with specific values of shear wave velocities at the top and bottom of the surface soil deposit:

$$v_T(z) = \left(v_T(L) - v_T(0)\right) \cdot \frac{z}{L} + v_T(0) \tag{3.1}$$

where, L is the thickness of the surface soil deposit. The shear wave velocities are modified to fluctuate randomly around the values given by Equation (3.1) so that the

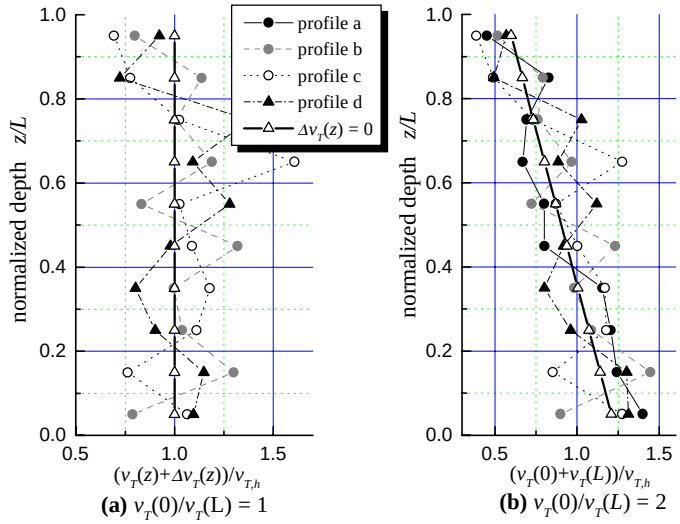

Figure 3.4 Soil profiles (The soil deposit is divided into 10 sub-layers)

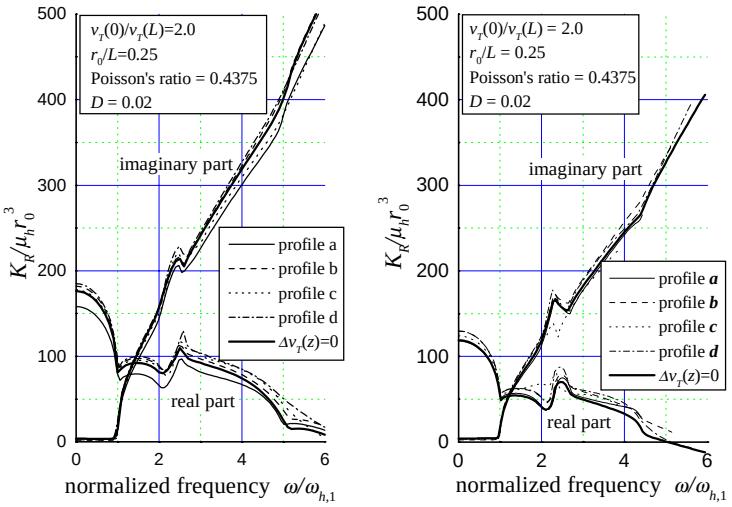

(a) $v_T(0)/v_T(H) = 1$ **(b)** $v_T(0)/v_T(H) = 2$

Figure 3.5 Impedance functions for rocking motion of an embedded body

ratio of the deviation $\Delta v_T(z)$ to $v_T(z)$ eventually exhibits the Gaussian distribution with the standard deviation of 20%. Finally, the obtained shear wave velocities at various depths are multiplied by a uniform factor throughout the depth, to keep the fundamental resonance frequency equal to that for the original simple soil profile described by Equation (3.1). Following this procedure, four different soil profiles are prepared for each of two different cases of $v_T(0)/v_T(L)=1$ and $v_T(0)/v_T(L)=2$ as shown in **Figures 7a** and **7b**. Impedance functions for the rocking mode of the embedded foundation were computed for these soil profiles by using Thin-Layered Element Method.

Figures 3.5a and **3.5b** show the computed rocking stiffnesses. It is noted that the change in the soil profile to the extent shown in **Figures 3.4a** and **3.4b** causes no serious change in the stiffness of the foundation. These examples suggest that the rocking stiffness of a stiff embedded foundation is strongly governed by the fundamental natural frequency of the surrounding soil deposit, and rather secondary detailed features can be eliminated. It is therefore worth examining the contribution of the first fundamental vibration mode of the soil deposit to the impedance function of the foundation.

The present simulation approach utilizes simple expressions for soil responses at the side of the embedded foundation, which are obtained neglecting the vertical soil response for the horizontal and rocking responses of the foundation. This assumption was first used by Tajimi (1969). Modified Tajimi's solution shows that the restoring moment M_r for the harmonic rotation $\varphi_0 e^{i\omega t}$ is expressed in the form of:

$$M_r = k_{R,side}\varphi_0 e^{i\omega t} \tag{3.2}$$

where,

$$k_{R,side} = \frac{8\mu {r_0}^3}{\pi}\frac{L}{r_0}\sum_{m=1,3,5..}^{\infty}\frac{{\zeta_m}^2\Omega_m}{m^4}$$

$$\Omega_m = \frac{4K_1(b_m)\cdot K_1(a_m)+a_m K_1(b_m)K_0(a_m)+b_m K_1(a_m)K_0(b_m)}{a_m K_0(a_m)K_1(b_m)+b_m K_0(b_m)K_1(a_m)+a_m b_m K_0(a_m)K_0(b_m)}$$

$$a_m=\zeta_m\frac{\omega_1 r_0}{v_T}, b_m=\zeta_m\frac{\omega_1 r_0}{v_L^*}, \omega_1=2\pi f_1=\frac{\pi v_T}{2L}$$

$$\zeta_m=\sqrt{m^2(1+iD)-\left(\frac{\omega}{\omega_1}\right)^2} \tag{3.3a)-(3.3f}$$

where K_m is modified Bessel function of order *m*. Though the original Tajimi's solution is based on the assumption of vanishing vertical displacement, the modified longitudinal wave velocity v_L * is used here to consider the stress free condition on the ground surface (Konagai and Maehara, 1992). The contribution of the first mode is isolated from the other modes in this expression. The impedances computed in this

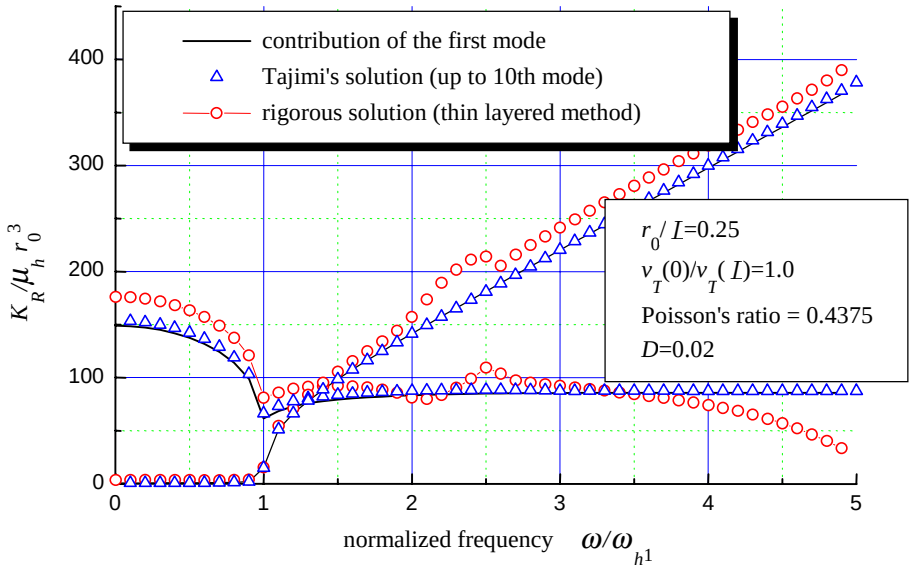

Figure 3.6 Contribution of the first vibration mode of surrounding soil to impedance function

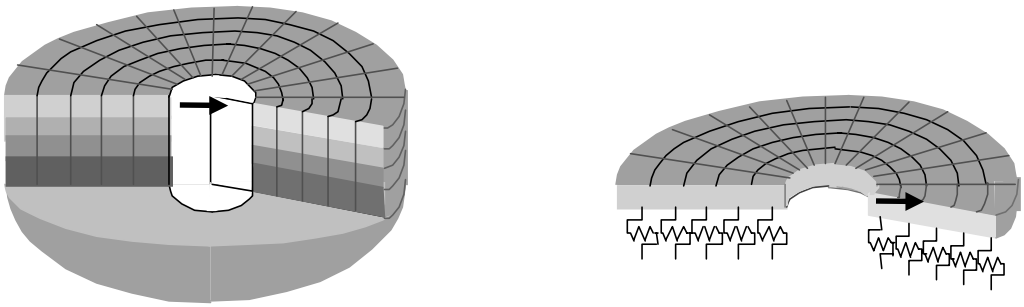

(a) soil deposit surrounding an embedded body (b) soil plane overlying Winkler springs

Figure 3.7 Vertically sliced soil deposit

manner is compared in **Figure 3.6** to those computed with up to 10 modes. They are also computed by the thin-layered element method which does not ignore the vertical soil response and is considered to be rigorous compared with Tajimi's method. It is clear in this figure that the exclusion of higher vibration modes in Tajimi's method affects little the dynamic stiffness, and the good agreement between the rigorous and approximate solutions proves the predominant contribution of the fundamental vibration mode.

All the examples mentioned above shows that salient features of the impedance function of a stiff embedded foundation are insensitive to the detailed variations of soil

profiles and, thus, this allows us to describe the impedance function by only a limited number of parameters.

The superior contribution of the fundamental vibration mode ψ_1 to soil-embedded rigid body interaction greatly simplifies the soil-embedded body interaction analysis. When the surface soil deposit is divided into vertical soil columns as shown in **Figure 3.7a**, these columns, given a prescribed vibration mode of ψ_1, can be replaced with simple-damped oscillators. Reducing the size of each soil column, the surface layer is modeled by a plane of infinite extent supported by Winkler-type springs (**Figure 3.7b**). The similarity is immediately apparent when **Figure 3.7** is compared with **Figure 2.7** in ***Chapter* 2**, and it is now obvious that the rocking stiffness, K_R, of the embedded foundation has the same form as k_s in Equation (2.15) (***Chapter* 2**), with L^2 added to its right-hand side as:

$$K_R = L^2 \cdot \xi_k(\nu^*) \cdot S^* \tag{3.4}$$

Further extended discussion on the stiffness could be made in the similar manner as that in ***Chapter* 2**. In ***Chapter* 2**, downward dips in the plots of rigorous variations of k_{xx} vs. frequency were ignored in discussing simplified expression of k_{xx} in terms of the frequency-independent mass, spring and damping parameters. **Figures 3.5** and **3.6**, however, show that these dips are rather clearer and more significant than those appeared in k_{xx} of pile groups. Substituting Equations (3.7a) and (3.7c) in Equation (3.4) yields both the real and the imaginary parts of K_R as

$$\frac{\mathrm{Re}(K_R)}{2\pi\mu_p\xi_k(\nu^*)} = \begin{cases} a_0 + 0.4 & \cdots \omega < \omega_0 \\ 0.4 & \cdots \omega > \omega_0 \end{cases} \tag{3.5a}$$

$$\frac{\mathrm{Im}(K_R)}{2\pi\mu_p\xi_k(\nu^*)} = \begin{cases} 0 & \cdots \omega < \omega_0 \\ a_0 & \cdots \omega > \omega_0 \end{cases} \tag{3.5b}$$

Noting that $a_0 = \omega_0 R_0 / v_T = (\pi/2)\cdot(R_0/L)$ at $\omega = 0$, the real part of K_R drops from $0.4 + (\pi/2)\cdot(R_0/L)$ down to 0.4 as ω approaches ω_0. The drop thus depends on the aspect ratio R_0/L of the foundation. For thick and short foundation, this drop is remarkable and cannot be ignored.

The stiffness S^* in Equation (3.4) or its inverse, namely, a flexibility function $H^*(=1/S^*)$ is the most frequently encountered expression in soil-structure interaction analyses. The flexibility function H^* is found to be closely approximated by the following form as:

$$H^*(\omega) = A_e \frac{1}{i\omega + \alpha_e} + A_c \frac{\omega_0}{(i\omega + \alpha_c)^2 + \omega_0^2} \tag{3.6}$$

where, $A_e = A_c \cdot \left(\frac{2L}{R_0} - 1\right)$, $A_c = 0.44 - 004 \cdot \log_2 \frac{L}{R_0}$

$$\alpha_e = \left(1.2 + 0.4 \cdot \log_2 \frac{L}{R_0}\right) \cdot \omega_0, \quad \alpha_c = \left(0.21 - 0.01 \cdot \log_2 \frac{L}{R_0}\right) \cdot \omega_0 \quad \text{and} \quad \omega_0 = \frac{\pi v_s}{2L} \tag{3.7a)-(3.7e)}$$

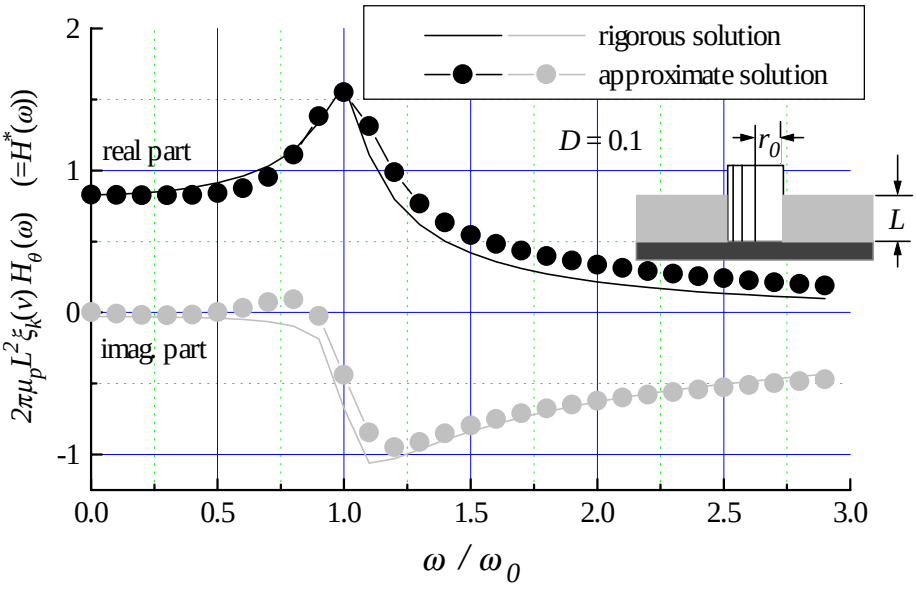

(b) Height-radius ratio ($=L/r_0$) = 2.0

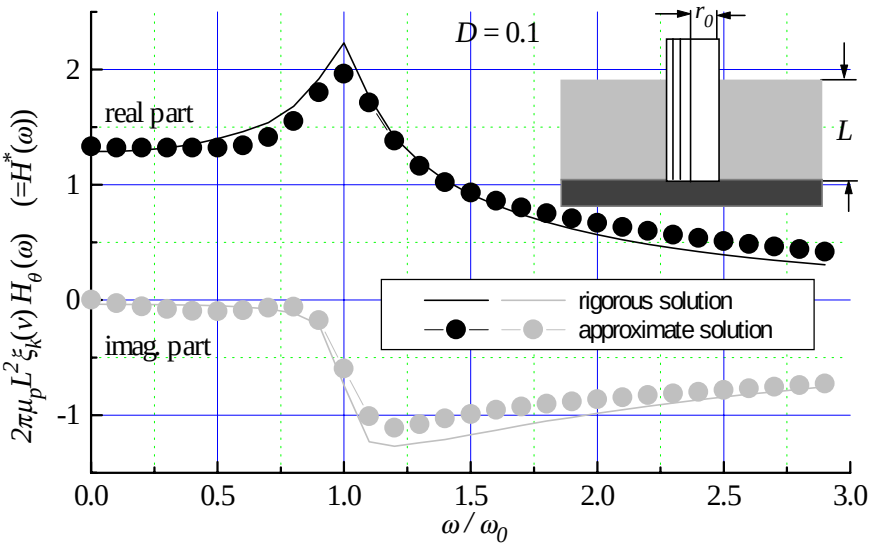

(c) Height-radius ratio (L/r_0) = 4.0

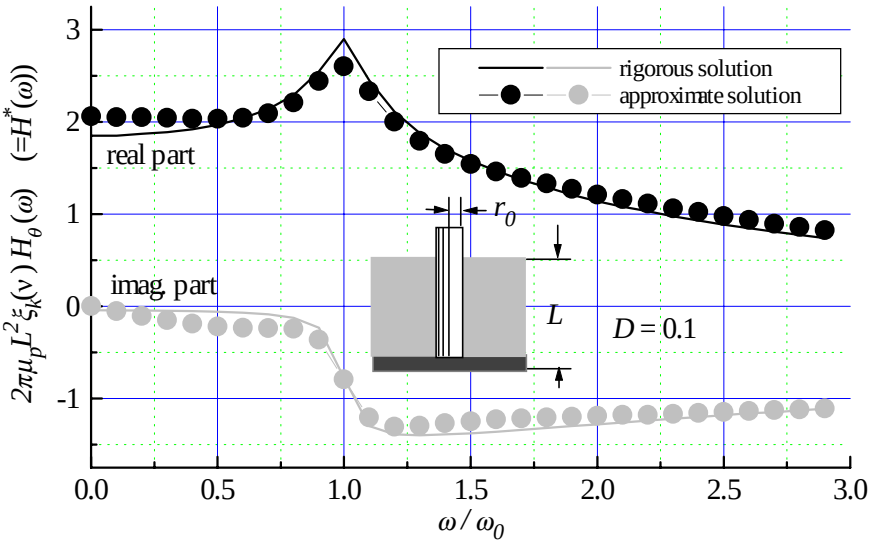

(d) height-radius ratio $(=L/r_0) = 8.0$

Figure 3.8 Flexibility functions $H^*(\omega)$ for different height-radius ratios

Figures 3.8a-3.8d show flexibility functions for the rocking motion of an embedded rigid cylinder for different height-radius ratios (L/R_0) 1, 2, 4 and 8, respectively. Within this range of radius-height ratio, the expression agrees well with the rigorous solution. Inverse Fourier transformation of H^* yields the impulse response function $h^*(t)$ as:

$$h^*(t) = A_e h_e(t) + A_c h_c(t) \tag{3.8}$$

where, $$h_e = e^{-\alpha_e t}, \quad h_c = e^{-\alpha_c t}\cos\omega_0 t \tag{3.9a), (3.9b)}$$

Equation (3.8) implies that the impulse response function $h^*(t)$ is approximated by adding up exponential and exponentially decaying cosine functions.

3.4 SIMPLE EXPRESSION OF STIFFNESS

Needless to say, use of the simple models that have been discussed so far leads to some loss of precision, to be sure, however, reviewing these expressions, it is found that the impulse responses of these models are closely approximated by summing up exponential and/or exponentially decaying sine and cosine functions of time t, $h_{e,m}(t)$, $h_{c,m}(t)$ and $h_{s,m}(t)$, namely,

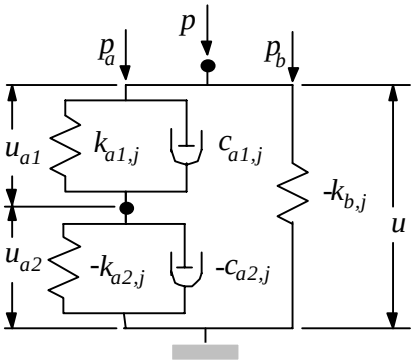

Figure 3.9 Mechanical model for basic response functions

$$h(t) = \sum_{m=1}^{n} (A_{e,m} h_{e,m}(t) + A_{c,m} h_{c,m}(t) + A_{s,m} h_{s,m}(t)) \tag{3.10}$$

where, $A_{e,m}$, $A_{c,m}$ and $A_{s,m}$ are unknown constants and

$$h_{e,m}, h_{c,m}(t), h_{s,m}(t) = \begin{cases} e^{-\alpha^{e,m}t}, e^{-\alpha_{c,m}t}\cos\omega_{c,m}t, e^{-\alpha_{s,m}t}\sin\omega_{s,m}t & t \geq 0 \\ 0 & t < 0 \end{cases} \tag{3.11}$$

Fourier transforms of $h_{e,m}(t)$, $h_{c,m}(t)$ and $h_{s,m}(t)$ in Equation (3.4) are:

$$\mathsf{F}(h_{e,m}(t)) = H_{e,m}(s) = \frac{1}{s+\alpha_{e,m}} = \frac{s+\alpha_{e,m}}{s^2 + 2\alpha_{e,m}s + \alpha_{e,m}{}^2} \tag{3.12a}$$

$$\mathsf{F}(h_{c,m}(t)) = H_{c,m}(s) = \frac{s+\alpha_{c,m}}{s^2 + 2\alpha_{c,m}s + \alpha_{e,m}{}^2 + \omega_{c,m}{}^2} \tag{3.12b}$$

$$\text{and} \quad \mathsf{F}(h_{s,m}(t)) = H_{s,m}(s) = \frac{\omega_{s,m}}{s^2 + 2\alpha_{s,m}s + \alpha_{e,m}{}^2 + \omega_{s,m}{}^2} \tag{3.12c}$$

where, $s = i\omega$ and F denotes Fourier transformation.

It is noted here that the flexibility function of an assembly of three springs, k_{a1}, k_{a2}, k_b, and two dashpots, c_{a1}, c_{a2}, shown in **Figure. 3.9**[4] is expressed in the following form as:

$$H(s) = \frac{(c_{a2}+c_{a1})s + (k_{a2}+k_{a1})}{c_{a1}c_{a2}s^2 + \{k_{a1}c_{a2} + k_{a2}c_{a1} + k_b(c_{a2}+c_{a1})\}s + k_{a1}k_{a2} + k_b(k_{a2}+k_{aj})} \tag{3.13}$$

which has the same form as any of Equations (3.12a), (3.12b) and (3.12c). Setting $c_{a1}c_{a2}$ in Equation (3.13) at a minus constant value -1, for example, and equating all the terms in Equation (3.13) with those of Equation (3.12a), five model parameters, k_{a1}, k_{a2}, k_b, c_{a1} and c_{a2} are given as real values as:

$$k_{a1} = 0.618\alpha_{e,m} \tag{3.14a}$$

$$k_{a2} = -1.618\alpha_{e,m} \tag{3.14b}$$

$$k_b = 0 \tag{3.14c}$$

$$c_{a1} = 0.618 \tag{3.14d}$$

$$c_{a2} = -1.618 \tag{3.14e}$$

It is noted here that the mechanical model with the above five parameters (Equations (3.14a)-(3.14e)) is identical to a simple Kelvin-Voigt model with a single spring, $-\alpha_{e,m}$, and a single dashpot, -1, arranged in parallel. Similarly, the parameters for Equation (3.12b) are obtained as:

$$k_{a1} = (0.618\alpha_{c,m} + \omega_{c,m}) \tag{3.15a}$$

$$k_{a2} = -(1.618\alpha_{c,m} + \omega_{c,m}) \tag{3.15b}$$

$$k_b = -2.236\omega_{c,m} \tag{3.15c}$$

$$c_{a1} = 0.618 \tag{3.15d}$$

$$c_{a2} = -1.618 \tag{3.15e}$$

and those for Equation (3.12c) are:

$$k_{a1} = \alpha_{s,m} - \frac{\omega_{s,m}}{2} \tag{3.16a}$$

$$k_{a2} = -\alpha_{s,m} - \frac{\omega_{s,m}}{2} \tag{3.16b}$$

$$k_b = 1.25\omega_{s,m} \tag{3.16c}$$

$$c_{a1} = 1 \tag{3.16d}$$

$$c_{a2} = -1 \tag{3.16e}$$

Needless to say, springs and dashpots should be positive in actuality. If these parameters were free from this restriction however, it would surely be possible for Equation (3.13) to be completely identical to any of Equations (3.12a), (3.12b) and (3.12c), and this assumption is possible in both analog circuits and digital signal processors.

The side soil stiffness, K_R (Equation (3.4)), for the rocking motion of an embedded rigid body is thus approximated by a simple mechanical model illustrated in **Figure 3.10**.

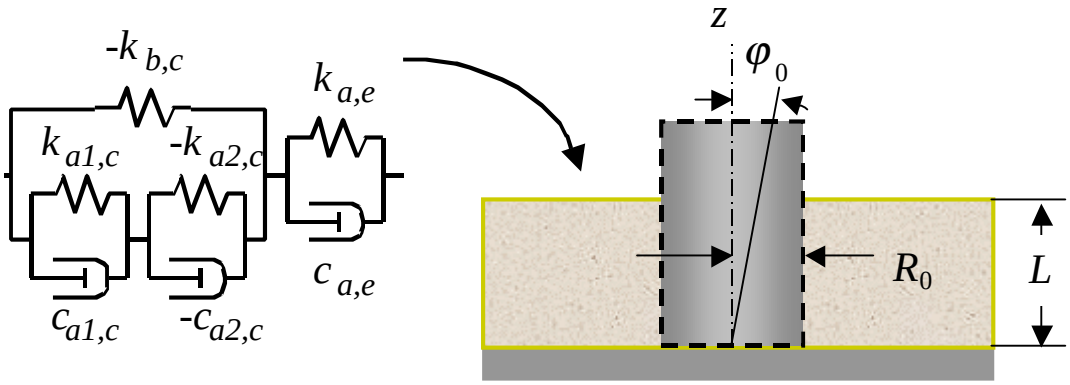

Figureure 3.10 Simple expression of side soil stiffness

3.5 BASE SOIL STIFFNESS

Differing from flexible pile foundations, the contribution of a base reaction to the stiffness of an embedded rigid body is not always small enough to be ignored. Unit impulse functions of soil/rock at the base of rigid embedded foundation are assumed to be those for a half space medium. According to the approach presented by Meek and Wolf (1992a-1993b), the soil is idealized as a truncated semi-infinite elastic cone with its own apex height (**Figure 3.11**) in order to develop unit-impulse functions for a surface foundation. The apex ratio z_0 / r_0, or the opening angle of the cone, is determined for each degree of freedom such that the static stiffness coefficient of the disk on the cone is equal to that on the semi-infinite soil half-space, although the wave propagating through the cone dominates the behavior in the high frequency range. For a translational cone, the unit-impulse response function $h_x(t)$ is thus obtained as:

$$h_x(t) = \begin{cases} \dfrac{1}{K_{x,static}} \dfrac{v_T}{z_0} e^{-\frac{v_T}{z_0}t} & t > 0 \\ 0 & t < 0 \end{cases} \tag{3.17}$$

with $K_{x,static} = \rho {v_T}^2 \cdot \pi {r_0}^2 / z_0$, where v_T is the shear wave velocity. The unit-impulse response function $h_\theta(t)$ for a rotational response is similarly obtained as:

$$h_\theta(t) = \begin{cases} \dfrac{1}{K_{\theta,static}} \dfrac{{v_L}^*}{z_0} e^{-\frac{3}{2}\frac{{v_L}^*}{z_0}t} \left(3\cos\dfrac{\sqrt{3}}{2}\dfrac{{v_L}^*}{z_0}t - \sqrt{3}\sin\dfrac{\sqrt{3}}{2}\dfrac{{v_L}^*}{z_0}t \right) & t > 0 \\ 0 & t < 0 \end{cases} \tag{3.18}$$

where $K_{\theta,static} = 3\rho {v_L}^2 I_0 / z_0$ with $I_0 = \pi {r_0}^4 / 4$, and ${v_L}^*$ is the modified longitudinal wave velocity (Meek and Wolf, 1992a-1993b).

The above expressions for unit-impulse functions are also found to be linear combinations of exponential and/or exponentially decaying sine and cosine functions

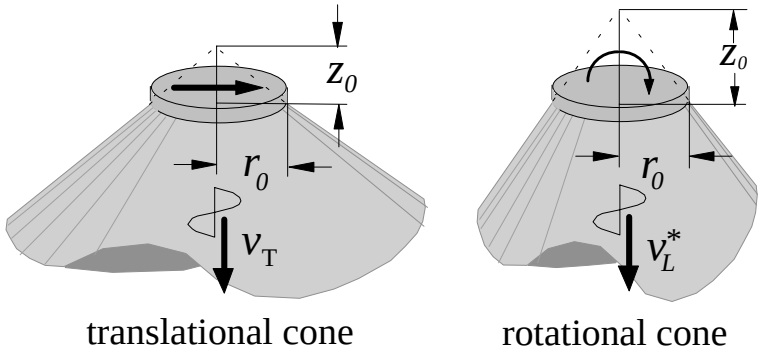

Figure 3.11 Cones for various degrees of freedom (Meek and Wolf, 1992a-1993b)

3.4 SUMMARY

Salient interaction features are often insensitive to the detailed variations of soil profiles. As for an embedded stiff foundation, its impedance function is strongly governed by the fundamental vibration mode of the surrounding soil deposit and the contributions by other modes can be ignored. This fact allows us to describe the impedance function (stiffness) by only a limited number of parameters. Such a small number of parameters are easily manageable even in commercially-available personal computers. This simplification thus certainly enhances the practicality of the present simulation approach and also will enable us to use the present simulation approach in the nonlinear soil environment.

REFERENCES

Konagai, K. and Maehara, M. [1992] "Study on hypotheses for simple numerical evaluation of soil-embedded structure interaction," *Bull., Earthquake Resistant Structure Research Center*, **25**, 39-60, 1992.

Konagai, K. and Nogami, T. [1998] "Analog circuit to simulate dynamic soil-structure interaction in shake table test," *International Journal of Soil Dynamics and Earthquake Engineering*, **17(5)**, 279-287, 1998.

Meek, J. W. and Wolf, J. P. [1992a]. "Cone models for homogeneous soil," *J. geotechnical eng., ASCE*, **118(5)**, 667-685.

Meek, J. W. and Wolf, J. P. [1992b]. "'Cone models for soil layer on rigid rock," *J. geotechnical eng., ASCE*, **118(5)**, 686-703.

Meek, J. W. and Wolf, J. P. [1992c]. 'Cone models for embedded foundation', *J. geotechnical eng., ASCE*, **120(1)**, 60-80, (1992c).

Meek, J. W. and Wolf, J. P. [1993a]. "Cone models for nearly incompressible soil," *Earthquake eng. struct. Dyn.*, **22**, 649-663.

Meek, J. W. and Wolf, J. P. [1993b]. "Why cone models can represent the elastic half space," *Earthquake eng. struct. Dyn.*, **22**, 759-771.

Tajimi, H. and Shimomura, Y. [1976] Dynamic analysis of soil-structure interaction by the thin layered element method, *Proc., Architectural Institute of Japan*, **243**, 41-51.

Tajimi, H. [1969] "Dynamic analysis of a structure embedded in an elastic stratum," *Proc. 4th World Conf., Earthquake Engineering*, Santiago, Chile, **III**(**A-6**), 53-69, 1969.

Chapter 4

REAL TIME CONTROL OF SHAKING TABLE FOR SOIL-STRUCTURE INTERACTION SIMULATION

4.1. INTRODUCTION

Simple descriptions of foundation stiffness parameters have been discussed in the first half of this report (***Chapters* 1-3**). The stiffness parameters are eventually approximated by a limited number of frequency-independent parameters. All these expressions may be such an oversimplification of reality that they cannot cover all cases of soil-structure interaction reality. They, however, allow the real-time production of the soil-structure interaction motions on a shaking table.

A faithful reproduction of input motions on a shaking table, however, is not easily done. Recent advances in robust and adaptive control theories have certainly enhanced the controllability of shaking tables to a great extent (Horiuchi et al., 1995, Stoten et al., 1998), and yet, the motions of a table often have to be adjusted, through iterative trials, to the intended base motions by modifying the input time histories; the iterative trials are not allowed to be done in the present approach. Generally, the larger a table is, the more difficult it is for the table to be controlled at will, and there often remains a time delay Δt between the produced motion and the input signal. This chapter shows in its first half a practical method for canceling the time-delay effects in shaking table tests. The latter part then describes simple examples of soil-structure interaction simulations.

4.2 CANCELLATION OF TIME DELAY EFFECT

It is noted that the system illustrated in **Figure 1.1** (***Chapter 1***) is realized on condition that a shaking table loses no time in producing faithfully its input motion. The motion produced by the shaking table, however, is not exactly identical to the intended time history because the ratio of output-to-input amplitude of the shaking table system does not remain the same over the desired frequency range. The performance of the system's transfer function is also affected by the presence of models on the shaking table; this fact may cause the motion of the table to further deviate from the intended time history. A controller with the transfer function T normally performs like a low pass filter, and experiments on the table are conducted below its *cut-off frequency*. Below this frequency yet, there remains a time delay Δt between the produced motion and the input signal. The effect of the time delay, described in the frequency domain as $T \cong e^{-i\omega\Delta t}$, could be canceled by multiplying the flexibility function H by T^{-1}. Assuming that the performance of a soil-foundation system is approximated by that of a simple-damped oscillator with spring, damping and mass parameters, *K*, *C* and *M* (**Figure 4.1**), the flexibility function H_{xx} is expressed as:

$$H_{xx} = \frac{1}{K - \omega^2 M + i\omega C} \tag{4.1}$$

Thus, the cancellation of the time-delay effects is made by

$$H_{xx}T^{-1} \cong \frac{e^{i\omega\Delta t}}{K - \omega^2 M + i\omega C} \tag{4.2}$$

For smaller values of $\omega\Delta t$, Equation (4.2) is rewritten as:

$$H_{xx}T^{-1} \cong \frac{1}{K - \omega^2 (M - \Delta M) + i\omega (C - \Delta C)} \tag{4.3}$$

where, $\Delta M = C \cdot \Delta t$ and $\Delta C = K \cdot \Delta t$ (4.4a) and (4.4d)

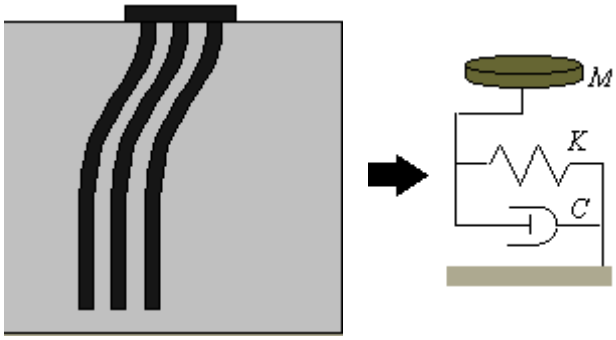

Figure 4.1 Modeling of a pile-group as a simple-damped oscillator

Equation (4.4b) shows that the equivalent mass and the viscous damping coefficient are reduced by $C\Delta t$ and $K \cdot \Delta t$, respectively. The reduced mass $M - \Delta M$ and the damping coefficient $C - \Delta C$ must be positive, calling for:

$$\frac{\Delta M}{M} = 4\pi^2 \frac{t_c \Delta t}{t_0^{\,2}} < 1 \quad \text{and} \quad \frac{\Delta C}{C} = \frac{\Delta t}{t_c} < 1 \qquad \text{(4.5a) and (4.5b)}$$

with $t_c = C / K$ and $t_0 = 2\pi\sqrt{M / K}$ (4.6a) and (4.6b)

The above conditions (Equations (4.5a) and (4.5b)) are usually satisfied in reality for many cases of soil-structure interaction, because radiation of waves from a foundation leads the motion of the structure to be noticeably damped.

It is, however, necessary for the time delay to be minimized when Equations (4.6a) and (4.6b) are not satisfied. One possible measure for reducing the time delay is to increase the feedback gain of a servo-amplifier of the shaking table (**Figure 4.2**). In **Figure 4.2**, u_{in} and u_{out} are the input signal and the signal of the motion produced by the shaking table, respectively. The deviation of the produced motion from the input signal, $u_{out} - u_{in}$, is multiplied by a negative factor $-\beta$, and is added to the input signal u_{in}. The following relationship between u_{in} and u_{out} is then satisfied with the original transfer function of the controller itself ($\beta = 0$) denoted by G:

$$u_{out} = G(u_{in} + \beta(u_{in} - u_{out})) \qquad (4.7)$$

From Equation (4.7), the overall transfer function T is described as:

$$T = \frac{u_{out}}{u_{in}} = \frac{G + G\beta}{1 + G\beta} \qquad (4.8)$$

It is noted in Equation (4.8) that T comes closer to 1 as the feedback gain, β, increases. The servo-amplifier shown in **Figure 4.2** was built in a one-dimensional shaking table system to check its performance. **Figure 4.3** shows that a servo-amplifier with a larger value of β offers more significant improvement in expanding the frequency range in which the ratio of output-to-input amplitude remains almost constant with little phase-shift. The increase of β, however, leads to a decrease in the margin for unstable clattering of the table that is caused by the noise echoing through the closed circuit of the servo-amplifier. The authors are trying out some other attempts in which a Robust-Adaptive way of control is utilized. They will be addressed in later publications.

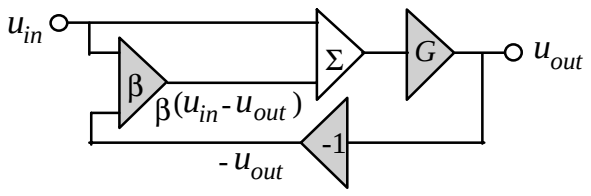

Figure 4.2 Servo-amplifier

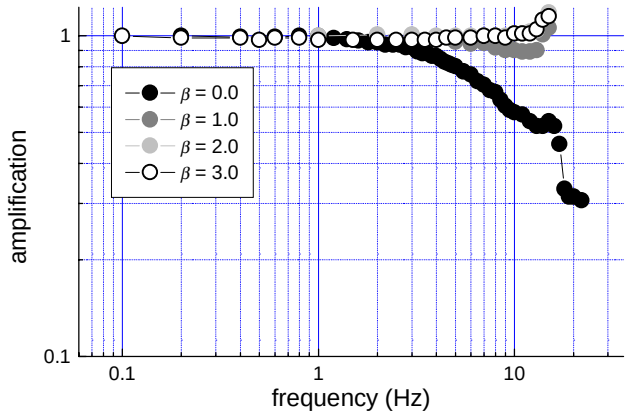

(a) Amplitude

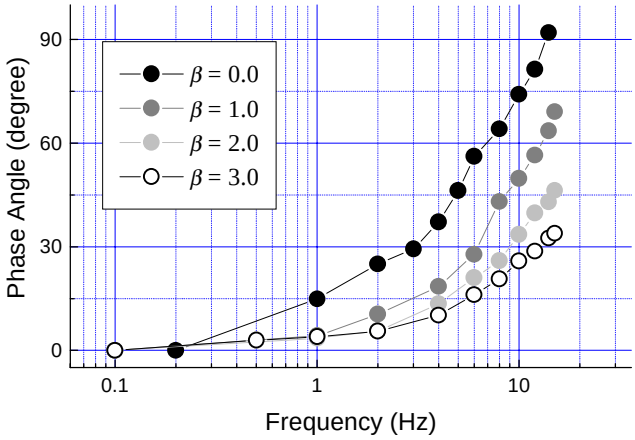

(b) Phase lag

Figure 4.3. Effect of feed-back gain on shaking-table transfer function

4.3 EXPERIMENTS

In order to provide a proper perspective on the usefulness of the present method, three simple examples of simulation of soil-structure interaction effects are introduced herein; (**4.3.1**) linear soil - linear structure, (**4.3.2**) linear soil - nonlinear structure and (**4.3.3**) nonlinear soil - nonlinear structure interactions. In the third example (**4.3.3**), the 'far field' soil non-linearity is taken into account through an equivalent linear approach. The non-linearity produced in the vicinity of foundations, which is usually associated with large strain and separation between soil and foundation, has not been considered in this example yet. It is, however, shown herein that a digital signal processor allows real time manipulation of the dynamic soil parameters to be made. The method on one hand captures the non-linear soil behavior of softening and re-hardening during the course of an earthquake, and on the other hand, allows testing of a bigger superstructure model by obviating the need of a heavy physical ground model.

4.3.1 *Flexible upright cantilever*

Eight steel plates (2000 mm×300mm×1 mm) were fastened together with rivets arranged in a grid to form a simple cantilever. The cantilever was then fixed upright on a shaking table with six degrees of freedom, as shown in **Figure 4.4** (Konagai et al., 1999), because it was expected that the bending of the cantilever would cause a rocking motion in its foundation. The feedback gains, β, of the servo-amplifier for this shaking table are set at 0.53 and 0.41 in respect to horizontal and rocking degrees of freedom. Mechanical properties of the cantilever are listed in **Table 4.1**. The cantilever is rather flexible, with its natural frequency set approximately at 1Hz, so that interaction forces (both shear force p_x and moment p_θ) are easily measured by bonding strain gages to the lower end of the cantilever. This flexible cantilever was assumed to be mounted virtually on a circular rigid mat foundation (radius (r_0) = 1.2 m, thickness (d) = 0.2 m, **Table 4.3**) resting on a soft semi-infinite half-space of soil ($v_s = 9$ m/s, **Table 4.2**). Meek and Wolf[6), 7)] have developed a unified approach for soil-structure interaction analysis by using truncated semi-infinite cone models representing an unbounded soil medium (See ***Chapter* 3**, **3.5**, p. 44). According to their approach, the soil supporting a rigid mat foundation is idealized for each degree of freedom as a truncated semi-infinite elastic cone with its own apex height z_0 (**Figure 4.5**). They also showed that the stiffness parameters for sway and rocking motions are approximated by those of discrete element models illustrated in **Figure 4.5**. The flexibility, $H_{xx}(s)$, of the discrete-element model in horizontal x direction is described as:

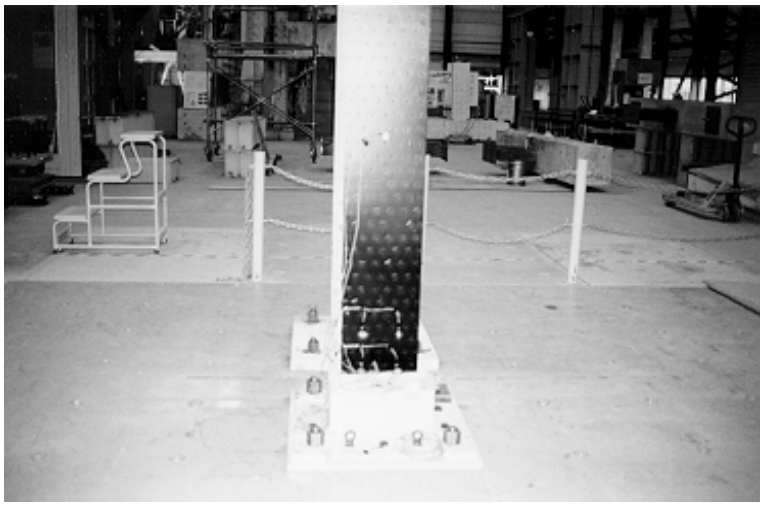

Fig. 4.4 Upright beam on shaking table

Table 4.1 Parameters of cantilever

width (m)	Height (m)	thickness (m)	Bending stiffness EI (Nm^2)	density ρ (kg/cm^3)
0.3	1.8	0.008	2132.5	0.00801

Table 4.2 Soil properties

Density ρ_s (kg/cm^3)	shear wave velocity v_s (m/s)	Poisson's ratio v
0.0016	4.8	0.5

Table 4.3 Parameters for foundation

Radius r_0 (m)	thickness d (m)	density ρ_c (kg/cm^3)
0.8	0.1	0.0025

$$H_{xx}(s) = \frac{1}{sC_x + K_x} \tag{4.9}$$

where,

$$K_x = \frac{\rho_s v_s^{\,2} \cdot \pi r_0^{\,2}}{z_0} \tag{4.10a}$$

$$C_x = \rho_s v_s \cdot \pi r_0^{\,2} \tag{4.10b}$$

and v_s is the shear wave velocity propagating through the cone that dominates the stiffness within considerably high frequency range. The apex ratio z_0 / r_0, or the opening angle of the cone, is determined by simply equating the static stiffness coefficient of the disk on the semi-infinite soil half-space to that of the corresponding cone, and is given by:

$$\frac{z_0}{r_0} = \frac{\pi}{8}(2-\nu) \tag{4.10c}$$

As far as the rocking motion of the disk is concerned, a rotational cone should be discussed. The flexibility, $H_{\theta\theta}(s)$, of the equivalent-discrete-element model in rocking motion is described as:

$$H_{\theta\theta}(s) = \frac{\frac{1}{C_\theta}s + \frac{1}{M_\theta}}{s^2 + \frac{K_\theta}{C_\theta}s + \frac{K_\theta}{M_\theta}} \tag{4.11}$$

where,

$$K_\theta = \frac{3\rho_s v^2 I_0}{z_0} \tag{4.12a}$$

$$C_\theta = \rho_s v I_0 \tag{4.12b}$$

$$M_\theta = \rho_s z_0 I_0 \tag{4.12c}$$

with $$I_0 = (\pi/4) r_0^{\,4} \tag{4.12d}$$

The velocity v is assumed to be identical to that of the longitudinal wave traveling through the cone when Poisson's ratio of the soil is less than 1/3. For larger values of Poisson's ratio, v is set at $2v_s$. The apex ratio z_0 / r_0 of the rotational cone is:

$$\frac{z_0}{r_0} = \frac{9\pi}{32}(1-\nu)\left(\frac{v}{v_s}\right)^2 \tag{4.12e}$$

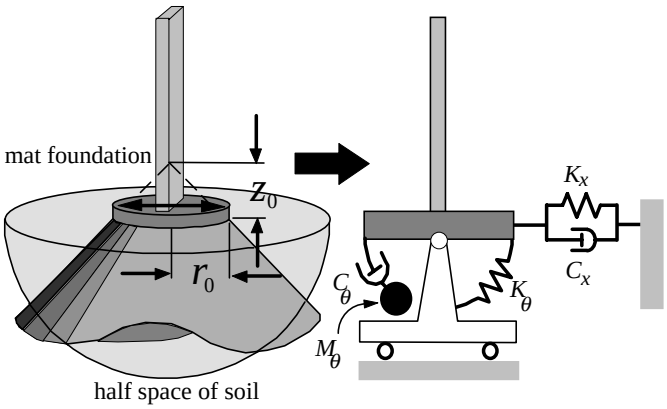

Figure 4.5 Mat foundation and equivalent discrete element model

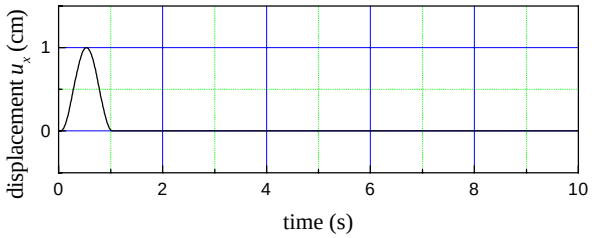

Figure 4.6 Input base motion $u_x^f + u_x^s$

In actuality, the lateral and rocking motions of a foundation are coupled, and the present method illustrated in **Figure 1.1** (***Chapter* 1**) allows the effect of the coupling to be simulated. The coupling effect, however, is ignored in this simulation.

As has been mentioned, electric-resistance strain gages were used as a sensing device for both shear-force and moment. A pair of strain gages were bonded on both sides of the lower end of the cantilever to sense the strain in the cantilever resulting from the bending motion of the cantilever. The outputs of strain gages are then connected to an appropriate bridge circuit that produces a signal proportional to the bending moment. Another pair of strain gages were then pasted 10 cm above them, and the measurement of moments at these two points permitted a determination of the shear force at the lower end of the cantilever. It is noted that the moment and the shear force sensed by these strain gages are not identical yet to the interaction forces, p_x and p_θ, on the soil-foundation interface. The interaction forces are to be evaluated taking into account the inertia forces of the foundation virtually resting on the half-space of soil. For this evaluation, both lateral and rocking accelerations, $\ddot{u}_x$ and $\ddot{u}_\theta$, were measured on the shaking table, and the signals of $\ddot{u}_x$ and $\ddot{u}_\theta$ were multiplied respectively by the foundation mass, M_x $(=\rho_c \cdot \pi r_0^{\,2} d)$, and the moment of inertia, M_p $(=\rho_c I_0 d + M_{trap})$, where M_{trap} is the contribution of the soil mass caught beneath the foundation, and is given by:

$$M_{trap} = 1.2\left(\nu - \frac{1}{3}\right)\rho_s I_0 r_0 \tag{4.13}$$

A horizontal impulse shown in **Figure 4.6** was given to the shaking table as an effective foundation input motion, $u_x^f + u_x^s$, and the acceleration response at the top end of the cantilever was measured. The dotted line in **Figure 4.7a** shows the acceleration time history without the interaction motions, u_x^r and u_θ^r, being added; whereas the dotted line in **Figure 4.7b** shows the response affected by the interaction motions. Thick lines in these figures show the computed responses of the discrete element model in **Figure 4.5**. In this numerical simulation, the finite difference method was utilized to obtain the solutions in the time domain. The thick and dotted lines are in good agreement in both figures; this fact clearly demonstrates that, for the simulation of soil-structure interaction motions, the present method works properly as expected. These figures show that incorporating the effect of the interaction motion leads to the increase of damping and to the slight decrease of natural frequency as well. Although only horizontal base motion was given to the shaking table, bending motion of the cantilever eventually caused the shaking table (the virtual foundation) to rock as shown in **Figure 4.8**. The observed rocking motion, u_θ^r, is also in good agreement with the numerical simulation (thick line).

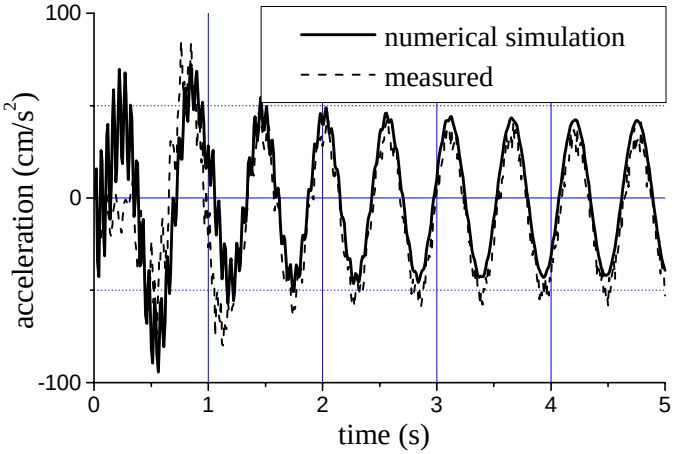

(a) without interaction

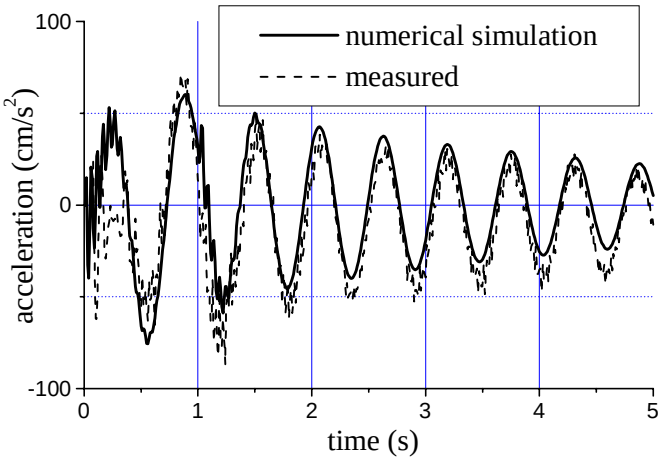

(b) with interaction

Figure 4.7 Accerelation at the top end of upright beam

The present system is conditionally stable as is often the case with feed-back control systems. Especially when a structure model with low damping ratio is shaken, the motion of the shaking table sometimes echoes through the circuit causing a serious clattering (howling) of the table. **Figure 4.9** shows one example of clattering that happened before the table was properly heated up and stabilized. The predominant frequency of the noise is 11 Hz, and is about identical to the fourth natural circular frequency of the model. When the predominant frequency is higher than the frequency range in which the desired signal exists, a low-pass filter may be used to reduce the noise. It is however noted that the use of a low-pass filter causes the response of the table to be more delayed. Some built-in device such as an adaptive echo canceller[10)] would be useful for further improving its performance.

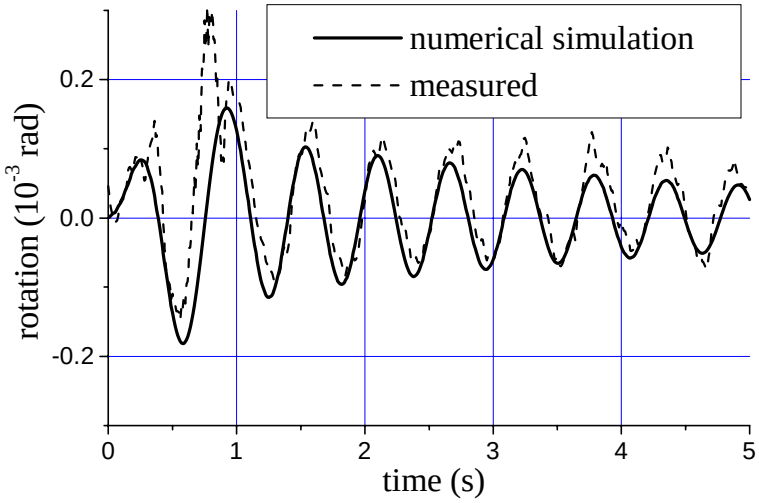

Figure 4.8 Rocking of shaking table

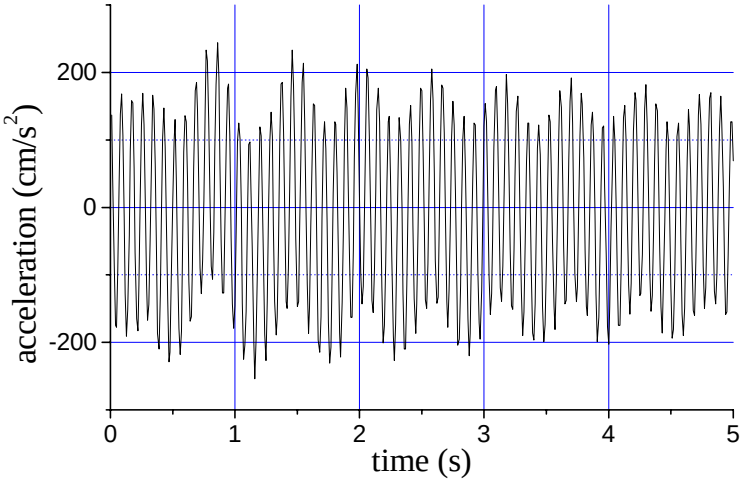

Figure 4.9 Howling observed at the top end of upright beam

4.3.2 *Slippage of rigid block on mat foundation*

A rigid cylindrical block is assumed to be put on a rigid and circular mat foundation resting on a semi-infinite half medium of soil (**Figure 4.10a**). The dimensions of both the prototype block and foundation are listed in **Table 4.4**, whereas **Table 4.5** shows the parameters for the soil medium. Poisson's ration of the soil was set at 0.5 on the assumption that the ground is an alluvial soft soil deposit that is totally saturated with water. In this case also, the soil supporting a circular mat foundation is idealized for each degree of freedom as a truncated semi-infinite cone (**Figure 4.10b**) with its own apex height z_0. Only translational motion of the foundation is discussed herein, and the soil-foundation is modeled by a damped one-degree-of-freedom system. The model of the soil-structure system is then prepared by reducing the parameters, *m*, *k* and *c* to the uniform scale of 1 to 100. Since the ratio of these parameters is kept unchanged, the time scale is not changed at all.

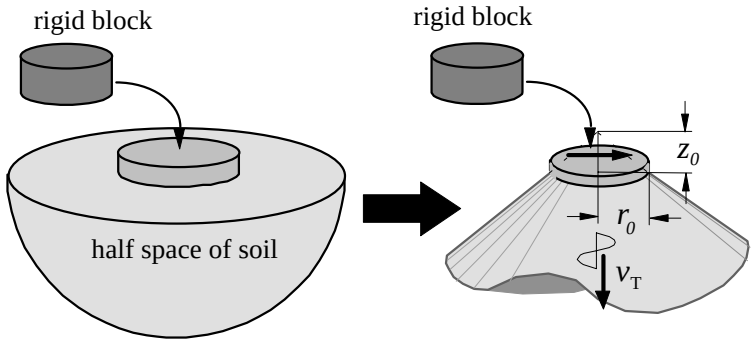

a Rigid block on mat foundation **b** translational cone

Figure 4.10 Rigid block put on a rigid mat foundation resting on a semi-infinite soil medium

Table 4.4 Dimensions of block and foundation

(a) block

Mass	Radius	Height
7.1×10^5 kg	7 m	2 m

(b) mat foundation

Mass	Radius	Height
1.4×10^6 kg	11 m	1.6 m

Table 4.5 Mechanical properties of soil

Density	Shear wave velocity	Poisson's ratio
1.6×10^3 kg/m^3	100 m/s	0.5

Figure 4.11 shows the model put on a shaking table. The steel block in the middle is the model of the rigid block, and the shaking table itself virtually represents the motion of the mat foundation on the semi-infinite soil half-space. The block is put not directly on the shaking table but on a flat steel plate supported by four stiff upright legs with strain gages pasted on them. These gages pick up the base shear force from the block. An impulse as shown in **Figure 4.12** is given to the shaking table as an input motion u_x. The test was also conducted for the above block model put on the rigid base. **Figure 4.13** shows time histories of both the displacement of the shaking table and the distance that the block has slipped. Dotted lines in this figure show the motions without the interaction effect being taken into account, whereas thick lines show the motions affected by the soil-structure (foundation-block) interaction. Incorporation of the soil-structure interaction leads to slight increase in the duration of the base motion and drastic decrease of the distance that the block has slipped. The mass of the block is the direct cause of the increase in the duration of the base motion, and the decrease of the sliding distance is closely linked with the increase of the energy that has dissipated as outwardly propagating waves into the virtually spreading soil medium. The present method allows both influx E_{input} and efflux $E_{dissipated}$ of energy through the foundation to be measured in real time. These two kinds of energy are respectively:

$$E_{input} = \int_0^t \left(p_x \dot{u}_x + p_\theta \dot{u}_\theta \right) \cdot dt \tag{4.14a}$$

$$E_{dissipaed} = \int_0^t \left(- p_x \dot{\tilde{u}}_x - p_\theta \dot{\tilde{u}}_\theta \right) \cdot dt \tag{4.14b}$$

The energy, $E_{consumed}$, used up within the model on the shaking table is then obtained as:

$$E_{consumed} = E_{input} - E_{dissipated} \tag{4.14c}$$

Figure 4.14a shows the variations of these energies with time where the interaction effects are ignored, and thus, the cumulative loss of energy through friction ends up to be the same amount as the energy influx. On the other hand, **Figure 4.14b**, in which soil-structure interaction effects are incorporated, shows that a part of influx energy dissipates away and just the remainder is used up through friction.

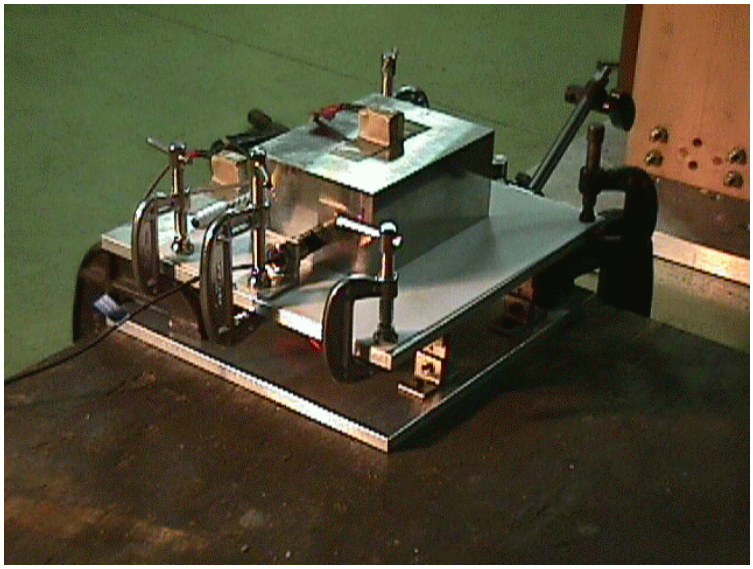

Figure 4.11 Block model on shaking table

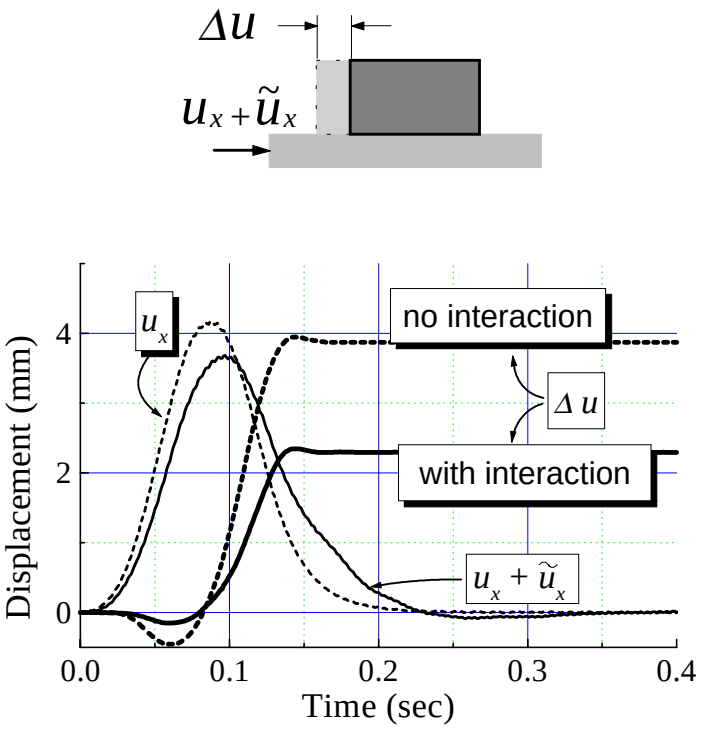

Figure 4.12 Displacement of shaking table and distance that block has slipped

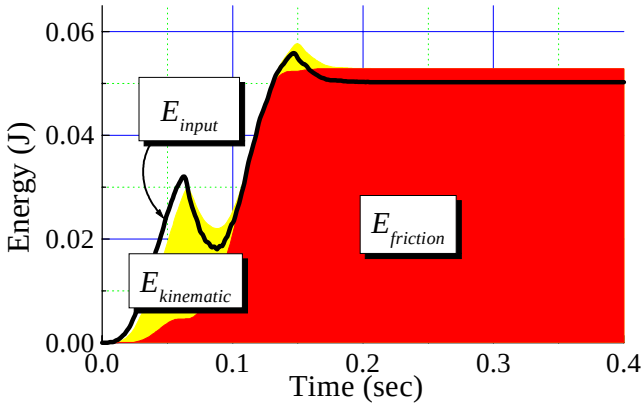

(**a**) no interaction

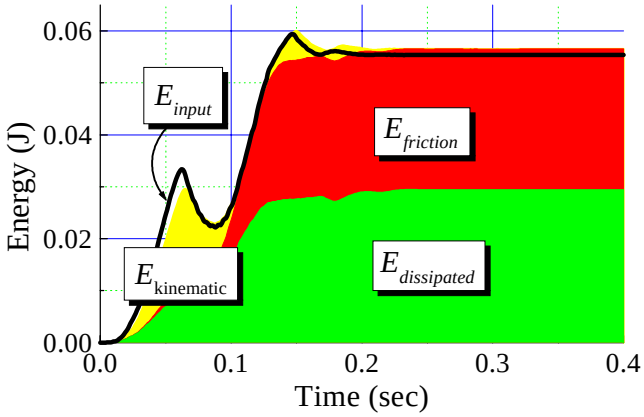

(**b**) with interaction

Fig. 4.13 Influx, efflux and consumption of energy

4.3.3 *Bilinear viaduct pier model on a pile group embedded in non-linear soil*

Ground response analysis

An application of the present method to a particular prototype is henceforth described to explain the steps of the method in an effective way. The prototype is an expressway viaduct supported by pile foundations. Information regarding the ground profile of the site is provided in **Table 4.6**. Since pile foundations are quite flexible in nature, it is assumed here that they follow the deformation of their surrounding soil. Therefore, in the non-linear ground response analysis, only the soil without the presence of any foundation was subjected to an earthquake excitation.

Table 4.6. Ground profile at the site of the prototype

Thickness h (m)	Unit weight γ (tf/m^3)	Shear wave velocity V_s (m/s)	Shear Modulus G_0 (tf/m^2)
3.8	1.9	144.0	4020
3.6	1.9	129.3	3241
12.2	1.4	159.8	3648
0.9	1.9	173.2	5816
11.5	1.4	159.5	3634
5.0	1.9	161.0	5026
6.0	1.9	188.2	6867

The ground response analysis was carried out considering only vertically propagating horizontal SH waves. Hence the ground profile of Table 4.6 was modeled as a one dimensional horizontally layered soil column having non-linear soil properties. For the analysis the Finite Element Method was adopted in spatial domain and the Finite Difference Method in time domain. To express the non-linear stress-strain relationship of each layer of the soil column, the Hardin-Drnevitch model was adopted in association with the Modified Masing rule. In order to take radiation damping into account, a dashpot was attached at the bottom of the soil column. For shear wave propagation through a one-dimensional semi-infinite medium, the damping coefficient of the dashpot is given by,

$$C = G_r / V_{s_r} \qquad (4.15)$$

Where, G_r and V_{s_r} are the shear modulus and shear wave velocity of the base rock, respectively.

The soil column was subjected to a sample base excitation for the non-linear ground response analysis. The north-south component of the acceleration record of the earthquake that occurred at Shizukuishi in Iwate prefecture, Japan on September 3, 1997 [Konagai et al., 1999] was used as the sample base excitation, shown in Figure 4.14. The analysis yields the displacement history at the surface layer, shown in Figure 4.15, and the stress-strain histories of all the layers. At each reversal point of the stress-strain history the corresponding secant shear modulus was determined. The method of determining the secant shear modulus is illustrated in Figure 4.16. Figures 4.17(a) and 4.17(b), respectively, show the variations of the secant shear moduli and the corresponding damping ratios of different layers of the soil profile with time.

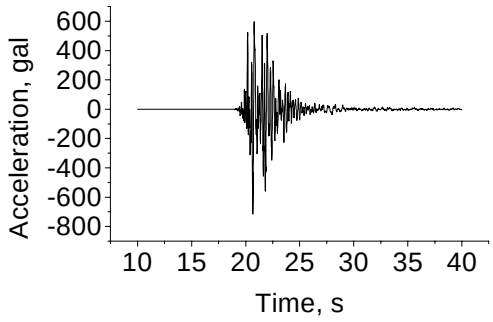

Figure 4.14. Sample base excitation

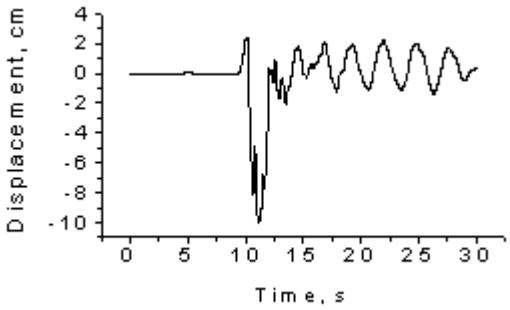

Figure 4.15. Displacement history at the surface layer

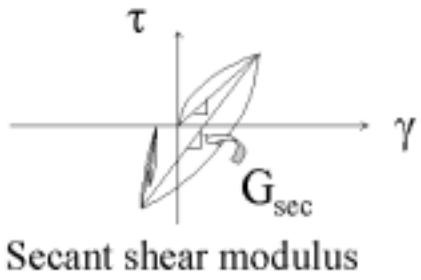

Figure 4.16 Determination of secant shear modulus

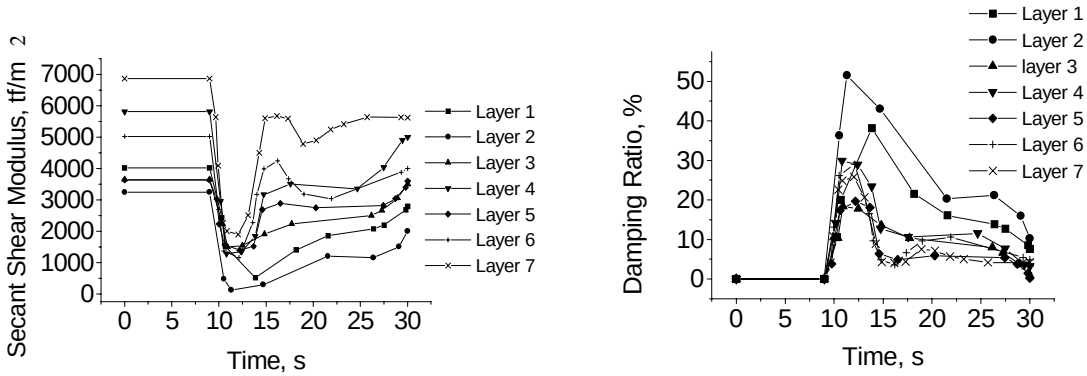

(a) Variation of secant shear modulus **(b)** Variation of damping ratio

Figure 4.17 Variation of equivalent linear parameters with time

Determination of stiffness function

In order to determine the stiffness function, *TLEM* (Ver. 1.2, See ***Chapter* 2** and **Appendix 3**) was employed to the soil-profile, correspoding to a particular time instant of the duration of the excitation, in order to obtain the dynamic stiffness at that time. The analysis yielded the dynamic stiffness of the substructure as a function of the forcing frequency. For pile-groups, some frequency invariant parameters (*K*, *C*, and *M*) can be defined to describe the stiffness function, as was explained in ***Chapter* 2**. Similar analyses are carried on for the soil profiles corresponding to other time instants as derived by the ground response analysis. The non-linear ground response analysis and the subsequent idealization of the non-linear parameters to equivalent linear parameters provided the necessary information of soil for the linear analysis of the pile-soil interaction. **Figure 4.18** shows a typical layout of the pile-groups of the viaduct. The outer and inner radii of each steel pile are 0.41m and 0.39m respectively.

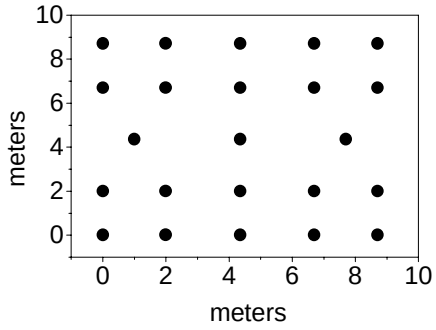

Figure 4.18 A typical pile-group layout of the Misato viaduct

The variations of K, C and time-constant, T (=C/K) are shown in Figures 4.19(a)-(c) with linear interpolation between the values obtained from the analysis. The value of M was found to remain nearly constant at 20 tf-s^2/m. Figures 4.19(a)-(c) show the non-linear feature of the initial softening of soil and then its subsequent rehardening in the course of an earthquake excitation.

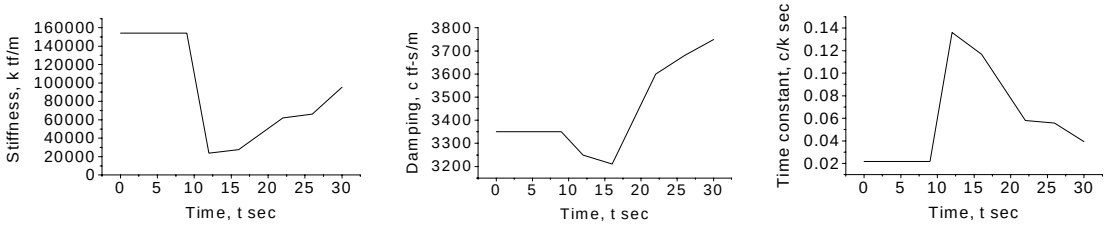

(a) Variation of stiffness **(b)** Variation of damping **(c)** Varation of time-constant

Figure 4.19 Variation of the different parameters of the substructure

Simulation

Since the experiment was mainly focused on studying the change in dynamic behavior of the structure due to the incorporation of soil-structure interaction effects, an exact physical model of the prototype structure was not necessary. Therefore, instead of making such an exact model, an attempt was made to model the dynamic features of the prototype.

A typical pier of the viaduct was considered as the prototype under study. The weight the pier sustains is around 666tf, and its resonance frequency is about 1Hz. The dynamic force displacement relationship of the pier is produced in Figure 4.20. From Figure 4.20, it is evident that the force-displacement curve can be approximated as a bilinear one. One simple way to model this bilinear force-displacement relationship is to

place a mass on top of a frame so that the mass slips when the acceleration exceeds beyond the level that the friction between the mass and the frame can resist. Below this level the mass moves with the frame. If the frame exhibits a linear feature, the mass-frame model posseses a bilinear force-displacement relationship.

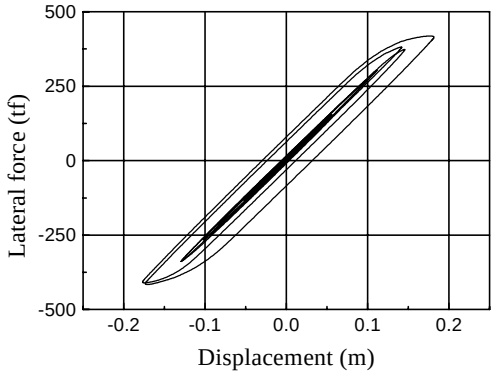

Figure 4.20. Force-displacement relationship of the pier

Experimental setup

In the present experiment, a mass of 6.75kg was placed on a steel frame. A teflon sheet was used to reduce friction between the mass and the crossbeam of the frame. A photograph of the experimental set-up is shown in **Figure 4.21**. The frequency of the steel frame was 2Hz. Since the frequency of the frame was two times of that of the prototype, the duration of the input motion as well as the time-constant of the interaction flexibility function was halved. From **Figure 4.20**, it is found that the pier carrying a mass of 666tf shows plastic deformation beyond an acceleration of 600gal. But the average frictional coefficient between the mass and the teflon sheet was found to be around 0.2. Therefore, the mass slipped when acceleration exceeded 200gal. Again the ratio of model displacement, u_m and prototype displacement, u_p can be expressed in terms of the ratio between model frequency, ω_m and prototype frequency, ω_p and the ratio between model acceleration, a_m and prototype acceleration, a_p as,

$$\frac{u_m}{u_p} = \frac{\omega_p{}^2 a_m}{\omega_m{}^2 a_p} \tag{4.16}$$

Therefore for the present case the input motion had to be scaled down by a factor of 1/12.

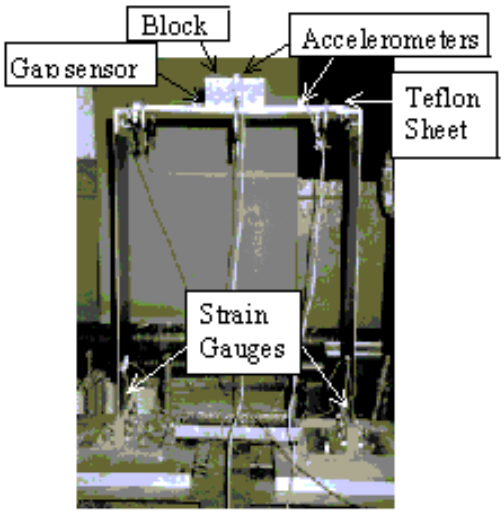

Figure 4.21. The experimental set up

A SIMULINK model, as is shown in Figure 4.22, was prepared to input shaking table motion and to add the soil-structure interaction motion to the input motion. The motion realized, by means of a digital signal processor, at the shaking table was adjusted by the FFM Gain so that it corresponds to the 1/12th of the prototype motion of Figure 4.15. The signals picked up by the force transducers attached at the bottom of the columns of the steel frame were fed into the SIMULINK model through AD converter of the digital signal processor. The signal was then passed through the flexibility function to produce soil-structure interaction motion.

The SSI Gain was used for consistent modeling of the substructure dynamics. The initial stiffness of the prototype substructure was found to be about 50 times the stiffness of the pier. The value of the SSI Gain was adjusted so that in the absence of any input motion, a static displacement of the frame produced a displacement of the shaking table 1/50th of that of the frame. The parameters of the flexibility function were changed in real time with an MLIB routine. A gap sensor was used to measure the relative displacement between the mass and the frame. The displacements of the frame and the shaking table were measured with laser sensors. Accelerometers were used to measure accelerations of the mass and the frame.

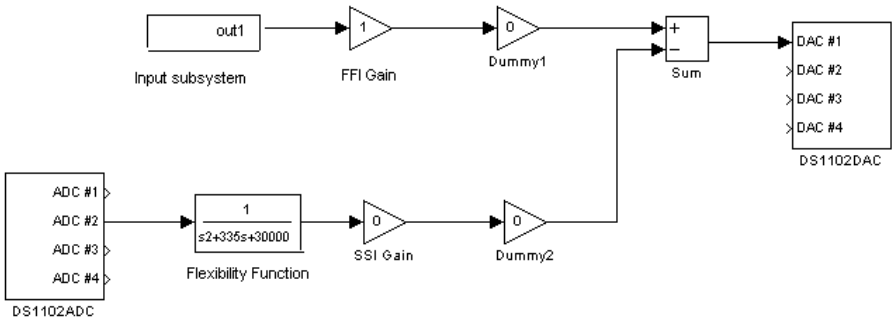

Figure 4.22. SIMULINK model

Results

One of the major concerns of the feedback control of dynamic systems is the reliability of the realized input motion. If the input motion is not realized at the shaking table in real time, the delay causes a delayed interaction motion which when added to the free-field motion fails to reflect appropriate interaction effects. For the purpose of checking the reliability of the realized motion, the signal of the input motion before inputting to the controller of the shaking table and the motion realized at the shaking table were both measured at the same time. During this measurement the SSI Gain was set at a value of zero i.e., there was no interaction effect involved. Both the measured signals are shown in **Figure 4.23**. **Figure 4.23** shows that the input motion was realized with adequate reliability.

When interaction effect is considered, the displacement of the frame was found to deviate from the displacement when there was no interaction (Figure 4.24(a)). Similar deviation can be observed in the displacement of the mass too (Figure 4.24(b)). Marked difference can be noticed in the displacement of the frame between the 7th and 10th second when the stiffness of the flexibility function is small and the time-constant is high due to the non-linearity of soil. At the latter part of the displacement history of the frame when input motion is about zero, the effect of increased damping due to soil-structure interaction is quite evident. It should be mentioned here that the slippage of the block is not always the same even for the same input motion and even without interaction. After repeating the same experiment a number of times, a representative result has been produced in Figure 4.24(b).

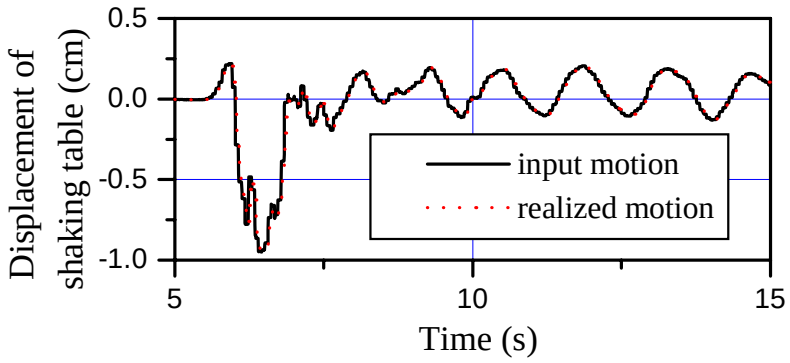

Figure 4.23 Reliability of the realized motion

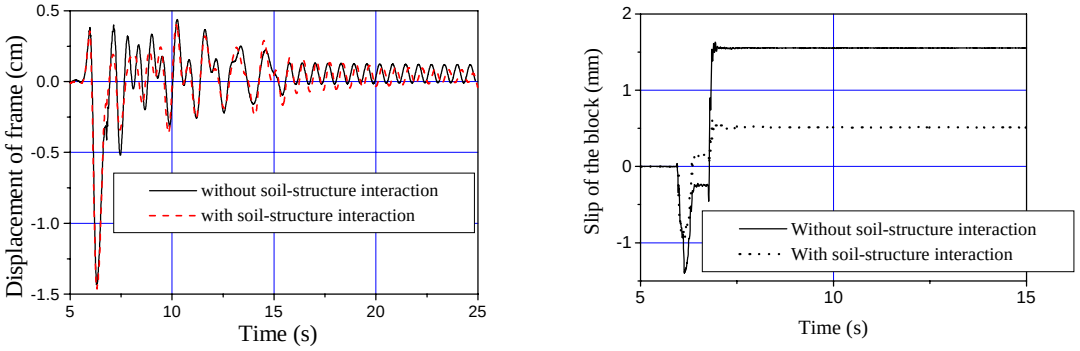

(a) **(b)**

Figure 4.24. Displacement of **(a)** the frame and **(b)** the mass with respect to the frame

At the absence of any soil-structure interaction the total input energy is consumed through the friction of the mass and the damping of the frame. Whereas the interaction between soil and structure causes a large amount of energy to dissipate as outwardly propagating waves into the virtually spreading soil medium. This dissipation of energy causes less energy to be consumed by friction and thereby reduces the slippage of the mass. As shown in 4.3.2 (pp. 58), the present method allows both influx of energy, E_{input} and efflux of energy $E_{dissipated}$ through the foundation to be measured in real time. These two quantities associated with lateral motions are respectively:

$$E_{input} = \int_0^t p_x \dot{u}_x \cdot dt \quad \text{and} \quad E_{dissipaed} = \int_0^t - p_x \tilde{\dot{u}}_x \cdot dt \qquad \text{(4.17a), (4.17b)}$$

The energy, $E_{consumed}$ used up within the model on the shaking table is then obtained as:

$$E_{consumed} = E_{input} - E_{dissipated} \tag{4.17c}$$

The energy is consumed within the model in two mechanisms: one due to the damping of the frame and the other through friction of the mass and the teflon sheet. The energy consumed due to the damping of the structure is given by,

$$E_{damp} = \int_0^t c\dot{u}_f{}^2 \cdot dt \tag{4.18a}$$

where c and $\dot{u}_f$ are respectively the damping coefficient and velocity of the frame. The energy used up due to friction can be calculated as,

$$E_{fric} = \int_0^t m\ddot{u}_b\dot{u}_{slip} \cdot dt \tag{4.18b}$$

where m and $\ddot{u}_b$ are respectively the mass and acceleration of the block and u_{slip} is the distance the block slips with respect to the frame. Thus $E_{consumed}$ can also be expressed as

$$E_{consumed} = E_{damp} + E_{fric} \tag{4.18c}$$

Figures 4.25(a) and 4.25(b) show the distribution of energy in two different cases: one without any consideration of the interaction and the other considering the interaction effects. The difference between the input energy and the total consumed energy in these figures corresponds to the kinetic and potential energy components of the mass and the frame when they are in motion. In relation to the prototype, it can be said that the soil-structure interaction causes dissipation of energy through soil which results in less plastic deformation of the pier. Any prediction based on experimental results not considering the interaction may overestimate the amount of plastic deformation accumulated in the pier after an earthquake.

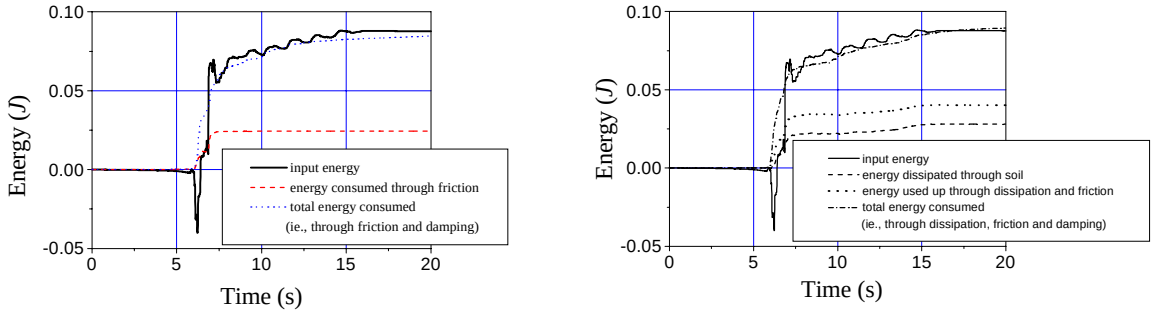

(a) without interaction (b) with interaction

Figure 4.25. Distribution of energy

4.4 SUMMARY

A new method for a model experiment on a shaking table has been examined. The present method allows soil-structure interaction to be simulated. In the present method, soil-structure interaction effects are simulated by adding appropriate soil-structure interaction motions to the free-field ground motions at the shaking table. The method was initially developed with the assumption that soil behaves linearly. In the present report, the method was extended to take the 'far field' soil non-linearity into account through an equivalent linear approach. The non-linearity produced in the vicinity of foundations, which is usually associated with large strain and separation between soil and foundation, has not been considered in this study. In this method, the dynamic soil parameters were varied in real time by means of a digital signal processor. The method on one hand captures the non-linear soil behavior of softening and re-hardening during the course of an earthquake, and on the other hand, allows testing of a bigger superstructure model by obviating the need of a heavy physical ground model. This method thus has the potential to be applied to a variety of experiments of soil-structure interaction without preparing any physical soil model. The conclusions of this study are summarized as follows:

(1) The present system is realized on condition that a shaking table produces faithfully its input motion. The motion produced by the shaking table, however, is not exactly identical to the intended time history because the ratio of output-to-input amplitude of the system does not remain the same over the frequency range desired. The performance of the system's transfer function is also affected by the presence of a model on the shaking table, a fact that may cause the motion of the table to further deviate from the input. This effect will be canceled by multiplying the flexibility function, H, of a soil-foundation system by the inverse transfer function, T^{-1}, of the shaking table system. This manipulation, however, leads to reducing both the mass, M, and the viscous damping coefficient, C, making up the discrete element model equivalent in mechanical properties to the soil-foundation system. Needless to say, the reduced mass, $M - \Delta M$, and the damping coefficient, $C - \Delta C$, must be positive. The conditions are usually satisfied in reality for many cases of soil-structure interaction because wave radiation from a foundation leads the motion of the structure to be noticeably damped. If not, it would be necessary for the time delay to be minimized. One possible measure for reducing the time delay is to increase the feedback gain of a servo-amplifier of the shaking table. It is, however, noted that the increase of feedback gain leads to a decrease in the margin for unstable clattering of the table that is caused by the noise echoing

through the closed circuit of the servo-amplifier.

(2) In order to provide a proper perspective on the usefulness of the present method, a simple upright 2,000 mm long steel cantilever was shaken on a shaking table. The observed responses of the beam showed that incorporating the effect of the interaction motion leads to the increase of damping and to the slight decrease of natural frequency as well. The numerical simulations were in good agreement with the observed responses, demonstrating that the present method for the simulation of soil-structure interaction motions works properly as expected. It is, however, noted that unexpected noise amplification can cause serious problem in operating the shaking table when a less-damped structure model is tested on a shaking table.

(3) A steel block was put on a shaking table that virtually represents the sway motion of a rigid circular mat foundation on a semi-infinite half space of soil. An impulsive displacement was then given to the shaking table as an input free-field motion, and both the displacement of shaking table and the distance that the block slipped were measured. Incorporation of the soil-structure interaction led to slight increase in the duration of the base motion and noticeable decrease of the distance that the block slipped.

(4) A steel block was placed on the top of a frame, which was assumed to dynamically correspond to a viaduct pier exhibiting a bilinear feature of force-displacement relationship. The prototype pier is supported by a pile-group foundation embedded in a nonlinear soft soil deposit. The model was subjected to an earthquake excitation. The results obtained from the experiment show some important features of the soil-structure interaction effects. The incorporation of soil-structure interaction led to a noticeable decrease of the distance that the block slipped.

REFERENCES

Horiuchi, T., Nakagawa, M., Sugano, M., and Konno, T. [1995] "Development of Real-Time Hybrid Experiments System with Actuator Delay Compensation," *Jour., JSME* (C), **61(584)**, 64-72 (in Japanese).

Konagai, K., Uemura, O., Katsukawa, T. and Suzuki, T. [1998] "Real Time Simulation of Soil-Structure Interaction Effects on Shaking Tables," *Proc., 10th Japan Earthquake Engineering Symposium*, **E1-13**, 1647-1652, 1998.

Konagai, K. and Nogami, T. [1997] "Simulation of Soil-Structure Interaction on a Shaking Table," Numerical and Physical Modeling for Dynamic Soil/Structure Interaction Phenomenon, *Geotechnical Special Technical Publication*, *ASCE*, **64**, 91-106.

Konagai, K. and Nogami, T. [1997] "Analog Circuits for Simulating Soil-Structure Interaction on a Shaking Table," *Intrn. Jour., Soil Dynamics and Earthquake Engineering*, **17(5)**, 279-287.

Konagai, K. and Katsukawa, T.[1997] "Real time control of a shaking table for soil-flexible

structure interaction," *Bull., Earthquake Resistant Structure Research Center,* IIS, Univ. of Tokyo, **30**.

Konagai, K., Nogami, T., Katsukawa, T., Suzuki, T. and Mikami, A. [1998] "Real Time Control of Shaking Table for Soil-Structure Interaction Simulation," *Jour. of Structural Mechanics and Earthquake Engineering, JSCE*, **16(1)**, 91s-95s.

Konagai, K., Mikami, K., Katagiri, K., Ahsan, R. and Maruyama, D. [1999] "Report of the Damage Caused by the Mid-North Iwate Earthquake of September 3, 1998," *Bulletin of Earthquake Resistant Structure Research Center*, IIS, University of Tokyo, **32**, 1-10.

Kanya, A. M. and Kauzel, E. [1982] "Dynamic Behavior of Pile Groups," *Proc., 2nd International Conference on Numerical Methods of Offshore Piling*, Austin, TX, 509-532.

Meek, J. W. and Wolf, J. P. [1992a] "Cone models for homogeneous soil," *J. Geotechnical Eng., ASCE*, **118(5)**, 667-685.

Meek, J. W. and Wolf, J. P.[1992b] "Cone models for embedded foundation," *J. Geotechnical Eng., ASCE*, **120(1)**, 60-80.

Sondhi, M. M.[1967] "An Adaptive Echo Canceller," Bell Syst. Tech. Jour., 46(3), 497.

Stoten, D.P. and Gomez, E [1998] "Recent Application: Results of Adaptive Control on Multi-Axis Shaking Tables," *Proc., 6th SECED Int. Conf., Seismic Design Practice into the Next Century*, Booth (ed.), 381-387.

Zadeh, L. A. and C. Desoer A. [1963] *Linear System Theory*, McGraw-Hill Book Co.

APPENDIX

APPENDIX I: *Stiffness matrix of equivalent single beam*

The soil and n_p piles system is divided into n_L horizontal slices as shown in **Figure 2.2**. Assumptions (1) and (2) imply that the deflections of the piles are all completely identical, allowing the deflections of all piles to be equally described by the same equation. Piece-wise increments of deflection angle $\{\Delta\boldsymbol{\theta}\}$ along the piles are described in terms of lateral displacements $\{\mathbf{u}\}$ as:

$$\{\Delta\boldsymbol{\theta}\}=[\mathbf{L}]\{\mathbf{u}\}+\left\{\frac{w_1}{R_0} \quad 0 \quad \cdots \quad 0\right\}^T \tag{A1}$$

where,

$$[\mathbf{L}]=\begin{bmatrix} -\frac{1}{h_1} & \frac{1}{h_1} & 0 & 0 & \cdots & 0 \\ \frac{1}{h_1} & -\frac{1}{h_1}-\frac{1}{h_2} & \frac{1}{h_2} & 0 & & \vdots \\ 0 & \frac{1}{h_2} & -\frac{1}{h_2}-\frac{1}{h_3} & \frac{1}{h_3} & & \vdots \\ 0 & 0 & \ddots & \ddots & \ddots & 0 \\ \vdots & & \ddots & \ddots & \ddots & \frac{1}{h_{n_L-1}} \\ 0 & \cdots & \cdots & 0 & \frac{1}{h_{n_L-1}} & -\frac{1}{h_{n_L-1}}-\frac{1}{h_{n_L}} \end{bmatrix} \tag{A2}$$ and

w_1 is the anti-symmetric vertical motion of the pile cap at $r=R_0$. The component, w_1/R_0, in short, is the deflection angle at the pile cap.

Given the piecewise increments of deflection angle $\{\Delta\boldsymbol{\theta}\}$, and applying the Method of Three Moments, the internal moments $\{\mathbf{M}_{\text{int}}\}$ induced in the beam are described as:

$$\{\mathbf{M}_{\text{int}}\}=[\mathbf{D}]^{-1}\{\Delta\boldsymbol{\theta}\} \tag{A3}$$

where,

$$[\mathbf{D}]=\frac{1}{6}\begin{bmatrix} 2\frac{h_1}{EI} & \frac{h_1}{EI} & 0 & 0 & \cdots & 0 \\ \frac{h_1}{EI} & 2\left(\frac{h_1}{EI}+\frac{h_2}{EI}\right) & \frac{h_2}{EI} & 0 & & \vdots \\ 0 & \frac{h_2}{EI} & 2\left(\frac{h_2}{EI}+\frac{h_3}{EI}\right) & \frac{h_3}{EI} & & \vdots \\ 0 & 0 & \ddots & \ddots & \ddots & 0 \\ \vdots & & \ddots & \ddots & \ddots & \frac{h_{n_L-1}}{EI} \\ 0 & \cdots & \cdots & 0 & \frac{h_{n_L-1}}{EI} & 2\left(\frac{h_{n_L-1}}{EI}+\frac{h_{n_L}}{EI}\right) \end{bmatrix} \tag{A4}$$

with $EI=n_pE_pI_p$ ($E_pI_p=$ bending stiffness of an individual pile). (A5)

It is noted that the moments $\{\mathbf{M}_{\text{int}}\}$ are expressed in terms of lateral external forces $\{\mathbf{p}_x\}$ as:

$$\{\mathbf{M}_{\text{int}}\} = [\mathbf{L}]^{-1} \cdot \{\mathbf{p}_x\} \tag{A6}$$

From Equations (A1), (A3) and (A6), one obtains

$$\{\mathbf{p}_x\} = [\mathbf{L}][\mathbf{D}]^{-1}\left\{[\mathbf{L}]\{\mathbf{u}\} + \left\{\frac{w_1}{R_0} \quad 0 \quad \cdots \quad 0\right\}^T\right\} \tag{A7}$$

Assumption (4) implies that the overall anti-symmetric rocking motion of a pile group is controlled by axial motions of the piles. In other word, external moments on the soil-pile composite from its surrounding soil are sustained by the piles which experience alternate push and pull in their axes. External moments due to the anti-symmetric vertical motions $\{\mathbf{w}\}$ are described as:

$$\left\{\frac{\mathbf{M}}{R_0}\right\} = [\mathbf{Q}]\{\mathbf{w}\} \tag{A8}$$

with,

$$[\mathbf{Q}] = \begin{bmatrix} \frac{EI^G}{R_0{}^2 h_1} & -\frac{EI^G}{R_0{}^2 h_1} & 0 & 0 & \cdots & 0 \\ -\frac{EI^G}{R_0{}^2 h_1} & \frac{EI^G}{R_0{}^2 h_1} + \frac{EI^G}{R_0{}^2 h_2} & -\frac{EI^G}{R_0{}^2 h_2} & 0 & & \vdots \\ 0 & -\frac{EI^G}{R_0{}^2 h_2} & \frac{EI^G}{R_0{}^2 h_2} + \frac{EI^G}{R_0{}^2 h_3} & -\frac{EI^G}{R_0{}^2 h_3} & & \vdots \\ 0 & 0 & & & & 0 \\ \vdots & & & & \ddots & -\frac{EI^G}{R_0{}^2 h_{n_L-1}} \\ 0 & \cdots & \cdots & 0 & -\frac{EI^G}{R_0{}^2 h_{n_L-1}} & \frac{EI^G}{R_0{}^2 h_{n_L-1}} + \frac{EI^G}{R_0{}^2 h_{n_L}} \end{bmatrix} \tag{A9}$$

The stiffness parameter EI^G in Equation (A9) is evaluated following the same procedure as that used for the evaluation of bending stiffness of a reinforced concrete beam. Namely, EI^G is assumed to be equal to the sum of the Young's-modulus-weighted products of all the elementary areas times their distances squared from the centroid of the cross-section A_G (**Figure 2.2a**).

Internal moment caused by the lateral motions of the beam appears as external moment ΔM_1 at the pile cap. This moment must be added to M_1. From Equation (A3), ΔM_1 is described as:

$$\Delta M_1 = \left\{1st\ row\ of\ matrix\ [\mathbf{D}]^{-1}[\mathbf{L}]\right\}\{\mathbf{u}\}^T + D_{1,1}^{-1} \cdot \frac{w_1}{R_0} \tag{A10}$$

where, $D_{1,1}^{-1}$ = upper-left corner component of the matrix, $[\mathbf{D}]^{-1}$.

Given Equations (A7), (A8) and (A10), the global stiffness matrix of the equivalent

single beam is finally expressed as:

$$\begin{Bmatrix} \mathbf{p}_x \\ \cdots \\ \dfrac{\mathbf{M}}{R_0} \end{Bmatrix} = \begin{bmatrix} [\mathbf{L}][\mathbf{D}]^{-1}[\mathbf{L}] & \vdots & \text{1st column of } [\mathbf{L}][\mathbf{D}]^{-1}/R_0 \text{ and zeros for other columns} \\ \cdots\cdots & & \cdots\cdots \\ \text{1st row of } [\mathbf{D}]^{-1}[\mathbf{L}]/R_0 \text{ and zeros for other rows} & \vdots & [\mathbf{Q}] \text{ with } D_{1,1}^{-1} \text{ added to its upper - left corner} \end{bmatrix} \begin{Bmatrix} \mathbf{u} \\ \cdots \\ \mathbf{w} \end{Bmatrix} \quad \text{(A11)}$$

APPENDIX II: *Effect of Winkler Spring k_p on Novak's Solution*

Novak's solution gives stiffness k_s for the lateral motion of a massless disk embedded in an infinite horizontal plane. The equation governing the motion of the plane with the inclusion of the disk is expressed in a compact form as:

$$\rho_p \{\ddot{\mathbf{u}}\} = [L]\{\mathbf{u}\} \quad \text{(A12)}$$

where, $[L]$ is a second-order differential spatial operator. In the frequency domain, Equation (A12) is rewritten as:

$$-\omega^2 \rho_p \{\mathbf{u}\} = [L]\{\mathbf{u}\} \quad \text{(A13)}$$

When the plane spreads over uniformly distributed discrete springs k_p, the reaction forces from the springs must be added as:

$$-\omega^2 \rho_p \{\mathbf{u}\} = [L]\{\mathbf{u}\} - k_p \{\mathbf{u}\} \quad \text{(A14)}$$

Transferring $k_p\{\mathbf{u}\}$ in Equation (A14) to the left-hand side, one obtains:

$$\left(k_p - \omega^2 \rho_p\right)\{\mathbf{u}\} = [L]\{\mathbf{u}\} \quad \text{(A15)}$$

Equation (A15) is re-expressed in the following form,

$$-(\omega_0 \eta)^2 \rho_p \{\mathbf{u}\} = [L]\{\mathbf{u}\} \quad \text{(A16)}$$

with $\omega_0 = \dfrac{k_p}{\rho_p}$ (Equation (2.6)) and $\eta = \sqrt{1 - \left(\dfrac{\omega}{\omega_0}\right)^2}$ (Equation (2.9c)).

It is noted that Equation (A16) has the same form as Equation (A13) with ω simply replaced with $\omega_0 \eta$. Thus, substituting $\omega_0 \eta$ in place of ω in Equation (2.8) (Novak's solution), the equation reflects the presence of the Winkler-type springs k_p.

APPENDIX III: *"BASPIA" and "TLEM"*

In the course of this study, the idea of treating a pile group beneath a super-structure as a single upright beam has yielded **BASPIA** (**B**eam **A**nalogy for **S**oil-**P**ile group **I**nteraction **A**nalysis), a program allowing soil-pile group interaction analysis to be made with less time and effort. **BASPIA** includes ***TLEM*** (Thin-Layered Element Method) as a solver that describes a soil stratum as an infinite stratified medium with the inclusion of a cylindrical hollow, in which a foundation is fitted. **BASPIA** with the restricted version of ***TLEM*** for WINDOWS is a freeware that can be downloaded from the from the following URL:

http://norway.iis.u-tokyo.ac.jp/BASPIA.htm

NOTES:

1) **BASPIA**: **B**eam **A**nalogy for **S**oil-**P**ile group **I**nteraction **A**nalysis, © 1998 Kazuo KONAGAI, IIS, University of Tokyo. All rights reserved.
2) This program uses EXCEL (Ver. 7.0 or EXCEL 98) as a post-processor. EXCEL must be installed in your computer in advance. EXCEL and Windows are registered trade marks of Microsoft Corporation.
3) The editor of BASPIA has been developed taking its prototype from ‘vbgrid.vbp’ by Haruhiko HAYASHI in his book ‘Advanced Programming with Visual Basic’, SOFTBANK 1997 (ISBN4-7973-0473-1). No part of this program including this editor may be reproduced or distributed in any form or by any means, or stored in a database or retrieval system, without the prior written permission of Kazuo KONAGAI, Prof., IIS, University of Tokyo, the developer of **BASPIA**.

INSTRUCTIONS FOR DOWNLOADING

(1) Visit the **BASPIA** download page:
http://norway.iis.u-tokyo.ac.jp/BASPIA.htm
(2) You can download both **BASPIA** and its manual (MS Word 97 document file). They are archived by using ZIP.
(3) After getting them stored in an appropriate folder in your computer, double-click them. And you get both automatically extracted in appropriate folders that you designate.
(4) Among those files extracted, find ‘setup.exe’. Double-click it, and you get **BASPIA** installed just by following instructions displayed one after another.
(5) A password is needed to run **BASPIA**. The default password is ‘**opensesame**’. You can change it from a hidden credits screen of **BASPIA**. This method, however, is secret. If you want to get your own password, e-mail me at **konagai@iis.u-tokyo.ac.jp**.

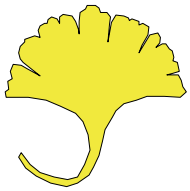

BASPIA for Windows

(Beam **A**nalogy for **S**oil-**P**ile group **I**nteraction **A**nalysis**)**

(Ver. 1.2B)

Kazuo KONAGAI

Dec. 28, 1998

Konagai Laboratory
Institute of Industrial Science
University of Tokyo

BASPIA for Windows (Solver: ***TLEM*** ver. 1.2)

BASPIA (**B**eam **A**nalogy for **S**oil-**P**ile group **I**nteraction **A**nalysis) offers a point-and-click **G**raphical-**U**sers-**I**nterface to ***TLEM*** (Ver. 1.2) that allows soil - pile group interaction to be rigorously evaluated in the frequency domain. The original series of ***TLEM*** programs (Vers. 1.0, 1.1 and 1.2, FORTRAN77) have been developed on the basis of the **T**hin **L**ayered **E**lement **M**ethod for the analyses of soil-embedded foundation interactions. Embedded foundations include upright vaults, mat foundations and pile foundations as well.

Piles, grouped beneath a superstructure, interact with the surrounding soil during an earthquake. Straight-forward evaluation of the pile-soil-pile interaction, however, is cumbersome especially in dealing with tens or hundreds of piles groped together. In ***BASPIA for Windows*** (***TLEM*** Ver. 1.2) a group of piles is viewed as an upright **Equivalent Single Beam**.

When you click the BASPIA icon, you will see the following window popping up.

Then, type the allotted password in the bottom text-box.

And you will get the following tag "**Post proc.**" automatically clicked.

Though the original versions of *TLEM* provide a variety of output files, this version of ***BASPIA for Windows*** allows you to examine dynamic **(1) pile cap stiffnesses** and **(2) effective input motions** which are graphically displayed by using **EXCEL** as a post-processor. **EXCEL** is thus needed to be installed in your computer in advance. Check if the correct path is displayed in the bottom text box. If not, type the correct path.

Then, click **OK**, and the third tab "**BASPIA**" comes up.

And you are ready to edit data files for ***BASPIA***. Needless to say, you are not allowed in

this stage to examine any output data without them. Click "**Edit data files**" to start the editor of ***BASPIA***.

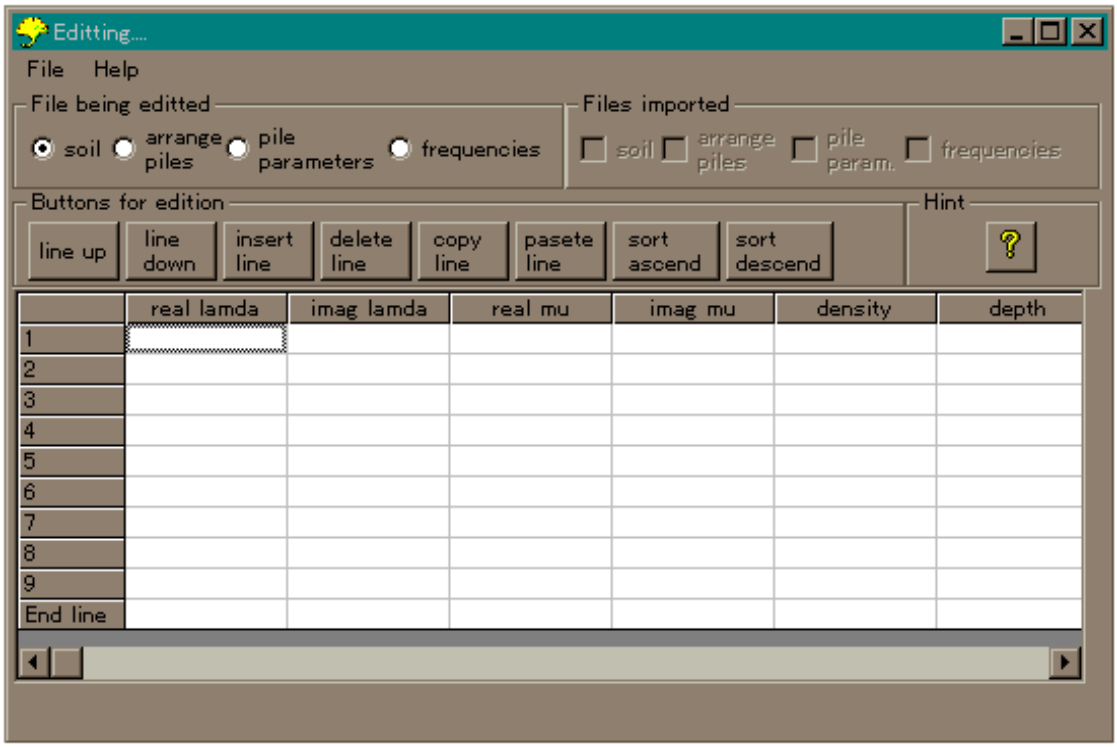

The following four data sets are to be prepared for running ***BASPIA for Windows***.

1. soil
2. pile arrangement
3. pile properties
4. frequencies

Units of the necessary parameters should be consistent with each other.

The editor allows you to line-edit necessary data. See **[Edit buttons]** and **[Key for edition]**

As the four data files are created in order, corresponding square check-boxes in the upper right area of the window are checked one by one. After creating all four files, you are allowed to exit the editor and to run ***BASPIA for Windows***. If you get lost in editing files, use **"What's this?" Help** ([**?**] button) that offers you important hints to get rid of your trouble.

1. soil

Parameters describing **soil properties** must be given layer by layer:

Lamda (real lamda, imag. Lamda) = Lamda of Lames constants. Complex number. (tf/m^2)
mu (real mu, imag. mu) = shear modulus of soil. Complex number. (tf/m^2)
density = Density of soil. Real number. (tf s^2/m^4)
depth = Depth of lower end of layer. Real number. (m)

2. pile arrangement

Locations of piles are described in ***x-y*** coordinates. When inertia interaction is concerned, lateral

force is assumed to be applied to a pile cap in *x* direction.

3. pile properties

Parameters describing **pile properties** must be given layer by layer:
outer radius = outer diameter of a single pile (m)
inner radius = inner radius of a single pile (m)
Young (Real Young, imag. Young) = Young's modulus of pile material. Complex number (tf/m^2)
density = density of pile material ($tf\ s^2/m^4$)

4. frequencies

BASPIA for Windows provides frequency-domain solutions of important soil-structure interaction parameters. It is therefore necessary to specify the following **frequencies**:
No of omegas = number of circular frequencies to be checked out. Integer value.
particular freq. = at this step of frequency-domain computation, a data file "space_dsp.dat" storing spatial distribution of soil displacement will be created.
initial omega = initial value of circular frequency
increment omega = incremental circular frequency

[Edit buttons]

Buttons for editing data files

line up	Moves the selected line one grid unit up.
Line down	Moves the selected line one grid unit down
insert line	Inserts a new empty line immediately above the selected insertion line
delete line	Deletes the selected line(s)
copy line	Copies the selection (line(s)) to the Clipboard.
Paste line	Pastes the Clipboard contents immediately above the selected insertion line
sort ascend	Sorts in ascending order
sort descend	Sorts in descending order

[Key for edition]

Start edition in the selected cell (Back color of the selected cell = white)

[Space]	Starts edition in the selected cell with the cursor set at the head of the existing string of letters
[Enter]	Starts edition in the selected cell with the cursor set at the end of the existing string of letters
[F2]	= **[Enter]**
[Back space]	Clears the selected cell and starts edition.
[Delete]	= **[Back space]**
others	Starts edition in the selected cell

Edit in the selected cell (Back color of the selected cell = yellow)

[Esc]	Quits editing in the selected cell with everything undone.
[Enter]	Quits editing in the selected cell

[Up arrow]	Quits editing in the selected cell, and moves one grid unit up
[Down arrow]	Quits editing in the selected cell, and moves one grid unit down
[Others]	Continues typing

When you returned from the **Editor**, you are now ready to run "***BASPIA***". Click "**Run BASPIA**" button.

After running ***BASPIA***, you will see the "Show result" button is enabled to be clicked.

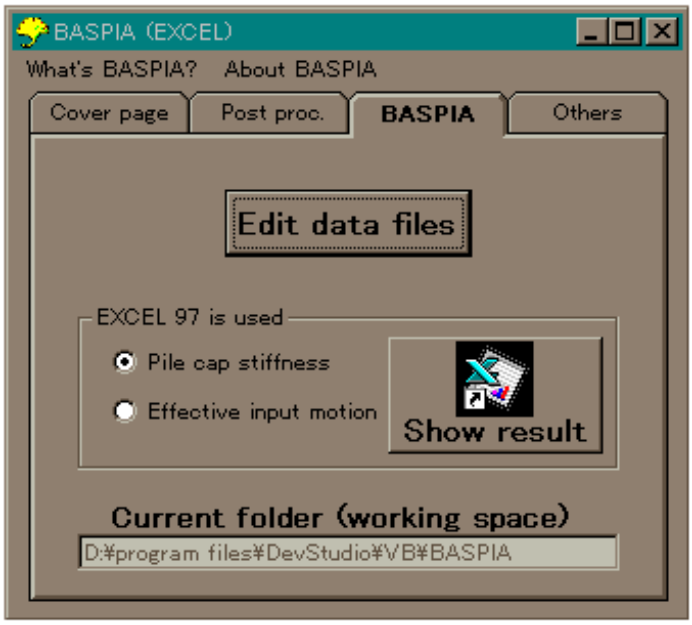

Then, click **"Show reslt"** button, and you can examine the result by using **EXCEL**.

Good Luck !

Program manual No. 6

Guide to "TLEM1.2"

(SOLVER in ***BASPIA***)

by

Kazuo KONAGAI

July 12, 1999

Konagai Laboratory
Institute of Industrial Science
University of Tokyo

July 12, 1999

Thin-Layered-Element Method for Dynamic Soil - Pile Group Interaction Analysis (Solver in BASPIA)

Kazuo KONAGAI

1. INTRODUCTION

This note has been prepared for the users of "*TLEM*" (**T**hin-**L**ayer-**E**lement **M**ethod, Ver. 1.2) that allows the soil - pile group interaction effects to be rigorously evaluated. A pile group is assumed to be an upright single beam embedded in a horizontally layered soil deposit with infinite extent.

2. WHAT CAN WE DO WITH "*TLEM*"?

A soil-structure system is divided into two substructures, the super-structure and the unbounded soil extending to infinity; the latter includes an embedded foundation as illustrated in **Fig. 2.1**. In the lower substructure of soil, an earthquake will cause soil displacements $\{\mathbf{u}^f\}$. The foundation embedded in this soil deposit, however, will not follow the free-field deformation pattern. This deviation of the displacements from the free-field soil displacements $\{\mathbf{u}^f\}$ is denoted by $\{\mathbf{u}^s\}$. The mass of the super-structure then causes it to respond dynamically, and the forces $\{\mathbf{P}\}$ transmitted to the lower substructure of soil and foundation will produce further deformation of soil $\{\mathbf{u}^r\}$ (***inertia interaction***) that would not occur in a fixed base structure. Thus, the displacements of soil $\{\mathbf{u}\}$ are eventually expressed by the following equation as:

$$\{\mathbf{u}\} = \{\mathbf{u}^f\} + \{\mathbf{u}^s\} + \{\mathbf{u}^r\} \tag{1.1}$$

In this program, ***TLEM***, a pile group is approximated by a single beam with a circular cross-section of radius R_0 embedded upright in a stratified soil, and this foundation is

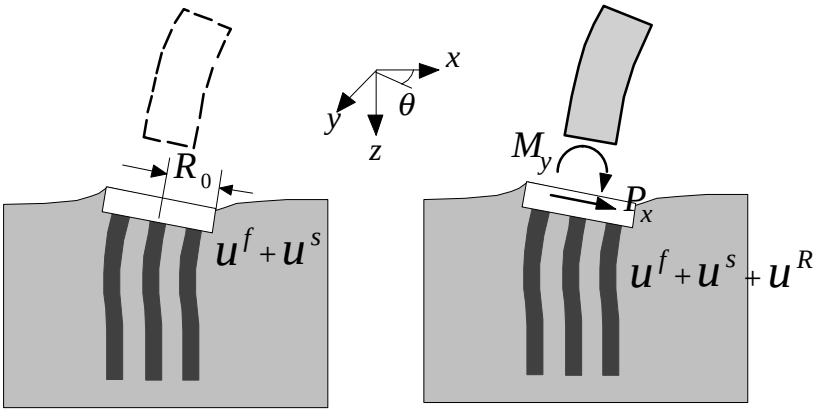

Fig. 2.1 Two primary causes of soil-structure interaction

excited in *x* direction. This assumption calls for the displacement components of the soil and its inclusion to be proportional to either $\cos\theta$ or $\sin\theta$, and it will be shown later on that displacements $\{\mathbf{u}^r\}$ on the wall of the embedded foundation are described in terms of displacement vectors, $\{V_r\}$ and $\{V_z\}$.

The interaction forces $\{\mathbf{p}\}(=\{P_x \quad M_y / R_0\}_{top}^T)$ from the super-structure causes the inertia interaction motions $\{\mathbf{u}^r\}_{top}(=\{V_r \quad V_z\}_{top}^T)$ in the frequency domain as:

$$\begin{Bmatrix} V_r \\ V_z \end{Bmatrix}_{top} = \begin{bmatrix} H_{xx}(s) & H_{xz}(s) \\ H_{zx}(s) & H_{zz}(s) \end{bmatrix} \begin{Bmatrix} P_x \\ \dfrac{M_y}{R_0} \end{Bmatrix}_{top} \tag{2.2}$$

where, $$\begin{bmatrix} H_{xx}(s) & H_{xz}(s) \\ H_{zx}(s) & H_{zz}(s) \end{bmatrix} = [\mathbf{H}] = [\mathbf{S}]^{-1} \tag{2.3}$$

is the flexibility (compliance) at the top of the foundation, with $s = i \cdot \omega$ and $i = \sqrt{-1}$, and ω is the excitement circular frequency.

This program provides the following pieces of information in the frequency domain:

1) **Free-field surface ground motion** $\{\mathbf{u}^f\}$ subjected to a sinusoidal shake given to its bedrock
2) **Foundation motions** $\{\mathbf{u}^f\}+\{\mathbf{u}^s\}$ caused by the free-field ground motion $\{\mathbf{u}^f\}$.
3) **Kinematic displacement factor** T_e for evaluation of the effective input motion $\left(u^f + u^r\right)_{top}$ at the top end of the foundation: $\left(u^f + u^r\right)_{top} = T_e \cdot u^f{}_{surface}$. (2.4)
4) **Flexibility components** H_{xx}, H_{xz} (= H_{zx}) and H_{zz} as well as **stiffness components** S_{xx}, S_{xz} and S_{zz} at the head of the foundation

3. FORMULATION

3.1 Soils

In ***TLEM***, an infinite soil medium surrounding a pile foundation is described by using the Thin-Layered Element Method, a semi-analytical finite element method developed by Tajimi and Shimomura (1976). The major part of this section is, thus, an abridged translation of their original Japanese paper appeared in the *Transaction of Architectural Institute of Japan*, **243**, 1976.

The idealized soil-embedded foundation system is shown in **Fig. 3.1**. In the idealized system, (1) the surrounding soil is divided into a number of homogeneous horizontal sub-layers holding (2) a circular column which is made of the foundation and (3) the soil beneath the bottom end of the foundation. (4) The mechanical features of the column (pile group) are described on the basis of the hypotheses whose description ("**3.2 *Piles Treated as a Single Upright Beam***") will follow this section, and the column has a perfect contact with the surrounding soil. (5) In each sub-layer, linear variation of displacement is assumed with respect to the depth, whereas, 3D equations of motion describe outwardly propagating wave in the radial direction.

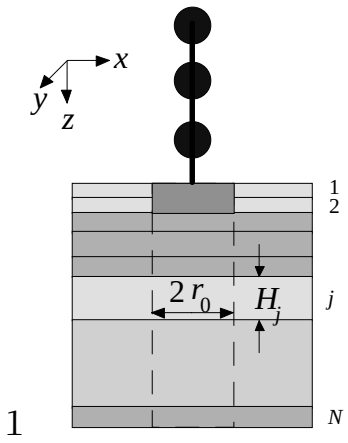

Fig. 3.1 Soil-Structure model

3-1 ***Motion of the Surrounding Soil***

Many wave motion problems regarding soil-circular embedded foundation systems are best described in terms of cylindrical coordinates. The governing equations are thus given as:

$$\left.\begin{aligned}
&(\lambda+2G)\frac{\partial \Theta}{\partial r}-\frac{2G}{r}\frac{\partial \varpi_z}{\partial \theta}+2G\frac{\partial \varpi_\theta}{\partial_z}=\rho\frac{\partial^2 u_r}{\partial t^2}\\
&(\lambda+2G)\frac{1}{r}\frac{\partial \Theta}{\partial \theta}-2G\frac{\partial \varpi_r}{\partial_z}+2G\frac{\partial \varpi_z}{\partial r}=\rho\frac{\partial^2 u_\theta}{\partial t^2}\\
&(\lambda+2G)\frac{\partial \Theta}{\partial z}-\frac{2G}{r}\frac{\partial}{\partial r}(r\varpi_\theta)+\frac{2G}{r}\frac{\partial \varpi_r}{\partial \theta}=\rho\frac{\partial^2 u_z}{\partial t^2}
\end{aligned}\right\} \qquad (3.1)$$

where,

$$\Theta=\frac{1}{r}\frac{\partial}{\partial r}(ru_r)+\frac{1}{r}\frac{\partial u_\theta}{\partial \theta}+\frac{\partial u_z}{\partial_z}$$

$$2\tilde{\omega}_r=\frac{1}{r}\frac{\partial u_z}{\partial \theta}-\frac{\partial u_\theta}{\partial_z},\quad 2\varpi_\theta=\frac{\partial u_r}{\partial_z}-\frac{\partial u_z}{\partial_r}$$

$$2\varpi_z=\frac{1}{r}\frac{\partial}{\partial r}(ru_\theta)-\frac{1}{r}\frac{\partial u_r}{\partial \theta}$$

Lame's constants λ and G are complex numbers whose imaginary parts describe internal damping of soil. The soil-foundation system is assumed to be excited in x direction (**Fig. 3.1**), and the displacement components of soil are described in terms of potential functions as:

$$\begin{bmatrix}u_r\\u_\theta\\u_z\end{bmatrix}=\begin{bmatrix}\cos\theta & 0\\ & \sin\theta\\0 & \cos\theta\end{bmatrix}\begin{bmatrix}v_r\\v_\theta\\v_z\end{bmatrix}e^{i\omega t} \qquad (3.2)$$

$$\begin{bmatrix} v_r \\ v_\theta \\ v_z \end{bmatrix} = \begin{bmatrix} H_2^{(2)}(\alpha\gamma) & H_0^{(2)}(\alpha\gamma) & 0 \\ H_2^{(2)}(\alpha\gamma) & -H_0^{(2)}(\alpha\gamma) & 0 \\ 0 & & H_1^{(2)}(\alpha\gamma) \end{bmatrix} \begin{bmatrix} \phi(z) \\ \varphi(z) \\ W(z) \end{bmatrix} \tag{3.3}$$

in which, $H_j^{(2)}(\alpha r)$ is the second kind Hankel function of order *j*.

Substituting equations (3.2) and (3.3) into equation (3.1), one obtains:

$$\alpha^2 G(\phi+\varphi) - G\frac{d^2}{dz^2}(\phi+\varphi) - \rho\omega^2(\phi+\varphi) = 0 \tag{3.4}$$

$$\alpha^2(\lambda+2G)(\phi-\varphi) - G\frac{d^2}{dz^2}(\phi-\varphi) + \alpha(\lambda+G)\frac{dW}{dz} - \rho\omega^2(\phi-\varphi) = 0 \tag{3.5}$$

$$-\alpha(\lambda+G)\frac{d}{dz}(\phi-\varphi) + \alpha^2 GW - (\lambda+G)\frac{d^2W}{dz^2} - \rho\omega^2 W = 0 \tag{3.6}$$

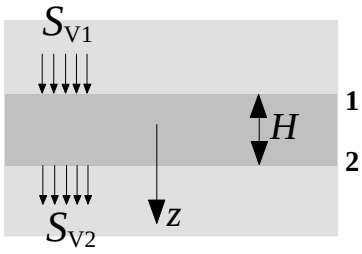

Fig. 3.2 Soil slice

Layer boundary forces-displacements relationship is obtained by using Galarkin's method. First, surface tractions in *p*-direction on both boundaries ($j = 1, 2$) of a sub-layer with the thickness H are denoted by S_{jp} (**Fig. 3.2**). Unit nodal-point displacement causes the sub-layer to be deformed into a prescribed shape of N_j. Thus, the equilibrium condition of virtual work is obtained by multiplying the equation of motion (equation (3.4), (3.5) or (3.6)) by N_j and integrating it over the entire extent of the element H as:

$$\int_{-H/2}^{H/2} -N_j F_p dz = \{K_{jp}\}^T \{U\} - s_{jp} = 0 \tag{3.7}$$

where, F_p is the equation of motion, and

$$N_j = \begin{cases} 1/2 - z/H & (j=1) \\ 1/2 + z/H & (j=2) \end{cases}$$

$\{K_{jp}\}$ = element stiffness matrix to be obtained,

$\{U\}$ = nodal point (boundary surface) displacements.

Just for preliminary arrangement, stress components are described in terms of potential functions:

$$\sigma_{zr} = G\left(\frac{\partial v_r}{\partial z} + \frac{\partial v_z}{\partial r}\right) = G\left[\left(\frac{d\phi}{dz} - \frac{\alpha}{2}W\right)H_2^{(2)}(\alpha r) + \left(\frac{d\varphi}{dz} + \frac{\alpha}{2}W\right)H_0^{(2)}(\alpha r)\right]$$

$$\sigma_{z\theta} = G\left(\frac{1}{r}\frac{\partial v_z}{\partial \theta} + \frac{\partial v_\theta}{\partial z}\right) = G\left[\left(\frac{d\phi}{dz} - \frac{\alpha}{2}W\right)H_2^{(2)}(\alpha r) + \left(\frac{d\varphi}{dz} + \frac{\alpha}{2}W\right)H_0^{(2)}(\alpha r)\right]$$

$$\sigma_{zz} = \lambda\left(\frac{1}{r}\frac{\partial}{\partial r}(rv_r) + \frac{v_\theta}{r} + \frac{\partial v_z}{\partial z}\right) + 2G\frac{\partial v_z}{\partial z} = \left[\lambda\alpha(\phi - \varphi) + (\lambda + 2G)\frac{dW}{dz}\right]H_1^{(2)}(\alpha r)$$

(3.8), (3.9), (3.10)

Equations (3.8), (3.9) and (3.10) are rewritten in the following matrix form as:

$$\begin{bmatrix}\sigma_{zr}\\ \sigma_{z\theta}\\ \sigma_{zz}\end{bmatrix} = \frac{1}{2}\begin{bmatrix} H_2^{(2)}(\alpha\gamma) - H_0^{(2)}(\alpha\gamma) & H_2^{(2)}(\alpha\gamma) + H_0^{(2)}(\alpha\gamma) & 0\\ H_2^{(2)}(\alpha\gamma) + H_0^{(2)}(\alpha\gamma) & H_2^{(2)}(\alpha\gamma) - H_0^{(2)}(\alpha\gamma) & 0\\ 0 & 0 & 2H_1^{(2)}(\alpha\gamma)\end{bmatrix}\begin{bmatrix}\tilde{\sigma}_1\\ \tilde{\sigma}_2\\ \tilde{\sigma}_3\end{bmatrix}$$

$$\tilde{\sigma}_1 = G\left[\frac{d}{dz}(\phi - \varphi) - \alpha W\right] \quad , \quad \tilde{\sigma}_2 = G\frac{d}{dz}(\phi + \varphi) \quad , \quad \tilde{\sigma}_3 = \alpha\lambda(\phi - \varphi) + (\lambda + 2G)\frac{dW}{dz}$$

(3.11), (3.12)

From equation (3), displacements are also described in similar manner as:

$$\begin{bmatrix}v_r\\ v_\theta\\ v_z\end{bmatrix} = \frac{1}{2}\begin{bmatrix} H_2^{(2)}(\alpha\gamma) - H_0^{(2)}(\alpha\gamma) & H_2^{(2)}(\alpha\gamma) + H_0^{(2)}(\alpha\gamma) & 0\\ H_2^{(2)}(\alpha\gamma) + H_0^{(2)}(\alpha\gamma) & H_2^{(2)}(\alpha\gamma) - H_0^{(2)}(\alpha\gamma) & 0\\ 0 & 0 & 2H_1^{(2)}(\alpha\gamma)\end{bmatrix}\begin{bmatrix}\phi - \varphi\\ \phi + \varphi\\ W\end{bmatrix}$$

(3.13)

It is noted that matrices in equations (3.11) and (3.13) are identical with each other, which fact eventually allows Galarkin's method (equation (3.7)) to be applied to the transformed equations described in terms of the transformed traction $(\tilde{\sigma}_1 \quad \tilde{\sigma}_2 \quad \tilde{\sigma}_3)$ and the displacement $(\phi - \psi \quad \phi + \psi \quad W)$. The transformed tractions and the displacements are described on the layer boundaries as:

$$\begin{bmatrix}\tilde{\sigma}_{11}\\ \tilde{\sigma}_{21}\end{bmatrix} = G\begin{bmatrix}\frac{d}{dz}(\phi - \varphi)\big|_1 - \alpha W_1\\ \frac{d}{dz}(\phi - \varphi)\big|_2 - \alpha W_2\end{bmatrix}, \begin{bmatrix}\tilde{\sigma}_{12}\\ \tilde{\sigma}_{22}\end{bmatrix} = G\begin{bmatrix}\frac{d}{dz}(\phi - \varphi)\big|_1\\ \frac{d}{dz}(\phi - \varphi)\big|_2\end{bmatrix}, \begin{bmatrix}\tilde{\sigma}_{13}\\ \tilde{\sigma}_{23}\end{bmatrix} = \begin{bmatrix}-\alpha\lambda(\phi - \varphi)_1 - (\lambda + 2G)\frac{dW}{dz}\big|_1\\ \alpha\lambda(\phi - \varphi)_2 + (\lambda + 2G)\frac{dW}{dz}\big|_2\end{bmatrix}$$

(3.14)

The transformed displacements within the sub-layer are described in terms of prescribed shape functions N_1 and N_2 as:

$$\begin{bmatrix}\phi\\ \varphi\\ W\end{bmatrix} = N_1\begin{bmatrix}\phi_1\\ \varphi_1\\ W_1\end{bmatrix} + N_2\begin{bmatrix}\phi_2\\ \varphi_2\\ W_2\end{bmatrix} \quad , \quad N_1 = \frac{1}{2} - \frac{z}{H} \quad , \quad N_2 = \frac{1}{2} + \frac{z}{H} \qquad (3.15)$$

As an example, Galarkin's method is applied to equation (3.5) in which equation (3.15) is substituted. Equation (3.7) thus is written for $j = 1$ as:

$$\int_{-2/H}^{2/H} N_1 F_1 dz = \alpha^2(\lambda+2G)\frac{H}{3}(\phi_1-\varphi_1)+\alpha^2(\lambda+2G)\frac{H}{6}(\phi_2-\varphi_2)+\frac{G}{H}(\phi_1-\varphi_1)-\frac{G}{H}(\phi_2-\varphi_2)$$
$$+\alpha\frac{\lambda+G}{2}(W_2-W_1)-\rho\omega^2\frac{H}{3}(\phi_1-\varphi_1)-\rho\omega^2\frac{H}{6}(\phi_2-\varphi_2)+G\frac{d}{dz}(\phi-\varphi)\Big|_1 \tag{3.16}$$

A similar expression is obtained for $j=2$. From equation (3.14), these expressions for $j=1$ and $j=2$ are arranged in the following matrix form as:

$$\alpha^2(\lambda+2G)\frac{H}{6}\begin{bmatrix}2 & 1\\ 1 & 2\end{bmatrix}\begin{bmatrix}\phi_1-\varphi_1\\ \phi_2-\varphi_2\end{bmatrix}+\frac{G}{H}\begin{bmatrix}1 & -1\\ -1 & 1\end{bmatrix}\begin{bmatrix}\phi_1-\varphi_1\\ \phi_2-\varphi_2\end{bmatrix}$$
$$+\alpha\begin{bmatrix}-(\lambda-G)/2 & (\lambda+G)/2\\ -(\lambda+G)/2 & (\lambda-G)/2\end{bmatrix}\begin{bmatrix}W_1\\ W_2\end{bmatrix}-\rho\omega^2\frac{H}{6}\begin{bmatrix}2 & 1\\ 1 & 2\end{bmatrix}\begin{bmatrix}\phi_1-\varphi_1\\ \phi_2-\varphi_2\end{bmatrix}=\begin{bmatrix}\tilde{\sigma}_{11}\\ \tilde{\sigma}_{21}\end{bmatrix} \tag{3.17}$$

Similarly, one obtains the following equation from equation (3.4):

$$\left(\alpha^2[A_s]^e+[G_s]^e-\omega^2[M]^e\right)\{\phi+\varphi\}^e=\{\tilde{\sigma}_2\} \tag{3.18}$$

where,

$$[A_s]^e=GH\frac{H}{6}\begin{bmatrix}2 & 1\\ 1 & 2\end{bmatrix}\quad,\quad [G_s]^e=\frac{G}{H}\begin{bmatrix}1 & -1\\ -1 & 1\end{bmatrix}$$
$$[M]^e=\rho H\frac{1}{6}\begin{bmatrix}2 & 1\\ 1 & 2\end{bmatrix}\quad,\quad \{\phi+\varphi\}^e=\begin{bmatrix}\phi_1+\varphi_1\\ \phi_2+\varphi_2\end{bmatrix}$$

The above matrices with superscript *e* imply that they are expressions for a particular sub-layer element. Using similar notations, transformed equations (3.5) and (3.6) are written as:

$$\left(\alpha^2[A_p]^e+[G_s]^e-\omega^2[M]^e\right)\{\phi-\varphi\}^e-\alpha\left([B]^e\right)^T\{W\}^e=\{\tilde{\sigma}_1\}$$
$$-\alpha[B]^e\{\phi-\varphi\}^e+\left(\alpha^2[A_s]^e+(\lambda+2G)\frac{H}{6}\begin{bmatrix}2 & 1\\ 1 & 2\end{bmatrix}-\omega^2[M]^e\right)\{W\}^e=\{\tilde{\sigma}_3\} \tag{3.19), (3.20}$$

where,

$$\left[A_p\right]^e=(\lambda+2G)\frac{H}{6}\begin{bmatrix}2 & 1\\ 1 & 2\end{bmatrix}$$
$$[G_p]^e=\frac{\lambda+2G}{H}\begin{bmatrix}1 & -1\\ -1 & 1\end{bmatrix}\quad,\quad \{\phi-\varphi\}^e=\begin{bmatrix}\phi_1-\varphi_1\\ \phi_2-\varphi_2\end{bmatrix}$$
$$[B]^e=\begin{bmatrix}(\lambda-G)/2 & (\lambda+G)/2\\ -(\lambda+G)/2 & -(\lambda-G)/2\end{bmatrix}\quad,\quad \{W\}^e=\begin{bmatrix}W_1\\ W_2\end{bmatrix}$$

The global equation of motion is then assembled with all element matrices provided. In this procedure, the layer-boundary displacements are arranged in the following order as:

$$\left.\begin{aligned}\{\phi-\varphi\}&=(\phi_1-\varphi_1,\phi_2-\varphi_2,\cdots,\phi_N-\varphi_N)^T\\ \{\phi+\varphi\}&=(\phi_1+\varphi_1,\phi_2+\varphi_2,\cdots,\phi_N+\varphi_N)^T\\ \{W\}&=(W_1,W_2,\cdots,W_N)^T\end{aligned}\right\} \tag{3.21}$$

in which, the subscripts, 1, 2, ... , N denote the numbers of layer boundaries starting from the ground surface. The displacement vectors are rewritten by using simpler notations as:

$$\{\phi-\varphi\}=\{X\},\quad \{\phi+\varphi\}=\{Y\},\quad \{W\}=\{Z\} \tag{3.22}$$

The global equations of motion are thus obtained by putting element matrices with the superscript *e* at the proper positions in the global matrix (**Fig. 3.3**) as:

$$\begin{aligned}&\left(\beta^2[A_s]+[G_s]-\omega^2[M]\right)\{Y\}=0\\ &\left(\alpha^2[A_p]+[G_s]-\omega^2[M]\right)\{X\}-\alpha[B]^T\{Z\}=0\\ &-\alpha[B]\{X\}+\left(\alpha^2[A_s]+[G_p]-\omega^2[M]\right)\{Z\}=0\end{aligned} \tag{3.23), (3.24), (3.25}$$

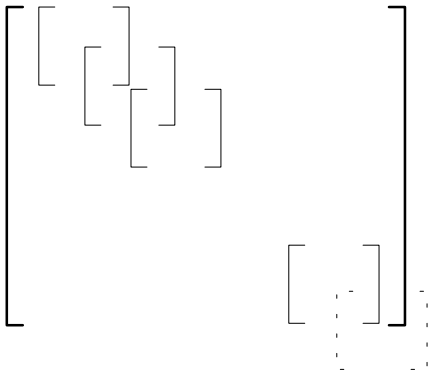

Fig. 3.3 Global matrix

The above equations are solved in the manner of an eigen-value problem, and it is noted that equation (3.23), of which eigen values are denoted by β, is completely independent of the mutually coupled equations (3.24) and (3.25) having the common eigen-values of α. Elimination of $\{Z\}$ in equations (24) and (25) leads to:

$$\begin{aligned}&\left(\alpha^4 S_4+\alpha^2 S_2+S_0\right)\{X\}=0\\ &S_4=[A_s]\left([B]^{-1}\right)^T[A_p]\\ &S_2=[A_s]\left([B]^{-1}\right)^T[G_s]+[G_p]\left([B]^{-1}\right)^T[A_p]\\ &-\omega^2[A_s]\left([B]^{-1}\right)^T[M]-\omega^2[M]\left([B]^{-1}\right)^T[A_p]-[B]\\ &S_0=\left([G_p]-\omega^2[M]\right)\left([B]^{-1}\right)^T\left([G_s]-\omega^2[M]\right)\end{aligned} \tag{3.26), (3.27}$$

A similar expression is also obtained by eliminating $\{X\}$:

$$\left(\alpha^4 S_4 + \alpha^2 S_2 + S_0\right)\{Z\} = 0$$

$$S_4 = \left[A_p\right][B]^{-1}\left[A_s\right]$$

$$S_2 = \left[A_p\right][B]^{-1}\left[G_p\right] + \left[G_s\right][B]^{-1}\left[A_s\right]$$

$$-\omega^2\left[A_p\right][B]^{-1}[M] - \omega^2[M][B]^{-1}\left[A_s\right] - [B]^T$$

$$S_0 = \left(\left[G_s\right] - \omega^2[M]\right)[B]^{-1}\left(\left[G_p\right] - \omega^2[M]\right)$$

Equation (3.26) is written in the following 2N×2N characteristic equations:

$$\left(\begin{bmatrix} 0 & S_0 \\ S_0 & S_2 \end{bmatrix} - \alpha^2 \begin{bmatrix} S_0 & 0 \\ 0 & -S_4 \end{bmatrix}\right)\begin{bmatrix} \{X\} \\ \{\hat{X}\} \end{bmatrix} = 0 \tag{3.29}$$

where, $\{\hat{X}\} = \alpha^2\{X\}$

Since equation (3.29) contains complex Lame's constants, 2N complex squared eigen-values, α^2, are obtained. This means that there exist total 4N solutions of α. The condition that the soil displacement converges on zero at $r \to \infty$ requires that the appropriate eigen-values must have negative imaginary parts. Thus, imposing this requirement yields the number of appropriate eigen-values to be cut by half (2N).

Boundary Conditions on the Upright Cylindrical Hollow

A foundation with a circular cross-section is assumed to be embedded upright in the stratified soil. Thus, the force-displacement relationship is to be obtained on the wall of the cylindrical hollow. Since the displacement components on the wall are proportional to either $\cos\theta$ or $\sin\theta$, displacements are described in terms of $(v_r \quad v_\theta \quad v_z)$. Thus displacement vectors, $\{V_r\}$, $\{V_\theta\}$, $\{V_z\}$, used in this formulation contain layer boundary displacement components. These displacement vectors are expressed in terms of the eigen-vectors of the stratified soil as:

$$\left.\begin{aligned}
\{V_r\} &= \frac{1}{2}\sum_\alpha \left\{H_2^{(2)}(\alpha R_0) - H_0^{(2)}(\alpha R_0)\right\}\{X\}_\alpha q_\alpha \\
&\quad + \frac{1}{2}\sum_\beta \left\{H_2^{(2)}(\beta R_0) + H_0^{(2)}(\beta R_0)\right\}\{Y\}_\beta q_\beta \\
\{V_\theta\} &= \frac{1}{2}\sum_\alpha \left\{H_2^{(2)}(\alpha R_0) + H_0^{(2)}(\alpha R_0)\right\}\{X\}_\alpha q_\alpha \\
&\quad + \frac{1}{2}\sum_\beta \left\{H_2^{(2)}(\beta R_0) - H_0^{(2)}(\beta R_0)\right\}\{Y\}_\beta q_\beta \\
\{V_z\} &= \sum_\alpha H_1^{(2)}(\alpha R_0)\{Z\}_\alpha q_\alpha
\end{aligned}\right\} \tag{3.30}$$

where, $\{X\}_\alpha$ and $\{Z\}_\alpha$ are the mutually coupled eigen-vectors corresponding to an eigen-value α, and the eigen-vector $\{Y\}_\beta$ corresponds to an eigen-value β. The effective contributions of these eigen-vectors are denoted by q_α and q_β, respectively.

A modal matrix is defined as:

$$\left.\begin{aligned}[X]&=\left[\{X\}_1,\{X\}_2,\cdots,\{X\}_{2N}\right]\\ [Y]&=\left[\{Y\}_1,\{Y\}_2,\cdots,\{Y\}_{2N}\right]\\ [Z]&=\left[\{Z\}_1,\{Z\}_2,\cdots,\{Z\}_{2N}\right]\end{aligned}\right\} \tag{3.31}$$

where, the dimensions of matrices $[X]$ and $[Z]$ are $N\times 2N$, whereas that of $[Z]$ is $N\times N$. Equation (3.30) is further simplified by virtue of the mathematical conveniences of Hankel functions, which are described as:

$$\left.\begin{aligned}\frac{H_2^{(2)}(\alpha R_0)+H_0^{(2)}(\alpha R_0)}{\dfrac{H_1^{(2)}(\alpha R_0)}{\alpha r_0}}&=2\\ \frac{H_2^{(2)}(\alpha R_0)-H_0^{(2)}(\alpha R_0)}{\dfrac{H_1^{(2)}(\alpha R_0)}{\alpha R_0}}&=2f_\alpha\end{aligned}\right\} \tag{3.32}$$

$$f_\alpha=1-\alpha R_0\frac{H_0^{(2)}(\alpha R_0)}{H_1^{(2)}(\alpha R_0)}\quad,\quad f_\beta 1-\beta R_0\frac{H_0^{(2)}(\beta R_0)}{H_1^{(2)}(\beta R_0)}$$

$$\tilde{q}_\alpha=q_\alpha\frac{H_1^{(2)}(\alpha R_0)}{\alpha R_0}\quad,\quad \tilde{q}_\beta=q_\beta\frac{H_1^{(2)}(\beta R_0)}{\beta R_0}$$

Introducing the newly defined parameters shown above, equation (3.30) is rewritten in the following matrix form as:

$$\begin{bmatrix}\{V_r\}\\ \{V_\theta\}\\ \{V_z\}\end{bmatrix}=\begin{bmatrix}[X]\left[\ddots f\alpha_{\cdot\cdot}\right] & [Y]\\ [X] & [Y]\left[\ddots f_\beta \ddots\right]\\ [Z]\left[\ddots \alpha R_0 \ddots\right] & 0\end{bmatrix}\begin{bmatrix}\{\tilde{q}_\alpha\}\\ \{\tilde{q}_\beta\}\end{bmatrix} \tag{3.33}$$

It is assumed that the cross-section of the cylindrical hollow is kept completely circle. This assumption requires the following equation to be satisfied.

$$\{V_r\}+\{V_\theta\}=0 \tag{3.34}$$

Substituting equation (3.34) in equation (3.33) yields:

$$[X]\left[\ddots 1+f_\alpha\ddots\right]\{\tilde{q}_\alpha\}+[Y]\left[\ddots 1+f_\beta\ddots\right]\{\tilde{q}_\beta\}=0 \tag{3.35}$$

From equation (35), $\{\tilde{q}_\alpha\}$ is described in terms of $\{\tilde{q}_\beta\}$ as:

$$\{\tilde{q}_\beta\}=-\left[\ddots 1+f_\beta\ddots\right]^{-1}[Y]^{-1}[X]\left[\ddots 1+f_\beta\ddots\right]\{\tilde{q}_\alpha\}=[E]\{\tilde{q}_\alpha\} \tag{3.36}$$

where, matrix $[E]$ has the dimension of $N\times 2N$. Equation (3.33) is degenerated into $2N\times 2N$ matrix form as:

$$\begin{bmatrix}\{V_r\}\\ \{V_z\}\end{bmatrix}=\begin{bmatrix}[X]\left[\ddots f\alpha_{\cdot\cdot}\right]+[Y][E]\\ [Z]\left[\ddots \alpha R_0 \ddots\right]\end{bmatrix}\cdot\{\tilde{q}_\alpha\}=[J_H]\{\tilde{q}_\alpha\} \tag{3.37}$$

Tractions $(p_r \quad p_\theta \quad p_z)$ on the wall of the cylindrical cavity are expressed as:

$$\begin{bmatrix}\sigma_{rr}\\ \sigma_{r\theta}\\ \sigma_{rz}\end{bmatrix} = -\begin{bmatrix}\cos\theta & 0 & \\ & \sin\theta & \\ 0 & & \cos\theta\end{bmatrix}\begin{bmatrix}P_r\\ P_\theta\\ P_z\end{bmatrix} \tag{3.38}$$

From equation (3.13), one can describe the tractions in terms of the transformed displacements $\phi-\psi$, $\phi+\psi$ and W as:

$$\begin{aligned}P_r &= -\left[\lambda\left(\frac{1}{r}\frac{\partial}{\partial r}(r v_r)+\frac{v_\theta}{r}+\frac{\partial v_z}{\partial z}\right)+2G\frac{\partial v_r}{\partial r}\right]_{r=R_0}\\ &= \left(\frac{2G}{R_0}H_2^{(2)}(\alpha R_0)-(\lambda+2G)\alpha H_1^{(2)}(\alpha R_0)\right)(\phi-\varphi)\\ &\quad+\frac{2G}{R_0}H_2^{(2)}(\beta R_0)(\phi+\varphi)-\lambda\frac{dW}{dz}H_1^{(2)}(\alpha R_0)\end{aligned} \tag{3.39}$$

$$\begin{aligned}P_\theta &= -G\left(\frac{\partial v_\theta}{\partial r}-\frac{v_\theta+v_r}{r}\right)_{r=R_0}\\ &= \frac{2G}{R_0}H_2^{(2)}(\alpha R_0)(\phi-\varphi)\\ &\quad+\left(\frac{2G}{R_0}H_2^{(2)}(\beta R_0)-G\beta H_1^{(2)}(\beta R_0)\right)(\phi+\varphi)\end{aligned} \tag{3.40}$$

$$\begin{aligned}P_z &= -G\left(\frac{\partial v_r}{\partial z}+\frac{\partial v_z}{\partial r}\right)_{r=R_0}\\ &= -\frac{G}{2}\left(H_2^{(2)}(\alpha R_0)-H_0^{(2)}(\alpha R_0)\right)\frac{d}{dz}(\phi-\varphi)\\ &= -\frac{G}{2}\left(H_2^{(2)}(\beta R_0)-H_0^{(2)}(\beta R_0)\right)\frac{d}{dz}(\phi+\varphi)\\ &\quad+\frac{G}{2}\alpha\left(H_2^{(2)}(\alpha R_0)-H_0^{(2)}(\alpha R_0)\right)W\end{aligned} \tag{3.41}$$

Given the above equations, resultant lateral force $\overline{P}_x$ in x direction and the moment $\overline{M}_y$ around y axis per unit depth are obtained as:

$$\begin{aligned}\overline{P}_x &= -2\int_{-1/2}^{1/2}\left(\sigma_{rr}\cos\theta-\sigma_{r\theta}\sin\theta\right)R_0 d\theta\\ &= 2\int_{-1/2}^{1/2}\left(P_r\cos^2\theta-P_\theta\sin^2\theta\right)R_0 d\theta\\ &= \pi R_0(P_r-P_\theta)\end{aligned} \tag{3.42}$$

$$\begin{aligned}\overline{M}_y &= -2\int_{-1/2}^{1/2}\sigma_{rz}R_0\cos\theta\,R_0 d\theta\\ &= 2\int_{-1/2}^{1/2}P_r R_0^{\,2}\cos^2\theta\,d\theta=\pi R_0 P_z\end{aligned} \tag{3.43}$$

$$\begin{aligned} P_r - P_\theta &= -(\lambda+2G)\alpha H_1^{(2)}(\alpha R_0)(\phi-\varphi) \\ &\quad + G\beta H_1^{(2)}(\beta R_0)(\phi+\varphi) - \lambda\frac{dW}{dz}H_1^{(2)}(\alpha R_0) \end{aligned} \tag{3.44}$$

The sub-layer boundary forces are then obtained by multiplying equations (3.42)-(3.44) by the prescribed shape of displacement N_j and integrating it over the entire thickness of the sub-layer.

$$\left.\begin{aligned} P_{jx} &= \pi R_0 \int_{-H/2}^{H/2} N_j (P_r - P_\theta) dz \\ M_{jy} &= \pi R_0^{\,2} \int_{-H/2}^{H/2} N_j P_z dz \end{aligned}\right\} \tag{3.45}$$

The obtained force-transformed displacement relationship is written in the following element matrix form as:

$$\begin{aligned} \frac{1}{\pi R_0}\{P_x\}^e &= \left(-\alpha\frac{(\lambda+2G)H}{6}\begin{bmatrix}2 & 1\\ 1 & 2\end{bmatrix}\begin{bmatrix}X_1\\ X_2\end{bmatrix} + \frac{\lambda}{2}\begin{bmatrix}1 & -1\\ 1 & -1\end{bmatrix}\begin{bmatrix}Z_1\\ Z_2\end{bmatrix}\right)H_1^{(2)}(\alpha R_0) \\ &\quad + \beta\frac{GH}{6}\begin{bmatrix}2 & 1\\ 1 & 2\end{bmatrix}\begin{bmatrix}Y_1\\ Y_2\end{bmatrix}H_1^{(2)}(\beta R_0) \\ \frac{1}{\pi R_0}\left\{\frac{M_y}{R_0}\right\}^e &= \frac{G}{4}\begin{bmatrix}1 & -1\\ 1 & -1\end{bmatrix}\begin{bmatrix}X_1\\ X_2\end{bmatrix}\cdot\left(H_2^{(2)}(\alpha R_0) - H_0^{(2)}(\alpha R_0)\right) \\ &\quad + \frac{G}{4}\begin{bmatrix}1 & -1\\ 1 & -1\end{bmatrix}\begin{bmatrix}Y_1\\ Y_2\end{bmatrix}\left(H_2^{(2)}(\beta R_0) + H_0^{(2)}(\beta R_0)\right) \\ &\quad + \beta\frac{GH}{12}\begin{bmatrix}2 & 1\\ 1 & 2\end{bmatrix}\begin{bmatrix}Z_1\\ Z_2\end{bmatrix}\left(H_2^{(2)}(\alpha R_0) + H_0^{(2)}(\alpha R_0)\right) \end{aligned}$$

These element matrices are then put in the proper locations in the global matrix.

$$\begin{aligned} \frac{1}{\pi R_0}\{P_x\} &= R_0\left(-[A_p][X]\begin{bmatrix}\ddots & & \\ & \alpha^2 & \\ & & \ddots\end{bmatrix}\right) \\ &\quad + [B_\lambda]^T[Z]\begin{bmatrix}\ddots & & \\ & \alpha & \\ & & \ddots\end{bmatrix}\{\tilde{q}_\alpha\} + R_0\left([A_s][Y]\begin{bmatrix}\ddots & & \\ & \beta^2 & \\ & & \ddots\end{bmatrix}\right)\{\tilde{q}_\beta\} \\ \frac{1}{\pi R_0}\left\{\frac{M_y}{R_0}\right\} &= \left(\frac{1}{2}[B_G]^T[X] + \frac{1}{2}[A_s][Z]\begin{bmatrix}\ddots & & \\ & \alpha & \\ & & \ddots\end{bmatrix}\right)\cdot\begin{bmatrix}\ddots & & \\ & 2f_\alpha & \\ & & \ddots\end{bmatrix}\{\tilde{q}_\alpha\} \\ &\quad + \frac{1}{2}[B_G]^T[Y]2\{\tilde{q}_\beta\} \end{aligned}$$

where, $[B_\lambda]^e = \frac{\lambda}{2}\begin{bmatrix}1 & 1\\ -1 & -1\end{bmatrix}$, $\quad [B_G]^e = \frac{G}{2}\begin{bmatrix}1 & 1\\ -1 & -1\end{bmatrix}$

These equations are rewritten in the following matrix form as:

$$\begin{aligned} \frac{1}{\pi R_0}\begin{bmatrix}\{P_X\}\\ \left\{\frac{M_y}{R_0}\right\}\end{bmatrix} &= \begin{bmatrix}\left(-[A_p][X]\begin{bmatrix}\ddots & & \\ & \alpha^2 & \\ & & \ddots\end{bmatrix} + [B_\lambda]^T[Z]\begin{bmatrix}\ddots & & \\ & \alpha & \\ & & \ddots\end{bmatrix} + [A_s][Y]\begin{bmatrix}\ddots & & \\ & \beta^2 & \\ & & \ddots\end{bmatrix}[E]\right)R_0 \\ [B_G]^T\left([X]\begin{bmatrix}\ddots & & \\ & f_\alpha & \\ & & \ddots\end{bmatrix} + [Y][E]\right) + [A_s][Z]\begin{bmatrix}\ddots & & \\ & \alpha f_\alpha & \\ & & \ddots\end{bmatrix}\end{bmatrix}\cdot\{\tilde{q}_\alpha\} \\ &= [D_H]\{\tilde{q}_\alpha\} \end{aligned}$$

(3.46)

From equations (3.37) and (3.46), the following layer boundary force-displacement relation is finally obtained.

$$\left.\begin{aligned}\begin{bmatrix}\{P_X\}\\ \left\{\dfrac{M_y}{R_0}\right\}\end{bmatrix} &= [R_H]\begin{bmatrix}\{V_r\}\\ \{V_z\}\end{bmatrix}\\ [R_H] &= \pi R_0 [D_H][J_H]^{-1}\end{aligned}\right\} \tag{3.47}$$

3.2 *Piles Treated as a Single Upright Beam*

Piles, grouped beneath a superstructure, interact with the surrounding soil during an earthquake, and the dynamic pile-soil-pile interaction often affects the motion of the superstructure to a considerable extent. Straight-forward evaluation of the pile-soil-pile interaction, however, is cumbersome especially in dealing with tens or hundreds piles groped together. Hence some simplified approach for the evaluation of such dynamic pile-soil-pile interaction is very much desirable for the purpose of treating the dynamic behavior of an entire soil-foundation-structure system. A number of researches have been carried out with the objective to develop such simplified approaches. These attempts include the Ring-Pile method (Takemiya, 1986) and Closely-Spaced-Plates model (Ohira and Tazo, 1985). In these methods, respectively, piles with the soil caught among them are re-grouped into several concentric cylinders (piles arranged in concentric circles) and soil-pile-striped upright plates, allowing close evaluation of interaction effects to be made with less time and trouble. This chapter presents further simplified approach in which a group of piles is viewed as a single equivalent upright beam.

Stiffness matrix of equivalent single beam

The soil and n_p piles system is divided into n_L horizontal slices as shown in **Fig. 3.4**. The following assumptions are tentatively adopted herein to derive the stiffness matrix of the equivalent single beam:

(1) Pile elements within a horizontal soil slice are deformed all at once keeping their intervals constant, and the soil caught among piles moves in a body with the piles. The cross-section, A_g, of the equivalent single upright beam, thus, comprises both the firmly joined piles and the soil.
(2) Frictional effects due to bending of piles (external moments on each pile from soil) are ignored.
(3) Top ends of the piles are fixed to a rigid cap.
(4) All upper or lower ends of the sliced pile elements arranged on the cut-end of a soil slice remain on one plane (Note this assumption does not necessarily mean that each pile's cross-section remains in parallel with this plane. See **Fig. 3.4(b)**).

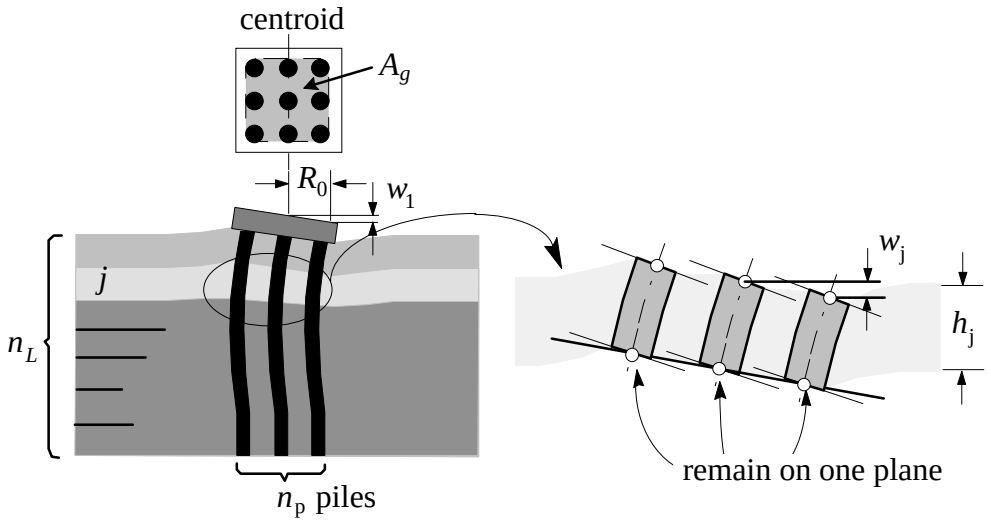

Fig. 3.4 Assumption for evaluation of equivalent single beam

With assumptions (1), (2) and (3), lateral external forces $\{\mathbf{P}_x\}$ are described in terms of lateral displacements $\{\mathbf{u}_x\}$ and anti-symmetric vertical motion of the cap w_1 as:

$$\{\mathbf{P}_x\} = [\mathbf{L}][\mathbf{D}]^{-1}\left\{[\mathbf{L}]\{\mathbf{u}_x\} + \left\{\frac{w_1}{R_0} \quad \vdots \quad 0 \quad \cdots \quad 0\right\}^T\right\} \tag{3.48}$$

where, R_0 is the radius of the equivalent single beam, and is assumed to be identical to the radius of a circle with the same area as the cross-section A_G that includes all the grouped piles enclosed by the broken line in **Fig. 3.4a**, and

$$[\mathbf{L}] = \begin{bmatrix} -\frac{1}{h_1} & \frac{1}{h_1} & 0 & 0 & \cdots & 0 \\ \frac{1}{h_1} & -\frac{1}{h_1}-\frac{1}{h_2} & \frac{1}{h_2} & 0 & & \vdots \\ 0 & \frac{1}{h_2} & -\frac{1}{h_2}-\frac{1}{h_3} & \frac{1}{h_3} & & \vdots \\ 0 & 0 & \ddots & \ddots & \ddots & 0 \\ \vdots & & \ddots & \ddots & \ddots & \frac{1}{h_{n_L-1}} \\ 0 & \cdots & \cdots & 0 & \frac{1}{h_{n_L-1}} & -\frac{1}{h_{n_L-1}}-\frac{1}{h_{n_L}} \end{bmatrix} \tag{3.49a}$$

$$[\mathbf{D}] = \frac{1}{6}\begin{bmatrix} 2\frac{h_1}{EI_p} & \frac{h_1}{EI_p} & 0 & 0 & \cdots & 0 \\ \frac{h_1}{EI_p} & 2\left(\frac{h_1}{EI_p}+\frac{h_2}{EI_p}\right) & \frac{h_2}{EI_p} & 0 & & \vdots \\ 0 & \frac{h_2}{EI_p} & 2\left(\frac{h_2}{EI_p}+\frac{h_3}{EI_p}\right) & \frac{h_3}{EI_p} & & \vdots \\ 0 & 0 & \ddots & \ddots & \ddots & 0 \\ \vdots & & \ddots & \ddots & \ddots & \frac{h_{n_L-1}}{EI_p} \\ 0 & \cdots & \cdots & 0 & \frac{h_{n_L-1}}{EI_p} & 2\left(\frac{h_{n_L-1}}{EI_p}+\frac{h_{n_L}}{EI_p}\right) \end{bmatrix} \tag{3.49b}$$

with $EI_p = n_p \times E_p I_p$ ($E_p I_p$ = bending stiffness of a single pile).

Moment M_1 at the top ends of rigidly capped piles due to the lateral displacements $\{\mathbf{u}_x\}$ is expressed as:

$$M_1 = \left\{ 1st\ row\ of\ matrix\ [\mathbf{D}]^{-1}[\mathbf{L}] \right\} \{\mathbf{u}_x\}^T + D_{1,1}^{-1} \cdot \frac{w_1}{R_0} \tag{3.49c}$$

where, $D_{1,1}^{-1}$ = upper-left corner component of the matrix, $[\mathbf{D}]^{-1}$.

Assumption (4) implies that the overall anti-symmetric rocking motion of a pile group is controlled by axial motions of the piles. In other word, the external moments on the overall soil-pile system from its surrounding soil are eventually sustained by the piles that experience alternate push and pull in their axes. External moments due to the anti-symmetric vertical motions $\{\mathbf{w}\}$ are described as:

$$\left\{ \frac{\mathbf{M}}{R_0} \right\} = [\mathbf{Q}]\{\mathbf{w}\} \tag{3.50}$$

where,

$$[\mathbf{Q}] = \begin{bmatrix} \frac{EI^G}{{R_0}^2 h_1} & -\frac{EI^G}{{R_0}^2 h_1} & 0 & 0 & \cdots & 0 \\ -\frac{EI^G}{{R_0}^2 h_1} & \frac{EI^G}{{R_0}^2 h_1} + \frac{EI^G}{{R_0}^2 h_2} & -\frac{EI^G}{{R_0}^2 h_2} & 0 & & \vdots \\ 0 & -\frac{EI^G}{{R_0}^2 h_2} & \frac{EI^G}{{R_0}^2 h_2} + \frac{EI^G}{{R_0}^2 h_3} & -\frac{EI^G}{{R_0}^2 h_3} & & \vdots \\ 0 & 0 & & & & 0 \\ \vdots & & & & \ddots & -\frac{EI^G}{{R_0}^2 h_{n_L-1}} \\ 0 & \cdots & \cdots & 0 & -\frac{EI^G}{{R_0}^2 h_{n_L-1}} & \frac{EI^G}{{R_0}^2 h_{n_L-1}} + \frac{EI^G}{{R_0}^2 h_{n_L}} \end{bmatrix} \tag{3.51}$$

where, EI^G is the bending stiffness of the equivalent single upright beam. This EI^G is evaluated following the same procedure as that used for the evaluation of bending stiffness of a reinforced concrete beam. Namely, EI^G is assumed to be equal to the sum of the Young's-modulus-weighted products of all the elementary areas times their distances squared from the centroid of the cross-section A_G (**Fig. 2.4a**).

Given equations (3.48)-(3.51), the global stiffness matrix of the equivalent single beam is finally expressed as:

$$\begin{Bmatrix} \mathbf{P}_x \\ \cdots \\ \frac{\mathbf{M}}{R_0} \end{Bmatrix} = \begin{bmatrix} [\mathbf{L}][\mathbf{D}]^{-1}[\mathbf{L}] & \vdots & \text{1st column of } [\mathbf{L}][\mathbf{D}]^{-1}/R_0 \text{ and zeros for other columns} \\ \cdots\cdots & & \cdots\cdots \\ \text{1st row of } [\mathbf{D}]^{-1}[\mathbf{L}]/R_0 \text{ and zeros for other rows} & \vdots & D_{1,1}^{-1} \text{ and } [\mathbf{Q}] \end{bmatrix} \begin{Bmatrix} \mathbf{u}_x \\ \cdots \\ \mathbf{w} \end{Bmatrix} \tag{3.52}$$

$$= [\mathbf{F}_H] \begin{Bmatrix} \mathbf{u}_x \\ \cdots \\ \mathbf{w} \end{Bmatrix}$$

The global equations of motion for the entire upright single beam are thus obtained as:

$$\left(\left[\mathbf{F}_H\right]-\omega^2\left[\mathbf{M}_H\right]\right)\begin{bmatrix}\{\mathbf{u}_x\}\\ \{\mathbf{w}\}\end{bmatrix}=\{P\}$$

where, $\{P\}=\left(\{\mathbf{P}_x\}^T \quad \{\mathbf{M}/R_0\}^T\right)^T$: external force vector.

Finally, the equations of motion for the entire soil-foundation system are obtained by combining equation (3.47) with the above equations of the upright column's motion ($\{V_r\}=\{\mathbf{u}_x\}$ and $\{V_z\}=\{\mathbf{w}\}$) as:

$$\left.\begin{aligned}\left(\left[R_H\right]+\left[F_H\right]-\omega^2\left[M_H\right]\right)\begin{bmatrix}\{V_r\}\\ \{V_z\}\end{bmatrix}&=\{P\}\\ \left[R_H\right]&=\pi R_0\left[D_H\right]\left[J_H\right]^{-1}\end{aligned}\right\} \tag{3.53}$$

Given the motions of the upright column from equation (3.53), displacements at an arbitrary point (r,θ) in the surrounding soil are obtained by solving the following equation:

$$\begin{bmatrix}\{V_r\}_r\\ \{V_\theta\}_r\\ \{V_z\}_r\end{bmatrix}=\begin{bmatrix}[X]\left[\ddots h_\alpha(r)\cdot f_{\alpha\cdots}\right]+[Y]\left[\ddots h_\beta{}^*(r)\cdots\right][E]\\ [X]\left[\ddots h_\alpha{}^*(r)\cdots\right]+[Y]\left[\ddots h_\beta(r)\cdot f_{\beta\cdots}\right][E]\\ [Z]\left[\ddots h_\alpha{}^*(r)\cdot\alpha r\cdots\right]\end{bmatrix}\cdot\left[J_H\right]^{-1}\begin{bmatrix}\{V_r\}\\ \{V_z\}\end{bmatrix} \tag{3.54}$$

where,

$$\left.\begin{aligned}h_\alpha(r)&=\frac{H_2{}^{(2)}(\alpha r)-H_0{}^{(2)}(\alpha r)}{H_2{}^{(2)}(\alpha R_0)-H_0{}^{(2)}(\alpha R_0)}\\ h_\alpha{}^*(r)&=\frac{H_2{}^{(2)}(\alpha r)+H_0{}^{(2)}(\alpha r)}{H_2{}^{(2)}(\alpha R_0)+H_0{}^{(2)}(\alpha R_0)}\\ &=\frac{H_1{}^{(2)}(\alpha r)}{H_1{}^{(2)}(\alpha R_0)}\frac{R_0}{r}\end{aligned}\right\} \tag{3.55}$$

h_β and $h_\beta{}^*$ are obtained by simply replacing α in equations (3.55) with β.

Pile Deflection Caused by the Motion of the Surrounding Soil

It is assumed that a virtual soil foundation having the same size and shape of an actual foundation is embedded in the soil, and the response of the virtual soil foundation is obviously identical to the free-field ground motion. We now consider an actual foundation whose stiffness and mass are cut down by the quantities that offset this virtual soil foundation. This procedure leads both the stiffness and mass matrices to be modified as:

$$\left[F_H\right]\Rightarrow\left[F_H{}^*\right],\ \left[M_H\right]\Rightarrow\left[M_H{}^*\right]$$

The change in $\left[F_H\right]$, however, turns out to be extremely small in many cases encountered, and can be ignored. The presence of this foundation with $\left[F_H\right]$ ($\left[F_H{}^*\right]$

correctly) and $[M_H{}^*]$ then causes the ground motion $\{V_r\}$ at the soil-foundation interface to deviate from the free-field ground motion $\{V_r{}^*\}$, and the equations of motion are written in the following form as:

$$\left([F_H]-\omega^2[M_H{}^*]\right)\begin{bmatrix}\{V_r\}\\ \{V_z\}\end{bmatrix}=-[R_H]\left(\begin{bmatrix}\{V_r\}\\ \{V_z\}\end{bmatrix}-\begin{bmatrix}\{V_r{}^*\}\\ \{0\}\end{bmatrix}\right) \tag{3.56}$$

where, $[R_H]=\pi R_0[D_H][J_H]^{-1}$ (See equation (3.47))

4. *Data Files*

TLEM1.2 requires four input data files to be provided. Among these files, "**equi_stiff.dat**" stores parameters describing a single upright beam which approximates closely the behaviors of a pile group. A program, "**pile_param.exe**", saves a lot of trouble creating parameters for "**equi_stiff.dat**". This program requires (1) **LAYER.dat** (5) **ARRANGE.dat** and (6) **PILEPRM.dat.**

After running ***TLEM1.2***, 14 output data files are created on the same directory where ***TLEM1.2*** exsits.

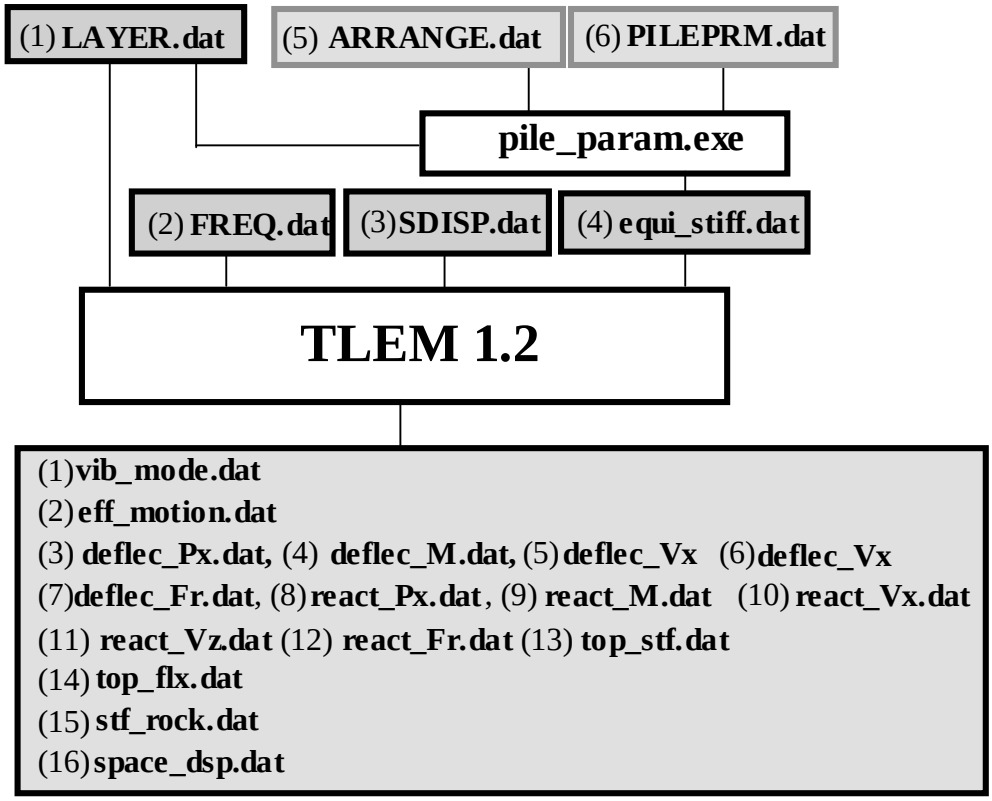

4.1 *Input data files*

(1) **LAYER.dat**

This data file provides the parameters that describe mechanical features of soil slices.

```
<-1->
   10
<---2----><---3----><---4----><---5----><---6----><---7---->
    4.80e4    4.80e3    9.79e2    9.79e1     0.153       2.0
    4.80e4    4.80e3    9.79e2    9.79e1     0.153       4.0
    4.80e4    4.80e3    9.79e2    9.79e1     0.153       6.0
    4.80e4    4.80e3    9.79e2    9.79e1     0.153       8.0
    4.80e4    4.80e3    9.79e2    9.79e1     0.153      10.0
    4.80e4    4.80e3    9.79e2    9.79e1     0.153      12.0
    4.80e4    4.80e3    9.79e2    9.79e1     0.153      14.0
    4.80e4    4.80e3    9.79e2    9.79e1     0.153      16.0
    4.80e4    4.80e3    9.79e2    9.79e1     0.153      18.0
    4.80e4    4.80e3    9.79e2    9.79e1     0.153      20.0
```

where,

<-1-> (I5): Number of soil slices,

<-2-> (F10.7): Real part of λ (Lame's constant: tf/m^2) for each soil slice,

<-3-> (F10.7): Imaginary part of λ (Lame's constant: tf/m^2) for each soil slice,

<-4-> (F10.7): Real part of μ (shear modulus: tf/m^2) for each soil slice,

<-5-> (F10.7): Imaginary part of μ (shear modulus: tf/m^2) for each soil slice,

<-6-> (F10.7): density of μ (shear modulus: tf/m^2) for each soil slice,

<-7-> (F10.7): depth of slice boundary (m)

(2) **FREQ.dat**

TLEM provides solutions in the frequency domain. The following index parameters must be provided:

```
<-1-><-2-><---3----><---4---->
   63    14       1.0       1.0
```

where,

<-1-> (I5): Number of stepwize increases of circular frequency

<-2-> (I5): Some large data files (**space_dsp.dat** etc.) are created at this step of increasing frequency

<-3-> (F10.7): Initial value of circular frequency

<-4-> (F10.7): Increment of circular frequency

(3) **SDISP.dat**

This data file "SDISP.dat" provides necessary parameters for storing spatial variation of soil displacements.

```
<-1-><-2-><-3-><---4----><---5---->
    1     4    10     1.000     0.100
```

where,
<-1-> (I5): IDR : direction of displacement component (IDR=1:radial, 2:tangential, 3:vertical)
<-2-> (I5): KF : direction of applied force or displacement
KF=1: Lateral unit force is applied
KF=2: Moment/R_0 (=1.0) is applied
KF=3: Lateral unit displacement is given keeping rotation zero
KF=4: Unit rotation is given keeping lateral displacement zero
<-3-> (I5): Number of stepwise increases of radial diatance
<-4-> (F10.7): Initial value of radial distance r / R_0
<-5-> (F10.7): Increment of radial distance $\Delta r / R_0$

(4) **Equi_stiff.dat**
As has been explained in Section 3.2, a pile group is treated as a single upright beam described in term of representative parameters, R_0, EI_p and EI^G (equations (3.49b) and (3.51)). These parameters for all sliced beam elements are provided by a data file "**equi_stiff.dat**". This data file also provides the masses of the sliced elements which are used in the mass matrix $[M_H]$

```
<---1---->
  .288E+01
<---2----><---3----><---4----><---5----><---6---->
  .245E+06  .000E+00  .160E+08  .000E+00  .350E+01
  .245E+06  .000E+00  .160E+08  .000E+00  .350E+01
  .245E+06  .000E+00  .160E+08  .000E+00  .350E+01
  .245E+06  .000E+00  .160E+08  .000E+00  .350E+01
  .245E+06  .000E+00  .160E+08  .000E+00  .350E+01
  .245E+06  .000E+00  .160E+08  .000E+00  .350E+01
  .245E+06  .000E+00  .160E+08  .000E+00  .350E+01
  .245E+06  .000E+00  .160E+08  .000E+00  .350E+01
  .245E+06  .000E+00  .160E+08  .000E+00  .350E+01
  .245E+06  .000E+00  .160E+08  .000E+00  .350E+01
```

where,
<-1-> (F10.7): Radius of the pile-group-equivalent single upright beam, R_0 (m).
<-2-> (F10.7): Real part of EI_p (tf m^2) for each sliced element.
<-3-> (F10.7): Imaginary part of EI_p (tf m^2) for each sliced element.
<-4-> (F10.7): Real part of EI^G (tf m^2) for each sliced element.
<-5-> (F10.7): Imaginary part of EI^G (tf m^2) for each sliced element.
<-6-> (F10.7): mass of each sliced element (tf s^2/m).

It actually takes time to obtain above mentioned parameters for pile groups. A program, "**pile_param.exe**", allows preparation of "**equi_stiff.dat**" to be made with less time and effort. This program requires (1) **LAYER.dat** and the following input data files:

(5) **ARRANGE.dat**

This data file "**ARRANGE.dat**" provides arrangement of piles grouped beneath a rigid pile cap.

```
<-1->
   16
<---2----><---3---->
       0.0       0.0
       1.5       0.0
       3.0       0.0
       4.5       0.0
       0.0       1.5
       1.5       1.5
       3.0       1.5
       4.5       1.5
       0.0       3.0
       1.5       3.0
       3.0       3.0
       4.5       3.0
       0.0       4.5
       1.5       4.5
       3.0       4.5
       4.5       4.5
```

where,

<-1-> (I5): number of piles

<-2-> (F10.7): *x* coordinate (m) (**NOTE**: piles are excited in *x* direction).

<-3-> (F10.7): *y* coordinate (m).

(5) **PILEPRM.dat**

This data file "**PILEPRM.dat**" provides mechanical properties of sliced pile elements.

```
<---1----><---2----><---3----><---4----><---5---->
    0.3000    0.2910     2.1e7       0.0     0.801
    0.3000    0.2910     2.1e7       0.0     0.801
    0.3000    0.2910     2.1e7       0.0     0.801
    0.3000    0.2910     2.1e7       0.0     0.801
    0.3000    0.2910     2.1e7       0.0     0.801
    0.3000    0.2910     2.1e7       0.0     0.801
    0.3000    0.2910     2.1e7       0.0     0.801
    0.3000    0.2910     2.1e7       0.0     0.801
    0.3000    0.2910     2.1e7       0.0     0.801
    0.3000    0.2910     2.1e7       0.0     0.801
    0.3000    0.2910     2.1e7       0.0     0.801
    0.3000    0.2910     2.1e7       0.0     0.801
    0.3000    0.2910     2.1e7       0.0     0.801
    0.3000    0.2910     2.1e7       0.0     0.801
    0.3000    0.2910     2.1e7       0.0     0.801
    0.3000    0.2910     2.1e7       0.0     0.801
```

where,

<-1-> (F10.7): outer radius of sliced pile element (m)

<-2-> (F10.7): inner radius of sliced pile element (m)

<-3-> and <-4-> (F10.7): Real and imaginary parts of Young's modulus of sliced pile element (tf/m^2)

<-5-> (F10.7): density of pile ($tf/m^3\ s^2/m$)

4.2 *Output data files*

(1) **vib_mode.dat**

This data file, "**vib_mode.dat**", stores the deflection of pile group caused by free-field ground motion (V_r^{f+s} and V_r^{f} in equation (3.56)).

```
<------1------><------2------><------3------><------4------><------5------><------6------>
     .1000E+01     .0000E+00     .1032E+01    -.3248E-02     .1032E+01    -.3249E-02
     .1000E+01     .2000E+01     .1031E+01    -.3209E-02     .1031E+01    -.3216E-02
     .1000E+01     .4000E+01     .1030E+01    -.3108E-02     .1030E+01    -.3118E-02
     .1000E+01     .6000E+01     .1029E+01    -.2944E-02     .1029E+01    -.2953E-02
     .1000E+01     .8000E+01     .1026E+01    -.2713E-02     .1027E+01    -.2723E-02
     .1000E+01     .1000E+02     .1024E+01    -.2416E-02     .1024E+01    -.2428E-02
     .1000E+01     .1200E+02     .1020E+01    -.2051E-02     .1020E+01    -.2068E-02
     .1000E+01     .1400E+02     .1016E+01    -.1619E-02     .1016E+01    -.1644E-02
     .1000E+01     .1600E+02     .1011E+01    -.1124E-02     .1011E+01    -.1155E-02
     .1000E+01     .1800E+02     .1006E+01    -.5770E-03     .1006E+01    -.6039E-03
     .2000E+01     .0000E+00     .1137E+01    -.1530E-01     .1137E+01    -.1532E-01
     .2000E+01     .2000E+01     .1136E+01    -.1512E-01     .1136E+01    -.1516E-01
     .2000E+01     .4000E+01     .1131E+01    -.1463E-01     .1132E+01    -.1468E-01
     .2000E+01     .6000E+01     .1124E+01    -.1383E-01     .1125E+01    -.1388E-01
     .2000E+01     .8000E+01     .1115E+01    -.1273E-01     .1115E+01    -.1278E-01
     .2000E+01     .1000E+02     .1102E+01    -.1131E-01     .1102E+01    -.1136E-01
     .2000E+01     .1200E+02     .1087E+01    -.9571E-02     .1087E+01    -.9646E-02
     .2000E+01                                -.7534E-02     .1069E+01    -.7638E-02
                                                             .1049E+01
```

where,

<-1-> (E15.7): circular frequency

<-2-> (E15.7): depth (m)

<-3-> (E15.7): real part of deformation of pile group, V_r^{f+s} (m)

<-4-> (E15.7): imaginary part of deformation of pile group, V_r^{f+s} (m)

<-5-> (E15.7): real part of free-field ground motion, V_r^{f} (m)

<-6-> (E15.7): imaginary part of free-field ground motion, V_r^{f} (m)

(2) **eff_motion.dat**

This data file "**eff_motion.dat**" stores transfer functions (kinematic displacement factor $T_{e,x}$ and $T_{e,z}$) for evaluation of effective input ground motion.

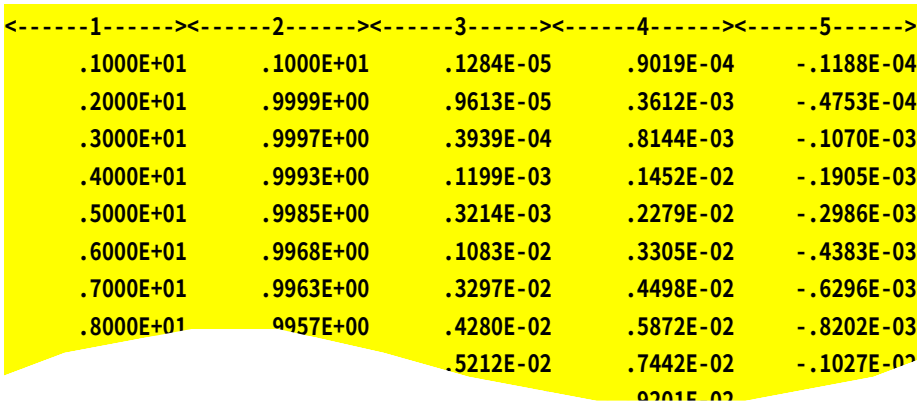

```
<------1------><------2------><------3------><------4------><------5------>
     .1000E+01     .1000E+01     .1284E-05     .9019E-04    -.1188E-04
     .2000E+01     .9999E+00     .9613E-05     .3612E-03    -.4753E-04
     .3000E+01     .9997E+00     .3939E-04     .8144E-03    -.1070E-03
     .4000E+01     .9993E+00     .1199E-03     .1452E-02    -.1905E-03
     .5000E+01     .9985E+00     .3214E-03     .2279E-02    -.2986E-03
     .6000E+01     .9968E+00     .1083E-02     .3305E-02    -.4383E-03
     .7000E+01     .9963E+00     .3297E-02     .4498E-02    -.6296E-03
     .8000E+01     .9957E+00     .4280E-02     .5872E-02    -.8202E-03
                                 .5212E-02     .7442E-02    -.1027E-02
                                               .9201E-02
```

where,

<-1-> (E15.7): circular frequency

<-2-> (E15.7) and

<-3-> (E15.7): Real and imaginary parts of kinematic displacement factor $T_{e,x}$ for evaluation of the effective input sway motion at the top end of the foundation:

$$T_{e,x} = \left(V_r^{\,f} + V_r^{\,r}\right)_{top} / V_r^{\,f}{}_{surface}$$

<-4-> (E15.7) and

<-5-> (E15.7): Real and imaginary parts of kinematic displacement factor $T_{e,z}$ for evaluation of the effective input rocking motion at the top end of the foundation:

$$T_{e,x} = \left(V_z^{\,f} + V_z^{\,r}\right)_{top} / \left(V_r^{\,f}\right)_{surface} = \left(V_z^{\,r}\right)_{top} / \left(V_r^{\,f}\right)_{surface}$$

(3) **deflec_Px.dat,** (4) **deflec_M.dat,** (5) **deflec_Vx**, (6) **deflec_Vx** and (7) **deflec_Fr**

Data files "**deflec_Px.dat**", "**deflec_M.dat**", "**deflec_Vx.dat**" and "**deflec_Vz.dat** store vibration modes of a pile group subjected to an unit lateral force, unit moment, M_y / R_0 =1, unit displacements V_x =1 and V_z =1, respectively, applied to its pile cap. "

Data file **deflec_Fr.dat** stores relative displacements between the pile group and far-field soil

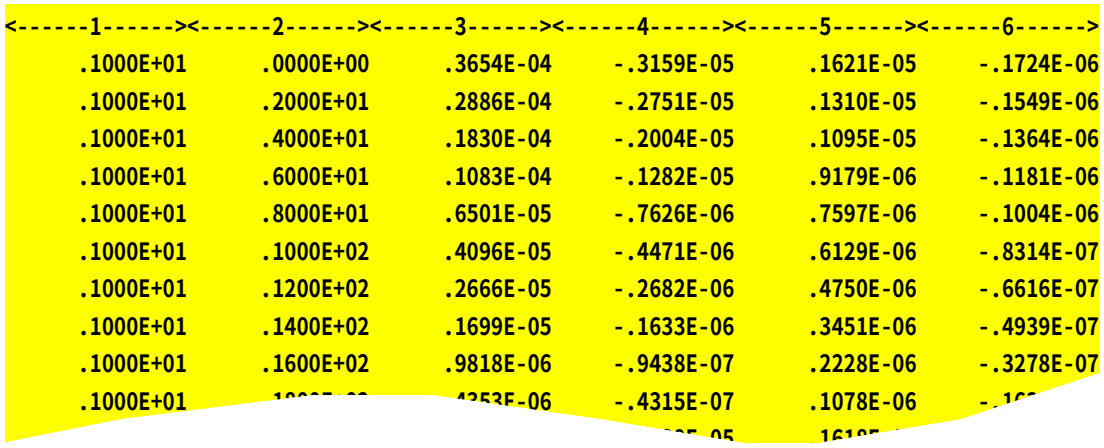

```
<------1------><------2------><------3------><------4------><------5------><------6------>
     .1000E+01     .0000E+00     .3654E-04    -.3159E-05     .1621E-05    -.1724E-06
     .1000E+01     .2000E+01     .2886E-04    -.2751E-05     .1310E-05    -.1549E-06
     .1000E+01     .4000E+01     .1830E-04    -.2004E-05     .1095E-05    -.1364E-06
     .1000E+01     .6000E+01     .1083E-04    -.1282E-05     .9179E-06    -.1181E-06
     .1000E+01     .8000E+01     .6501E-05    -.7626E-06     .7597E-06    -.1004E-06
     .1000E+01     .1000E+02     .4096E-05    -.4471E-06     .6129E-06    -.8314E-07
     .1000E+01     .1200E+02     .2666E-05    -.2682E-06     .4750E-06    -.6616E-07
     .1000E+01     .1400E+02     .1699E-05    -.1633E-06     .3451E-06    -.4939E-07
     .1000E+01     .1600E+02     .9818E-06    -.9438E-07     .2228E-06    -.3278E-07
     .1000E+01                   .4353E-06    -.4315E-07     .1078E-06
```

where,

<-1-> (E15.7): circular frequency
<-2-> (E15.7): depth (m)
<-3-> (E15.7): real part of sway motion of pile group V_r (m)
<-4-> (E15.7): imaginary part of sway motion of pile group V_r (m)
<-5-> (E15.7): real part of vertical motion V_z (m)
<-6-> (E15.7): imaginary part of vertical motion V_z (m)

(8) **react_Px.dat**, (9) **react_M.dat**, (10) **react_Vx.dat**, (11) **react_Vz.dat** and (12) **react_Fr.dat**

Data files "**react_Px.dat**", "**react_M.dat**", "**react_Vx.dat**" and "**react_Vz.dat**" store reaction forces from the soil surrounding a pile group subjected to an unit lateral force, unit moment, $M_y / R_0 = 1$, unit displacements $V_r = 1$ and $V_z = 1$, respectively, applied to its pile cap. Data file **react_Fr.dat** stores kinematic interaction forces.

```
<------1------><------2------><------3------><------4------><------5------><------6------>
     .1000E+01     .0000E+00     .4159E+00     .1016E-01     .1140E+00     .2307E-02
     .1000E+01     .2000E+01     .4517E+00     .2759E-02     .9328E-01     .9282E-03
     .1000E+01     .4000E+01     .1530E+00    -.7822E-02     .3651E-01    -.2419E-03
     .1000E+01     .6000E+01     .2252E-01    -.5780E-02     .1813E-01    -.5195E-03
     .1000E+01     .8000E+01    -.1342E-01    -.1746E-02     .1098E-01    -.4298E-03
     .1000E+01     .1000E+02    -.1479E-01     .4071E-03     .8540E-02    -.2868E-03
     .1000E+01     .1200E+02    -.8879E-02     .8773E-03     .7752E-02    -.1964E-03
     .1000E+01     .1400E+02    -.3916E-02     .6195E-03     .7357E-02    -.1525E-03
     .1000E+01     .1600E+02    -.4989E-03     .2450E-03     .6935E-02    -.1331E-03
     .1000E+01     .1800E+02     .2493E-02     .7824E-05     .7039E-02    -.1674E-03
     .2000E+01     .0000E+00     .4160E+00     .1015E-01     .1141E+00     .2302E-02
     .2000E+01     .2000E+01     .4519E+00     .2752E-02     .9342E-01     .9130E-03
     .2000E+01     .4000E+01     .1532E+00    -.7835E-02     .3673E-01    -.2679E-03
     .2000E+01     .6000E+01     .2267E-01    -.5796E-02     .1841E-01    -.5526E-03
                                              -.1761E-02     .1128E-01    -.4670E-03
                                              -.2959E-03     .8859E-02    -.3265E-
```

where,

<-1-> (E15.7): circular frequency
<-2-> (E15.7): depth (m)
<-3-> (E15.7): real part of lateral reaction P_x (tf)
<-4-> (E15.7): imaginary part of lateral reaction P_x (tf)
<-5-> (E15.7): real part of restoring moment M_y / R_0 (tf)
<-6-> (E15.7): imaginary part of restoring moment M_y / R_0 (tf)

(13) **top_stf.dat**

This data file "**top_stf.dat**" stores pile cap stiffness S_{xx}, S_{xz} $(= S_{zx})$ and S_{zz}.

<-----1------><------2------><------3------><------4------><------5------><------6------><------7------>

.1000E+01	.2744E+05	.2343E+04	-.6224E+04	-.8212E+01	.1400E+06	.2949E+04
.2000E+01	.2714E+05	.2352E+04	-.6141E+04	-.1584E+02	.1399E+06	.2954E+04
.3000E+01	.2660E+05	.2375E+04	-.5989E+04	-.3131E+02	.1397E+06	.2963E+04
.4000E+01	.2572E+05	.2429E+04	-.5739E+04	-.6209E+02	.1394E+06	.2980E+04
.5000E+01	.2425E+05	.2592E+04	-.5314E+04	-.1365E+03	.1391E+06	.3016E+04
.6000E+01	.2127E+05	.3625E+04	-.4439E+04	-.5057E+03	.1385E+06	.3153E+04
.7000E+01	.2079E+05	.8581E+04	-.4403E+04	-.2051E+04	.1381E+06	.3648E+04
.8000E+01	.2239E+05	.1064E+05	-.4966E+04	-.2682E+04	.1378E+06	.3863E+04
.9000E+01				-.3072E+04	.1374E+06	.4031E+04

where,

<-1-> (E15.7): circular frequency
<-2-> (E15.7): real part of S_{xx} (tf/m)
<-3-> (E15.7): imaginary part of S_{xx} (tf/m)
<-4-> (E15.7): real part of S_{xz} $(=S_{zx})$ (tf/m)
<-5-> (E15.7): imaginary part of S_{xz} $(=S_{zx})$ (tf/m)
<-6-> (E15.7): real part of S_{zz} (tf/m)
<-7-> (E15.7): imaginary part of S_{zz} (tf/m)

(14) **top_flx.dat**

This data file "**top_flx.dat**" stores pile cap flexibility H_{xx}, H_{xz} $(=H_{zx})$ and H_{zz}.

<-------1------><------2------><------3------><------4------><------5------><------6------><------7------>

.1000E+01	.3654E-04	-.3159E-05	.1621E-05	-.1724E-06	.7211E-05	-.1595E-06
.2000E+01	.3693E-04	-.3239E-05	.1618E-05	-.1722E-06	.7216E-05	-.1597E-06
.3000E+01	.3766E-04	-.3400E-05	.1611E-05	-.1715E-06	.7223E-05	-.1602E-06
.4000E+01	.3889E-04	-.3708E-05	.1599E-05	-.1694E-06	.7234E-05	-.1609E-06
.5000E+01	.4111E-04	-.4422E-05	.1572E-05	-.1627E-06	.7248E-05	-.1619E-06
.6000E+01	.4600E-04	-.7828E-05	.1500E-05	-.1172E-06	.7266E-05	-.1637E-06
.7000E+01	.4143E-04	-.1694E-04	.1574E-05	.3389E-07	.7287E-05	-.1680E-06
.8000E+01				.4659E-07	.7311E-05	-.1709E-06

where,

<-1-> (E15.7): circular frequency
<-2-> (E15.7): real part of H_{xx} (m/tf)
<-3-> (E15.7): imaginary part of H_{xx} (m/tf)
<-4-> (E15.7): real part of H_{xz} $(=H_{zx})$ (m/tf)
<-5-> (E15.7): imaginary part of H_{xz} $(=H_{zx})$ (m/tf)
<-6-> (E15.7): real part of H_{zz} (m/tf)
<-7-> (E15.7): imaginary part of H_{zz} (m/tf)

(15) **stf_rock.dat**

This data file "**stf_rock.dat**" stores restoring moment for a particular case of a rigid massless foundation rocking on a bedrock.

```
<------1------><------2------><------3------>
      .1000E+01      .1631E+08      .1642E+07
      .2000E+01      .1600E+08      .1643E+07
      .3000E+01      .1543E+08      .1649E+07
      .4000E+01      .1455E+08      .1673E+07
      .5000E+01      .1316E+08      .1766E+07
      .6000E+01      .1059E+08      .2411E+07
      .7000E+01      .9192E+07      .5942E+07
      .8000E+01      .9463E+07      .8001E+07
                     .9607E+07      .9515E+07
```

where,

<-1-> (E15.7): circular frequency

<-2-> (E15.7): real part of restoring moment M_y / R_0 (tf)

<-3-> (E15.7): imaginary part of restoring moment M_y / R_0 (tf)

(16) **space_dsp.dat**

This data file "**space_dsp.dat**" stores spatial variation of soil displacements. As has been mentioned, "**SDISP.dat**" provides the following necessary parameters for storing spatial variation of soil displacements.

<1> IDR : direction of displacement component (V_r (IDR=1), V_θ (IDR=2) or V_z (IDR=3))

<2> KF : direction of applied force or displacement

KF=1: Lateral unit force is applied

KF=2: Moment/R_0 (=1.0) is applied

KF=3: Lateral unit displacement is given keeping rotation zero

KF=4: Unit rotation is given keeping lateral displacement zero

<3> (I5): Number of stepwise increases of radial diatance

<4> (F10.7): Initial value of radial distance r / R_0

<5> (F10.7): Increment of radial distance $\Delta r / R_0$

```
<------1------><------2------><------3------><------4------>
      .2880E+01      .0000E+00     -.1348E-15      .5787E-17
      .2880E+01      .2000E+01     -.3404E+00      .4228E-01
      .2880E+01      .4000E+01     -.3105E+00      .1051E+00
      .2880E+01      .6000E+01     -.2018E+00      .1482E+00
      .2880E+01      .8000E+01     -.1130E+00      .1686E+00
      .2880E+01      .1000E+02     -.6000E-01      .1715E+00
      .2880E+01      .1200E+02     -.3502E-01      .1603E+00
      .2880E+01      .1400E+02     -.2690E-01      .1367E+00
      .2880E+01      .1600E+02     -.2473E-01      .1009E+00
      .2880E+01      .1800E+02     -.1764E-01      .5411E-01
      .3168E+01      .0000E+00     -.8249E-02      .1562E-02
      .3168E+01      .2000E+01     -.3194E+00      .4389E-01
                                   -.2934E+00      .1054E+00
                                                   .1481E+00
```

where,

<-1-> (E15.7): radial distance r (m)

<-2-> (E15.7): depth z (m)

<-3-> (E15.7): real part of displacement (V_r (IDR=1), V_θ (IDR=2) or V_z (IDR=3)) (m)

<-4-> (E15.7): imaginary part of displacement (V_r (IDR=1), V_θ (IDR=2) or V_z (IDR=3)) (m)

5. *Numerical Examples*

Steel pile groups

Steel piles (**Table 5.1**) grouped together beneath a rigid massless pile cap are embedded in a homogeneous soil deposit (**Table 5.2**) overlying a rigid bedrock.

Table 5.1 Parameters for steel piles

E_p (tf/m^2)	ρ_p (t/m^3)	r_0 (m)	thickness (m)	length (m)
2.1×10^7	7	0.3	0.0089	20

Table 5.2 Parameters for soil

ρ_p (t/m^3)	v_s (m/s)	ν	thickness (m)
1.5	80	0.49	20

The soil deposit with the inclusion of piles is cut equally into 10 slices. Piles are arranged side by side in squares with equal interval of 2.5 times as large as the pile diameter. Two pile groups (2×2 and 3×3, **Fig. 5.1**) are discussed herein.

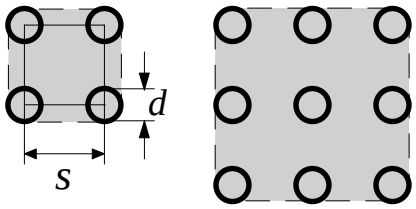

Fig. 5.1 pile groups

Prepared input data files

(1) **LAYER.dat**

```
10
 4.80e4    4.80e3    9.79e2    9.79e1    0.153      2.0
 4.80e4    4.80e3    9.79e2    9.79e1    0.153      4.0
 4.80e4    4.80e3    9.79e2    9.79e1    0.153      6.0
 4.80e4    4.80e3    9.79e2    9.79e1    0.153      8.0
 4.80e4    4.80e3    9.79e2    9.79e1    0.153     10.0
 4.80e4    4.80e3    9.79e2    9.79e1    0.153     12.0
 4.80e4    4.80e3    9.79e2    9.79e1    0.153     14.0
 4.80e4    4.80e3    9.79e2    9.79e1    0.153     16.0
 4.80e4    4.80e3    9.79e2    9.79e1    0.153     18.0
 4.80e4    4.80e3    9.79e2    9.79e1    0.153     20.0
```

(2) **FREQ.dat**

```
63   15        1.0        1.0
```

(3) **SDISP.dat**

```
 1    4   10      1.000      0.100
```

(4) **equi_stiff.dat** (See next page).

(5) **ARRANGE.dat**

2×2 piles

```
4
   0.0      0.0
   1.5      0.0
   0.0      1.5
   1.5      1.5
```

3×3 piles

```
9
   0.0      0.0
   1.5      0.0
   3.0      0.0
   0.0      1.5
   1.5      1.5
   3.0      1.5
   0.0      3.0
   1.5      3.0
   3.0      3.0
```

(6) **PILEPRM.dat**

```
   0.3      0.291    2.1e7    0        0.801
   0.3      0.291    2.1e7    0        0.801
   0.3      0.291    2.1e7    0        0.801
   0.3      0.291    2.1e7    0        0.801
   0.3      0.291    2.1e7    0        0.801
   0.3      0.291    2.1e7    0        0.801
   0.3      0.291    2.1e7    0        0.801
   0.3      0.291    2.1e7    0        0.801
   0.3      0.291    2.1e7    0        0.801
   0.3      0.291    2.1e7    0        0.801
```

(4) **equi_stiff.dat**

2×2 piles

```
 .118E+01
 .613E+05  .000E+00  .851E+06  .000E+00  .555E+00
 .613E+05  .000E+00  .851E+06  .000E+00  .555E+00
 .613E+05  .000E+00  .851E+06  .000E+00  .555E+00
 .613E+05  .000E+00  .851E+06  .000E+00  .555E+00
 .613E+05  .000E+00  .851E+06  .000E+00  .555E+00
 .613E+05  .000E+00  .851E+06  .000E+00  .555E+00
 .613E+05  .000E+00  .851E+06  .000E+00  .555E+00
 .613E+05  .000E+00  .851E+06  .000E+00  .555E+00
 .613E+05  .000E+00  .851E+06  .000E+00  .555E+00
```

3×3 piles

```
 .203E+01
 .138E+06  .000E+00  .488E+07  .000E+00  .171E+01
 .138E+06  .000E+00  .488E+07  .000E+00  .171E+01
 .138E+06  .000E+00  .488E+07  .000E+00  .171E+01
 .138E+06  .000E+00  .488E+07  .000E+00  .171E+01
 .138E+06  .000E+00  .488E+07  .000E+00  .171E+01
 .138E+06  .000E+00  .488E+07  .000E+00  .171E+01
 .138E+06  .000E+00  .488E+07  .000E+00  .171E+01
 .138E+06  .000E+00  .488E+07  .000E+00  .171E+01
 .138E+06  .000E+00  .488E+07  .000E+00  .171E+01
```

5.1 *Deflection of pile group caused by free-field ground motion* (vib_mode.dat)

Fig. 5.2a shows the real part of the soil response to sine shake given to its bottom end (bedrock); the motion is referred to as the "free-field ground motion". The grouped piles (3×3) are flexible enough to follow closely the free-field ground motion in a low frequency range (**Fig. 5.2b**), but they become inflexible as the frequency increases and the motion of piles V_r^{f+s} gradually deviates from the free-field ground displacement V_r^{f}.

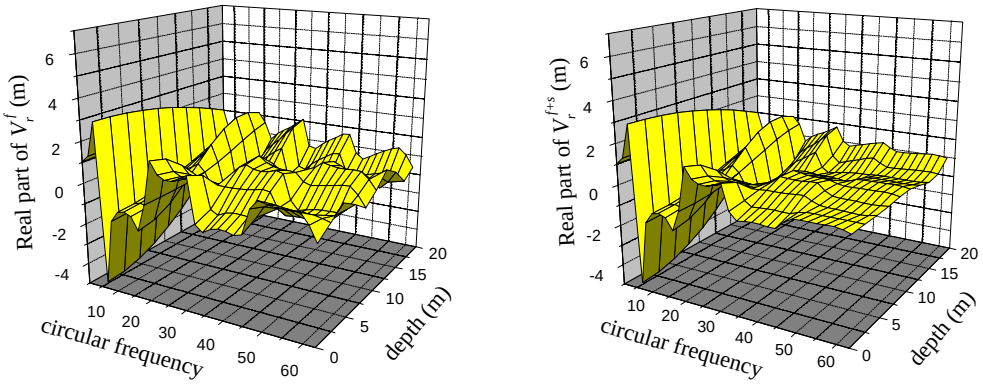

(a) Free-field ground motion V_r^{f} **(b)** Pile deflection V_r^{f+s}

Fig. 5.2 Free-field ground motion and pile deflection

5.2 *Kinematic displacement factors* (eff_motion.dat)

The effects of soil-pile group kinematic interaction evaluated at its pile cap are portrayed in the form of two kinematic displacement factors in sway and rocking motions

$$T_{e,sway} = \frac{V_r^{f+s}}{V_r^{f}}, \qquad T_{e,rocking} = \frac{V_z^{f+s}}{V_r^{f}} \tag{5.1), (5.2}$$

plotted as functions of frequency.

Fig. 5.3 shows the kinematic displacement factors of the 3×3 pile group. This figure shows that the motion of the pile group is about identical to the free-field ground motion, and the kinematic interaction effect in a lower frequency range ($\omega < 20$) case can be ignored. As the frequency increases, however, the pile cap gradually starts rocking.

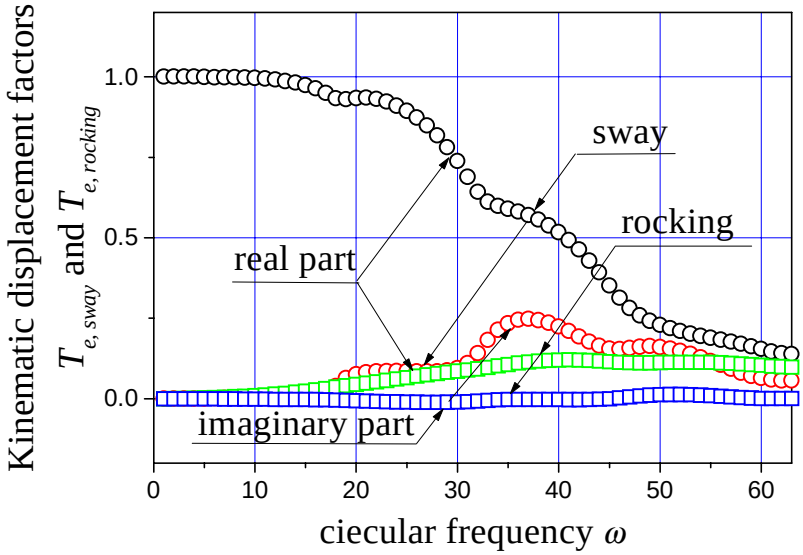

Fig. 5.3 Kinematic displacement factors

5.3 Pile deflection caused by a unit lateral force P_x applied to pile cap (**deflec_Px.dat**)

Deflection ($(V_r)_{r=R_0}$) of the 3×3 pile group subjected to a unit lateral force applied to its pile cap is show in **Fig. 5.4** for different excitement frequency. The other data files "**deflec_M.dat**", "**deflec_Vx.dat**" and "**deflec_Vz.dat**" store pile deflections caused by an unit moment, M_y / R_0 =1, unit displacements V_x =1 and V_z =1, respectively, applied to its pile cap.

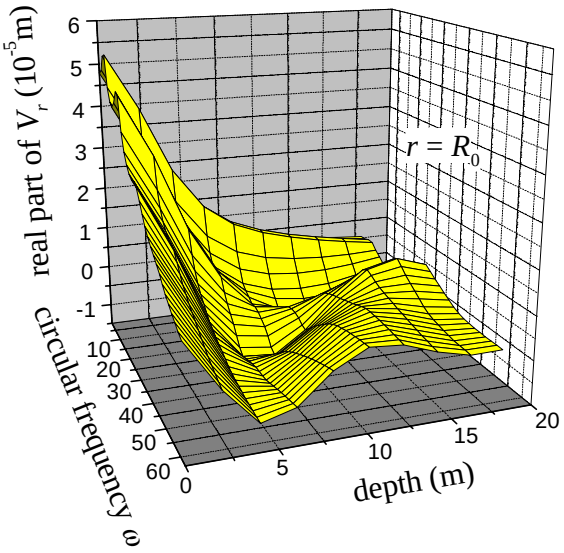

Fig. 5.4 Pile deflection caused by a unit lateral force P_x

5.4 Soil reactions to pile group caused by a unit lateral force P_x applied to pile cap (**react_Px.dat**)

Soil reactions at laterally-sliced element boundaries to the 3×3 pile group subjected to a unit lateral force applied to its pile cap is show in **Fig. 5.5** for different excitement frequency. The other data files "**react_M.dat**", "**react_Vx.dat**" and "**react_Vz.dat**" store reaction forces from the soil surrounding a pile group subjected to an unit moment, M_y / R_0=1, unit displacements V_r=1 and V_z=1, respectively, applied to its pile cap.

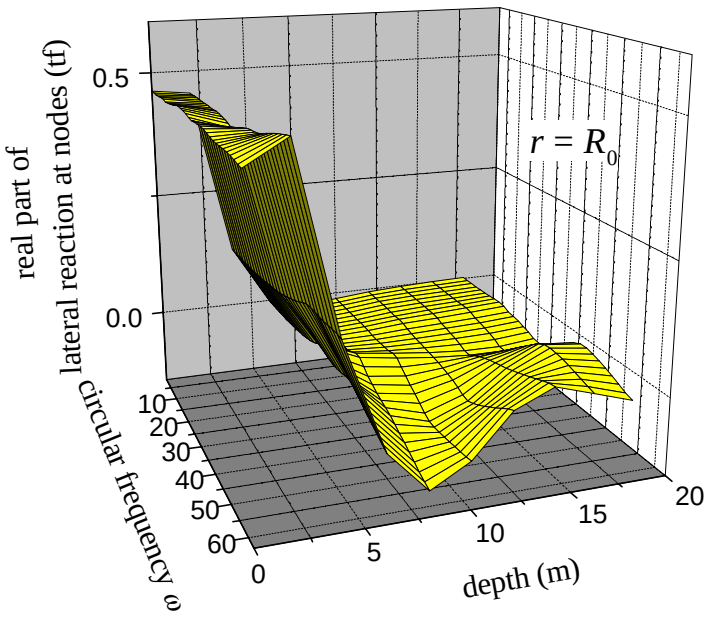

Fig. 5.5 Soil reactions to 3×3 pile group subjected to an unit lateral force given to its pile cap

5.5 *Pile cap stiffness* (**top_stf.dat**)

Fig. 5.6 shows the variations of pile cap stiffnesses for sway motions of 2×2 and 3×3 steel pile groups. The curves for the equivalent single beams agree well with rigorous solutions from "***TLEM***" **(Ver. 1.1)**.

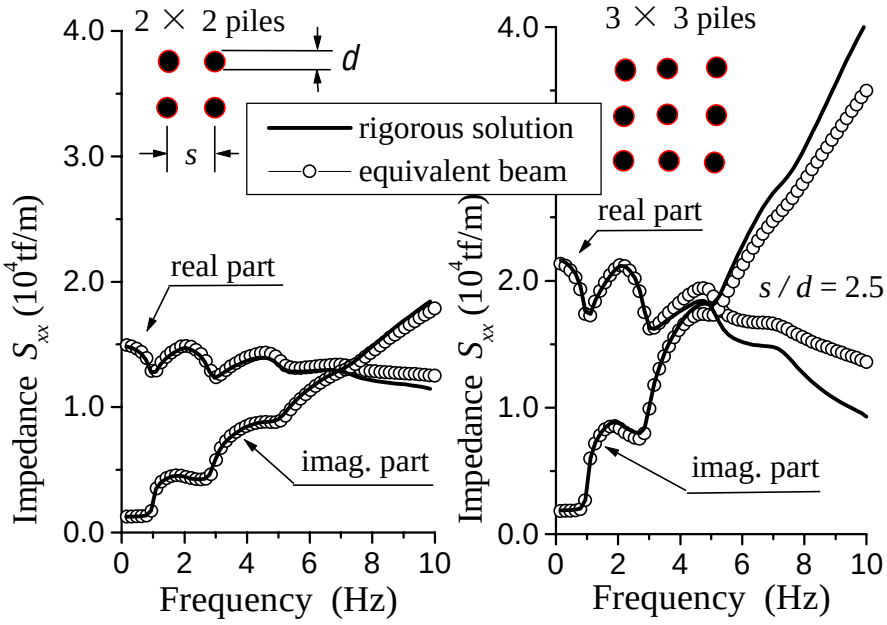

Fig. 5.6 Variations of stiffness parameters for sway motions of pile groups

5.6 *Pile cap flexibility* (**top_flx.dat**)

Fig. 5.7 shows the variations of pile cap flexibilities for sway, coupling, rocking motions of the 3×3 steel pile group.

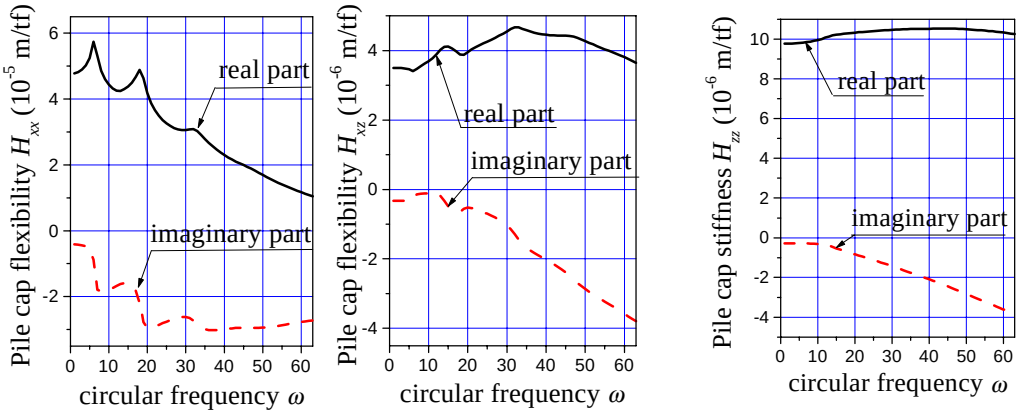

Fig. 5.7 Pile cap flexibilities

5.7 *Soil deformation* (**space_dsp.dat**)

Fig. 5.8 shows the spatial variation of soil displacement caused by a unit lateral force given to the pile cap of a 3×3 pile group. Directions of displacement component and the unit force or displacement given to the pile cap can be controlled by the following indexes in "**SDISP.dat**".

<1> IDR : direction of displacement component (V_r (IDR=1), V_θ (IDR=2) or V_z (IDR=3))

<2> KF : direction of applied force or displacement

KF=1: Lateral unit force is applied

KF=2: Moment/R_0 (=1.0) is applied

KF=3: Lateral unit displacement is given keeping rotation zero

KF=4: Unit rotation is given keeping lateral displacement zero

<3> (I5): Number of stepwise increases of radial diatance

<4> (F10.7): Initial value of radial distance r / R_0

<5> (F10.7): Increment of radial distance $\Delta r / R_0$

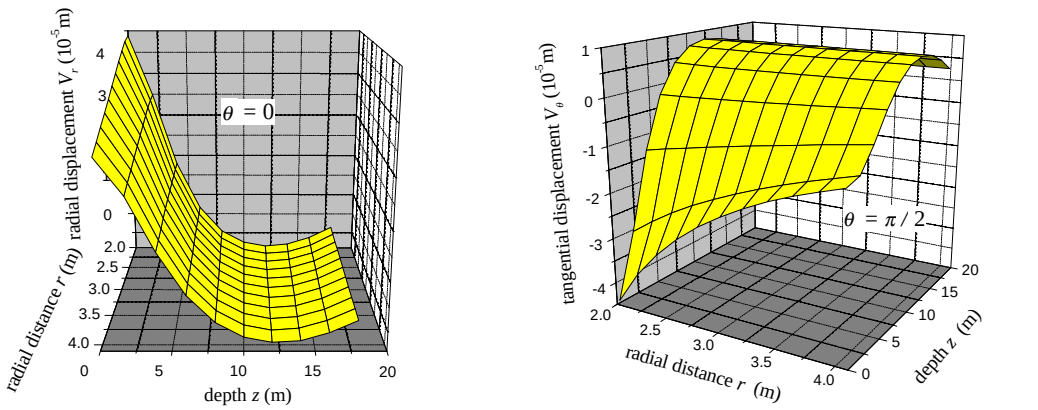

(a) radial displacement (ID=1) **(b)** tangential displacement (IDR=2)

Fig. 5.8 Spatial variation of soil displacement (KF=1)